Investigating the role of lipid metabolism in *C. elegans* mitochondrial *isp-1;ctb-1* mutant

Inaugural-Dissertation

zur
Erlangung des Doktorgrades
der Mathematisch-Naturwissenschaftlichen Fakultät
der Universität zu Köln

vorgelegt von

Sarah Eveline Iris Maciej

aus Hilden

Köln, 2020

Berichterstatter: **Prof. Dr. Aleksandra Trifunovic**
Dr. David Vilchez

Tag der mündlichen Prüfung: 26.06.2020

To my family and friends

Table of Contents

List of Figures

List of Tables

Abbreviations

°C	Degree Celsius
%	Percent
AA	Antimycin A
ACAD	Acyl-CoA dehydrogenase
ACC	Acetyl-CoA carboxylase
ACS	Acyl CoA synthetase
ATP	Adenosine triphosphate
ACOX	Acyl-CoA oxidase
Ca^{2+}	Calcium
C-C	Carbo-Carbon bond
CACT	Carnitine-acyl-carnitine translocase
C_2H_2	Acetylene
C. elegans	*Caenorhabditis elegans*
CHRS	Cerebro-hepato-renal syndrome
CoA	Coenzyme A
CO_2	Carbon dioxide
CoA	Coenzyme A
CPT	Carnitine palmitoyl transferase
CPZ	Chlorpromazine
CR	Caloric restriction
CYP	Cytochrome P450
dsRNA	Double-stranded RNA
D1	Day one of adulthood
DGAT-2	Diacylglycerol acyltransferase 2
E. coli	*Escherichia coli*
ECL	Enhanced chemiluminescence
EDTA	Ethylenediaminetetraacetic acid
ER	Endoplasmic reticulum
ETC	Electron transport chain
ETF	Electron transfer flavoprotein
ETFDH	ETF dehydrogenase

FAD	Flavin adenine-dinucleotide
FAO	Fatty acid oxidation
FAS	Fatty acid synthase
Fe^{2+}	Iron sulfate
Fe-S	Iron-sulfur
GFP	Green fluorescent protein
GPX4	Glutathione peroxidase 4
GS	Glyoxylate shunt
GSH	Glutathione
GST-4	Glutathione S-transferase 4
h	Hour
HECT	Homologous to the E6-AP-Carboyl Terminus
H_2O	Water
H_2O_2	Hydrogen peroxide
$HOO\cdot$	Hydroperoxyl radical
IMM	Inner mitochondrial membrane
IMS	Intermembrane space
IPTG	Isopropyl β-D-1-thiogalactopyranoside
K_2HPO_4	Dipotassium phosphate
KAT	3-Ketoacyl-coA Thiolase
KH_2PO_4	Monopotassium phosphate
KLF	Krüppel-like factor
KPI	Phosphate buffer
KSS	Kears-Sayre syndrome
L1-L4	Larval stage 1-Larval stage 4
LD	Lipid droplets
LHON	Leber's hereditary optic neuropathy
LOPs	Lipid oxidation products
LS	Leigh syndrome
M	Molar
MDA	Malondialdehyde
MELAS	Mitochondrial encephalopathy with lactic acidosis and stroke like episodes

MERRF	Myoclonic epilepsy with ragged-red fibers
$MgCl_2$	Magnesium chloride
$MgSO_4$	Magnesium sulfate
MIB	Mitochondria isolation buffer
min	Minute
mm	Millimeter
mM	Millimolar
mRNA	Messenger RNA
MRWB	2x Modified Ruvkun's witches brew
mtDNA	Mitochondrial DNA
NaCl	Sodium chloride
NaN_3	Sodium azide
NADH	Nicotinamide adenine dinucleotide
Na_2HPO_4	Disodium phosphate
NaOH	Sodium hydroxide
NGM	Nematode growth media
NP-40	Nonyl phenoxypolyethoxylethanol
O_2	Molecular oxygen
O_2^-	Superoxide
OMM	Outer mitochondrial membrane
OXPHOS	Oxidative phosphorylation
PBS	Phosphate-Buffered saline
PBST	Phosphate buffered saline (with Tween)
PC	Phosphatidylcholine
PCR	Polymerase chain reaction
PE	Phosphatidylethanolamine
PI	Phosphatidylinositol
PLIN1	Perilipin1
PLs	Phospholipids
PPARs	Peroxisome proliferator-activated receptors
PQ	Paraquat (1,1'-Dimethyl-4,4'-bipyridiniumdichloride)
PRX	Peroxisome assembly factor
PTS	Peroxisomal targeting signal

PUFA	Polyunsaturated fatty acid
RNA	Ribonucleic acid
RNAi	RNA interference
ROS	Reactive oxygen species
ROO·	Peroxyl radical
ROOH	Hydroxyl radical
ROS	Reactive oxygen species
RT	Room temperature
rpm	Revolutions per minute
SEM	Standard error of the mean
SDS	Sodium Dodecyl Sulfate
TAGs	Triglycerides
TBST	Tris-buffered saline with Tween
TCA cycle	Citric acid cycle
t-Test	Student`s t-Test
µg	Microgram
µl	Microliter
µM	Micromolar
UPR^{mt}	Mitochondrial unfolded protein response
V	Volt
VLCFA	Very-long-chain-fatty acid
ZS	Zellweger syndrome

Abstract

Fatty acids are essential components of all living organisms and the fatty acid metabolism mechanisms are conserved across species. Fatty acids are important for membrane biogenesis, energy storage and they serve as signaling molecules and modulate growth and development. *Caenorhabditis elegans* (*C. elegans*) does not have adipocytes dedicated to fat storage like in mammals, hence they store fats as triglycerides (TAGs) in lipid droplets and yolk. In *C. elegans*, the intestine is the major organ where food absorption, incorporation of nutrients into metabolic pathways, fat storage and utilization take place. Fatty acid synthesis, elongation, and desaturation, such as mitochondrial and peroxisomal ß-oxidation of fatty acids, are conserved in *C. elegans*.

Previously, we identified Krüppel-like factor 1 (KLF-1) as a major regulator of the longevity assurance caused by mitochondrial dysfunction in *C. elegans*. Now, we show that KLF-1 negatively regulates neutral lipid levels in *C. elegans* mitochondrial *isp-1(qm150);ctb-1(qm189)* mutants, a defect that can be fully corrected upon *klf-1* knockdown. The role of KLF-1 in the regulation of genes involved in lipid metabolism and storage in *isp-1;ctb-1* mutants is further emphasized by our microarray study.

Moreover, we identified ACS-1, a peroxisomal acyl-CoA synthetase, to be essential for the longevity of mitochondrial *isp-1;ctb-1* mutants. We also showed that PRX-5, a putative peroxisomal membrane protein, involved in protein import, has a similar role in suppression of increased lifespan in *isp-1;ctb-1* worms. We further showed that both, ACS-1 and PRX-5 are important to sustain respiration in *isp-1;ctb-1* mutants. Therefore, our data highlight the crosstalk between mitochondria and peroxisomes, especially lipid metabolism and shared fatty acid oxidation, as central to the response beneficial for organismal survival. Furthermore, we showed that loss of ACS-1 in *isp-1;ctb-1* mutant induces massive lipid peroxidation and can trigger KLF-1 translocation to the nucleus, independent of mitochondrial ROS production. Finally, our preliminary data suggest that this increased lipid peroxidation and insufficient capacity to reduce lipid peroxides might result in the initiation of ferroptosis.

Zusammenfassung

Fettsäuren sind ein essenzieller Bestandteil aller lebenden Organismen. Sie sind ein wichtiger Baustein für die Membranbiogenese, der Energiespeicherung und dienen darüber hinaus als Signalmoleküle, die Wachstum und Entwicklung modulieren. So ist der Fettsäurestoffwechsel speziesübergreifend zu finden. Bei Säugetieren dienen Adipozyten der Fettspeicherung. Der Fadenwurm *Caenorhabditis elegans* (*C. elegans*) besitzt keine Adipozyten, sondern speichert Fette als Triglyceriden in Lipidtröpfchen. Der Darm des Wurms ist das Hauptorgan und dient sowohl der Nahrungsaufnahme als auch der Aufnahme von Nährstoffen für weitere Stoffwechselwege, sowie der Fettspeicherung- und Verwertung von Fetten. Verschiedene Funktionen wie die Synthese, die Verlängerung und Entsättigung, aber ebenso die mitochondriale und peroxisomale Beta-Oxidation von Fettsäuren ist in *C. elegans* konserviert.

Kürzlich wurde unsererseits der Krüppel-like Faktor 1 (KLF-1), als ein Hauptregulator für Sicherung der Langlebigkeit, identifiziert. Diese Langlebigkeit wird bei *C. elegans* durch eine mitochondriale Dysfunktion verursacht. In dieser Studie konnten wir zeigen, dass KLF-1 die Menge an Lipiden in der *C. elegans* mitochondrialen *isp-1(qm150);ctb-1(qm189)* Mutante negativ reguliert. Die geringe Lipidmenge, kann bei einem Knockdown des *klf-1* Gens vollständig korrigiert werden. Unsere Microarrayergebnisse spiegeln auch die Rolle von KLF-1 in der Regulierung von Genen, die am Lipidstoffwechsel und der Speicherung in *isp-1(qm150);ctb-1(qm189)* Mutanten beteiligt sind, wider. Darüber hinaus identifizierten wir ACS-1, eine peroxisomale Acyl-CoA-Synthetase, die für die Langlebigkeit mitochondrialer *isp-1(qm150);ctb-1(qm189)* Mutanten essenziell ist. Ergänzend konnte gezeigt werden, dass PRX-5, ein peroxisomales Membranprotein, eine ähnliche Rolle bei der Unterdrückung der verlängerten Lebensdauer bei *isp-1;ctb-1* Würmern spielt.

Des Weiteren konnte gezeigt werden, dass sowohl ACS-1 als auch PRX-5 wichtig sind, um die Zellatmung in *isp-1(qm150);ctb-1(qm189)* Mutanten aufrechtzuerhalten. Unsere Ergebnisse heben ein Zusammenspiel von Mitochondrien und Peroxisomen, insbesondere im Lipidstoffwechsel und bei der Oxidation von Fettsäuren hervor, die für das Überleben des Organismus von zentraler Bedeutung sind. Der Verlust von ACS-1 in der *isp-1(qm150);ctb-1(qm189)* Mutante führt zu einer massiven oxidativen Degradation von Lipiden, was wiederum eine Translokation von KLF-1 in den Zellkern begünstigt. Das geschieht unabhängig von der mitochondrialen ROS-Produktion. Schließlich legen

unsere vorläufigen Daten nahe, dass die erhöhte Peroxidation von Lipiden und die unzureichende Fähigkeit zur Reduktion von Lipidperoxiden, zur Einleitung einer Ferroptose führen kann.

1 Introduction

1.1 *C. elegans* as a model organism

Caenorhabditis elegans (*C. elegans*) was introduced as a model organism in development and molecular biology by Sydney Brenner (Brenner, 1974). Since then, *C. elegans* turned out to be an important model organism in many fields of biology such as regulating development, cell death, and aging (Brenner, 1974). Advantages of the nematode, as an experimental model for biological studies, are *C. elegans* simplicity, full transparency, easy growth and maintenance in culture, short lifespan, high progeny, suitability for genetic analysis and their small genome size (Wood, 1988). Moreover, the transparent body of the nematode allows using microscopy on a cellular level in the living organism (Altun, 2009). Small body size and fast life cycle, with a reproduction cycle of just three days, makes it an efficient tool for scientific research (Riddle, 1997). Approximately 99.9% of all worms in the population are hermaphrodites that can reproduce by self-fertilization and lay up to 300 eggs (Altun, 2009). Thus, populations with low genetic variability can be grown. Males, which appear with a frequency of just 0.1%, allow the cross between different strains and can increase the genetic variability (Corsi AK, 2005-2018). Adult hermaphrodites reach an average length of 1 mm, while the male is smaller and thinner. Besides the smaller size, the male can be easily identified by the shape of its tail, which has a blunt end, compared to the pointed end of the hermaphrodite (Altun, 2009). *C. elegans* genome was the first multicellular genome which was fully sequenced and, as it shares 35% homology with *Homo sapiens,* the nematode is an optimal tool for studying conserved pathways. One of the additional very important advantages of *C. elegans* is that along with a large number of genetic mutants available, there is the possibility to silence any gene of interest through feeding double-stranded RNAi-expressing bacteria (Fire et al., 1998). This tool allows running large-scale RNAi screens to identify the functions of genes through the correlation between genotype and phenotype. The nematode has become an essential organism for studying aging and age-related diseases (Kaletta and Hengartner, 2006). The life cycle of *C. elegans* is temperature-dependent and takes approximately 20 days at 20°C. Adult hermaphrodites lay around 300 fertilized eggs in 3-4 days. During postembryonic development, *C. elegans* eggs hatch and go through four larval stages L1 to L4. Larval stages L1-L4 can be differentiated by their size as shown in the scheme below (Fig. 1.1). Under

stress conditions such as starvation, a dauer stage is formed , in which the nematode can last up to four months without food (Altun, 2009).

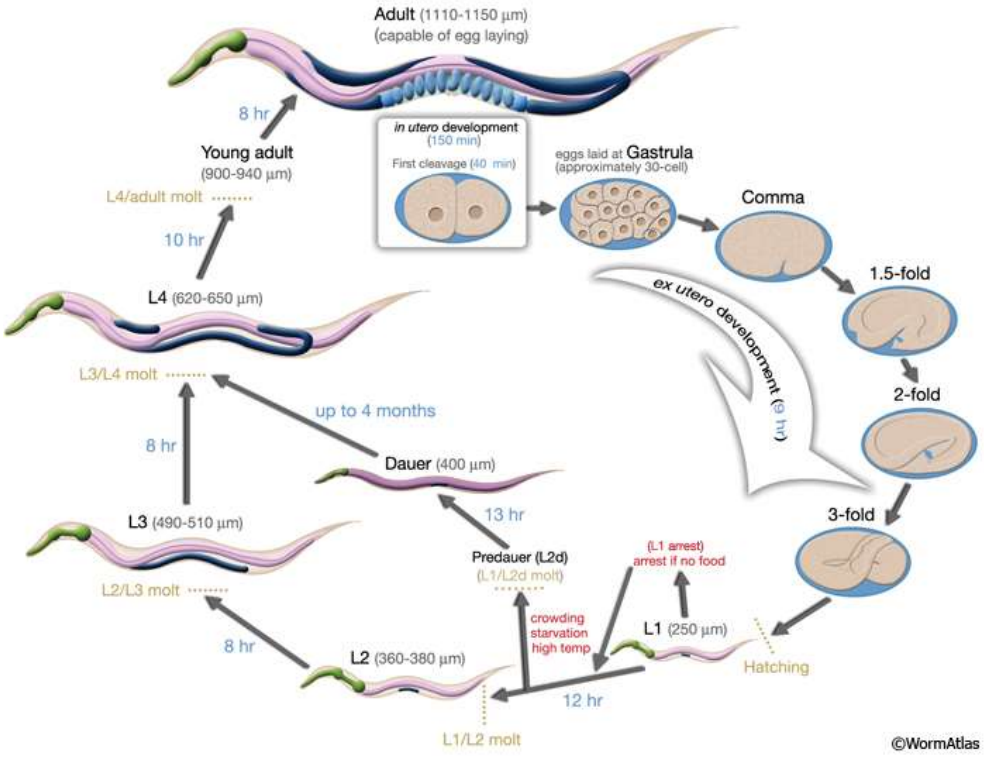

Figure 1.1 *C. elegans* life cycle.
Adult hermaphrodites lay eggs that hatch and go through four larval stages (L1 to L4). When the animals reach the gravid adult stage the life cycle is completed and worms are capable of egg-laying. In conditions like crowding, starvation, or high-temperature, L1 larvae change to dauer form in which worms can survive up to four months. As soon as the food is available the standard development resumes. Figure adapted from WormAtlas (www.wormatlas.org).

1.2 Mitochondria

1.2.1 Mitochondria structure and function

The mitochondria originated two billion years ago, and many features of the organelle reflect its endosymbiotic origin. Mitochondria are found in almost all eukaryotic cells, except for erythrocytes. Mitochondria are organelles defined by a double membrane system that separates four different compartments: the outer membrane (OMM), intermembrane space (IMS), inner membrane (IMM) and the matrix as seen in Figure 1.2 (McBride et al., 2006). Due to the presence of porins that allow free diffusion of molecules with low molecular weight, the OMM is highly permeable to small molecules. The IMM is

folded into cristae and encloses the matrix. The IMM has more protein content and is less permeable than OMM. So, it is acting as a functional barrier for small molecules between the cytosol and matrix. The matrix harbors the mitochondrial DNA (mtDNA) a unique feature of mitochondria (Sherratt, 1991). *C. elegans* mtDNA is similar to human mtDNA, but encodes only 12, not 13 mitochondrial respiratory chain subunits (excluding *ATP8*). Both undergo heteroplasmy, polyploidy, and maternal inheritance. (Dancy et al., 2015). Heteroplasmy means that there are multiple mtDNA variants in a cell. The mtDNA is predominantly maternally inherited and mitochondrial genome is polyploid, since it is present in the cell in multiple copies (Wallace et al., 1988, Carugno et al., 2012).

Most of the approximal 1500 mitochondrial proteins are encoded in the nucleus and needs to be imported into the mitochondria. Mitochondria are essential for the generation of cellular energy, adenosine triphosphate (ATP), through the process of oxidative phosphorylation (OXPHOS). Moreover, mitochondria are involved in various other cellular processes, such as iron-sulfur (Fe-S) cluster biogenesis, lipid biosynthesis, calcium homeostasis, apoptosis and generation of reactive oxygen species (ROS) (Wallace, 2005, Chan, 2006, Nunnari and Suomalainen, 2012).

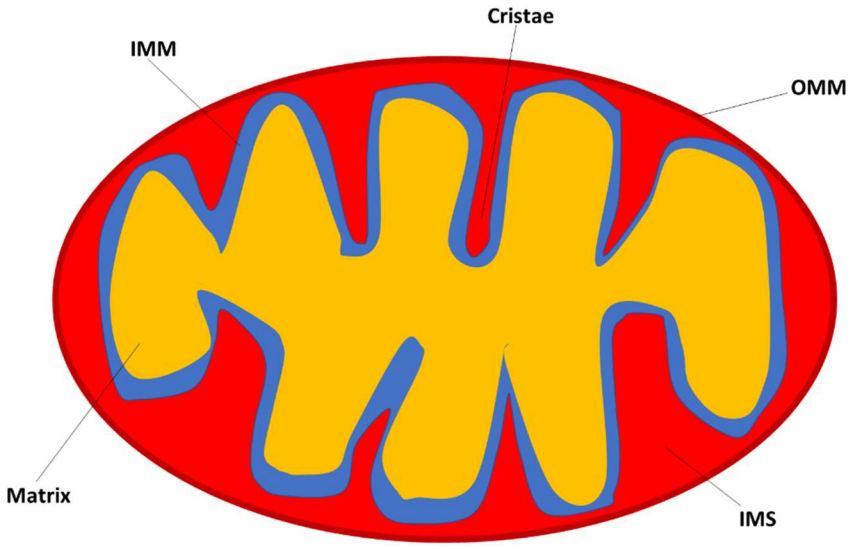

Figure 1.2 Mitochondria inner structure

The scheme represents the key characteristics of a mitochondrial structure. Mitochondria are defined by a double membrane composed of the outer membrane (OMM) and inner membrane (IMM). Between both membranes, there is the intermembrane space (IMS). The IMM forms cristae and encloses the interior of the organelle or matrix, which contains multiple copies of mtDNA.

1.2.2 Mitochondrial dysfunction and diseases

Some of the most common metabolic disorders are caused by mitochondrial dysfunction. The first mitochondrial dysfunction was described in the 1962 by Luft and colleagues. Since then, the knowledge acquired of mitochondria in health, disease, and aging exponentially grew. Mitochondria play an essential role in the regulation of metabolism and energy production and mitochondrial dysfunction generally results from dysfunction of the mitochondrial oxidative phosphorylation (OXPHOS) system. Mutations in both mitochondrial and nuclear genes encoding subunits of mitochondrial respiratory chain complexes, proteins involved in their import and assembly or enzymes that control mitochondrial DNA replication, transcription or translation all lead to the development of mitochondrial diseases (Leonard and Schapira, 2000, Viscomi and Zeviani, 2020). In humans, mitochondrial disorders are a genetically heterogeneous group of diseases, caused by mutations in mitochondrial and nuclear DNA. Depending on where the gene defect is located, mitochondrial diseases can be inherited from an autosomal chromosome, the X-chromosome, or maternally. Besides that, mitochondrial diseases can appear in any organ system as highlighted in Figure 1.3 (Suomalainen and Battersby, 2018).

The mitochondrial genome has an excessive mutation rate. The mutation rate varies between 10- to 17-fold higher than seen in nuclear DNA (Ingman et al., 2000). The main mtDNA modifications are neutral polymorphisms (Ingman et al., 2000). The first pathogenic mtDNA mutations were identified in 1988 (Holt et al., 1988, Wallace et al., 1988). Since then, over 250 pathogenic mtDNA mutations have been characterized in the “Human Mitochondrial Genome Database” (Tuppen et al., 2010).

In mtDNA diseases, the patients are often heteroplasmic, meaning that they have two different mtDNA populations in the same cell or tissue. A heteroplasmic person will develop a disease just if the mutant mtDNA reaches a certain threshold that varies with both tissue and mutation type, usually in the range 50 to 100% (Ylikallio and Suomalainen, 2012). Examples for most common mtDNA diseases are mitochondrial diseases with onset in early infancy like the Leigh syndrome (LS). LS is a progressive neurodegenerative disease, which predominantly affects the brainstem, diencephalon, and basal ganglia and it is caused by failure of oxidative metabolism and a variety of different genetic defects affecting either the mitochondrial or nuclear genome (Tuppen et al., 2010).

There are also reports of classic phenotypes caused by mtDNA deletions, for example Kearns–Sayre syndrome (KSS) and Pearson syndrome (PS). The Pearson syndrome is a rare disorder of infancy characterized by sideroblastic anemia with pancytopaenia and exocrine pancreatic failure. KSS is a disorder caused by single, large-scale deletions (Maceluch and Niedziela, 2006). Patients often develop other neurological complications including cerebellar ataxia, cognitive impairment, and deafness, as well as non-neurological features of cardiomyopathy, complete heart block, short stature, endocrinopathies, and dysphagia (Maceluch and Niedziela, 2006).

There are mitochondrial diseases which are accompanied with oxidative stress. One of the five most common is Friedreich's ataxia and antioxidant enzymes such as superoxide dismutase (SOD) and glutathione transferase (GST) activity are reduced in these patients (Chantrel-Groussard et al., 2001, Tozzi et al., 2002). Other examples include Leber's hereditary optic neuropathy (LHON), Mitochondrial encephalopathy with lactic acidosis and stroke like episodes (MELAS), Myoclonic epilepsy with ragged-red fibers (MERRF), and Lean-Syndrome (LS) (Hayashi and Cortopassi, 2015).

The major cause of oxidative damage is reactive oxygen species (ROS). However, over the last decade, the ROS is being more investigated as a signaling molecule, especially as promoters of mitohormesis, in which low, non-cytotoxic concentrations of ROS support mitochondrial homeostasis. For example, caloric restriction (CR) and physical exercise can induce a mild increase in mitochondrial-derived ROS and have been reported to have a pro-longevity effect through mitohormesis (Ristow and Zarse, 2010). Thus, a mitohormetic response is proposed to be activated by mitochondrial stress in which low concentrations of ROS can act as signals to mitochondrial and antioxidant signaling pathways and this promotes changes in the antioxidant defense system and mitochondrial dynamics resulting in extended lifespan (Palmeira et al., 2019)

There is also a relationship between mitochondria and aging. On one hand, mitochondrial dysfunction contributes to numerous age-related diseases like diabetes, cardiomyopathy, and neurodegeneration, on another hand mild reduction of mitochondrial function prolongs the lifespan from yeast to mammals (Cristina et al., 2009, Durieux et al., 2011). The lifespan extension in *C. elegans* comes along with slower development, and a smaller body and brood size (Palikaras et al., 2015). The impaired mitochondrial function can be achieved either by genetic or pharmaceutical interventions in *C. elegans* (Palikaras et al., 2015).

The mechanisms by which mild mitochondrial dysfunction delays aging are not yet completely understood, but specific quality control mechanisms like the mitochondrial unfolded protein response (UPR^{mt}), autophagy and mitophagy are proposed to play an important role (Cristina et al., 2009, Durieux et al., 2011, Palikaras et al., 2015).

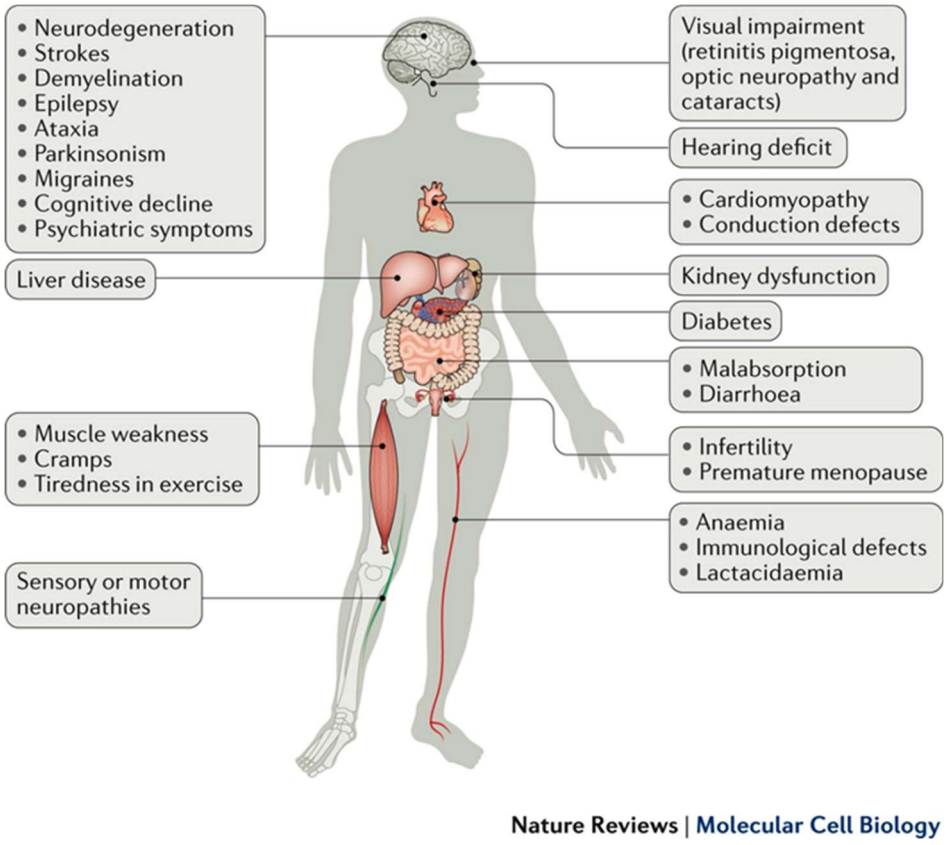

Figure 1.3 Mitochondrial diseases can appear in any organ
Figure adapted from (Suomalainen and Battersby, 2018).

1.2.3 *C. elegans* mitochondrial mutants

Publications of two individual groups drew interest to the role of mitochondrial chain dysfunction in lifespan determination. These two studies have shown that RNA interference (RNAi) of subunits of some mitochondrial respiratory chain complexes were able to extend the lifespan in *C. elegans* (Dillin et al., 2002, Lee et al., 2003). Later, similar findings were reported that a minor mitochondrial dysfunction of the mitochondrial electron transport chain (ETC) display a beneficial effect on lifespan in many organisms such as *Drosophila melanogaster* (Copeland et al., 2009) and *Surf1*$^{-/-}$ mouse, which was the first mouse model with increased lifespan (Lapointe and Hekimi, 2008, Agostino et al., 2003).

There are many genetic mutants and RNAi defined models of *C. elegans* with a deficiency in one of the electron transport chain components (Butler et al., 2010). Collectively they are called mitochondrial mutants ("mit-mutants"). In *C. elegans,* longevity induced by mitochondria dysfunction can be divided into three different groups, according to the way the ETC is affected.

The first group consists of mitochondrial dysfunction created via RNAi which inactivates genes either directly or indirectly involved in the functionality of the electron transport chain. The second group are "mit-mutants" with genetic mutations in electron transport chain regulatory subunits and the third group represents mitochondrial dysfunction induced by chemicals which either partially or specifically inhibit electron transport chain activity. Oftentimes, the phenotypes studied in *C. elegans* "mit-mutants" reflect genetic mitochondrial disorders in human patients (Ventura and Rea, 2007, Ventura et al., 2006, Dancy et al., 2015, Dancy et al., 2014). A study by Hartman et al. in 2001 showed that not all "mit-mutants" have increased, but instead also show decreased lifespan (Hartman et al., 2001). For example, *gas-1* encodes a 49 kDa subunit of complex I of the electron transport chain and *gas-(fc21)* mutant is short-lived, has less progeny, shows delayed development and is extremely sensitive to oxidative stress (Hartman et al., 2001, Kayser et al., 1999). One more example is *nuo-6* which encodes the *C. elegans* orthologous of mammalian NUDFB4/B15 subunit of complex I (Yang and Hekimi, 2010). These animals exhibit an increased lifespan and an accumulation of mitochondrial ROS (Yang and Hekimi, 2010). These two models show that mutations in the same complex can cause two different phenotypes. Another example is mutation in a complex II gene, *mev-1* which encodes an integral membrane protein the *C. elegans* ortholog of the succinate dehydrogenase cytochrome b560 subunit (SDHC in mammals). These animals exhibit shorter lifespan, decreased fecundity, increased oxidative damage and hypersensitivity to oxidative stress (Ishii et al., 1998, Ishii et al., 2002, Yanase et al., 2002). In turn, the knockdown of complex IV subunits has been shown to have a beneficial effect on the lifespan (Lee et al., 2003, Suthammarak et al., 2010). The RNAi depletion of *cco-1*, an orthologue of cytochrome c oxidase 4 (COX4), showed an increased lifespan (Durieux et al., 2011).

In this study we worked with the double mutant *isp-1(qm150);ctb-1(qm189)* (Fig. 1.4). The mutation in iron-sulfur protein *isp-1(qm150)* of mitochondrial complex III was first described in 2001 (Feng et al., 2001). The *isp-1(qm150)* mutant is characterized by increased

resistance to ROS, increased lifespan and decreased mitochondrial respiration (Feng et al., 2001). The *isp-1(qm150)* single mutant has a dramatically defective complex III function. Besides, the I:III:IV super-complex is severely disturbed and complex I activity, as well as complex I-III activity, is also dramatically impaired (Suthammarak et al., 2010). Another complex III mutation affecting cytochrome b, *ctb-1(qm189)*, partly suppresses the phenotypes observed in *isp-1(qm150)* without affecting the longevity phenotype (Feng et al., 2001).

The *ctb-1(qm189)* mutant shows decreased complex III and complex I-III activity, although not to the same extent as *isp-1(qm150)* mutant, while the I:III:IV super-complex is not disrupted. But this additional mutation in the cytochrome b, improves complex I and III activity and is stabilizing super-complex assembly, which altogether partially suppresses the slow development and reproductive features, while the prolonged lifespan is not affected (Suthammarak et al., 2010, Dancy et al., 2015, Feng et al., 2001).

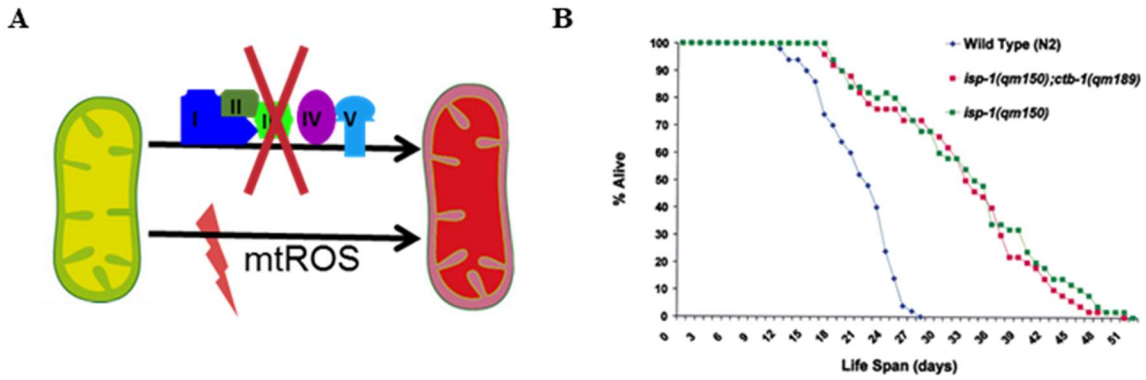

Figure 1.4 The life span of the wild-type, the *isp-1 (qm150)* mutant and *isp-1(qm150);ctb-1(qm189)* double mutant
A) Scheme of electron transport chain, consisting of complex I-V. Deficiency in complex II leads to increased mtROS. B) Life span curve of *isp-1(qm150)* single and *isp-1(qm150);ctb-1(qm189)* double mutant.
Figure adapted from (Feng et al., 2001).

1.3 Fatty acids

1.3.1 Fatty acids general features

Fatty acids are important for membrane biogenesis and energy storage. They serve as signaling molecules and modulate growth and development. They are essential

components of all living organisms and the fatty acid metabolism mechanisms are conserved across species (Towle et al., 1997, Arrese and Soulages, 2010, Letunic et al., 2008). For humans, the most important dietary source of fatty acids are vegetable oils, milk products, meat products, grains, and fatty fish or fish oils (Watts, 2016). The most common saturated fatty acid in animals, plants, and microorganisms is palmitic acid (16:0). Stearic acid (18:0) is a minor fatty acid in animals, fungi, and a major component in plants. Fatty acids can be saturated and unsaturated. Saturated fatty acids do not have any double bonds between carbon molecules. Unsaturated fatty acids can be monounsaturated, meaning they contain one C-C double bond or polyunsaturated then they contain two or more C-C double bonds (Watts, 2009, Srinivasan, 2015). C-C double bonds in *C. elegans* are configurated in so-called "cis" orientation and are methylene intermitted (Watts, 2016, Watts and Ristow, 2017, Wallis et al., 2002). Methylene intermitted stands for C-C double bonds that are spaced along the carbon chain at stated intervals of three carbons.

As in all eukaryotes, fatty acids in *C. elegans* are composed exclusively of even chains of saturated and unsaturated carbon-carbon bonds. The major fatty acids are products of 16-, 18- and 20-carbon chains (Fig.1.5). Fatty acids gained from the bacterial diet are converted to triglycerides and turn into the body fat in *C. elegans* (Watts, 2009, Watts and Browse, 2002). *C. elegans* stores fat predominantly as triglycerides (Fig. 1.5). Triglycerides compose of three fatty acid chains anchored by glycerol backbone (Srinivasan, 2015, Watts and Ristow, 2017).

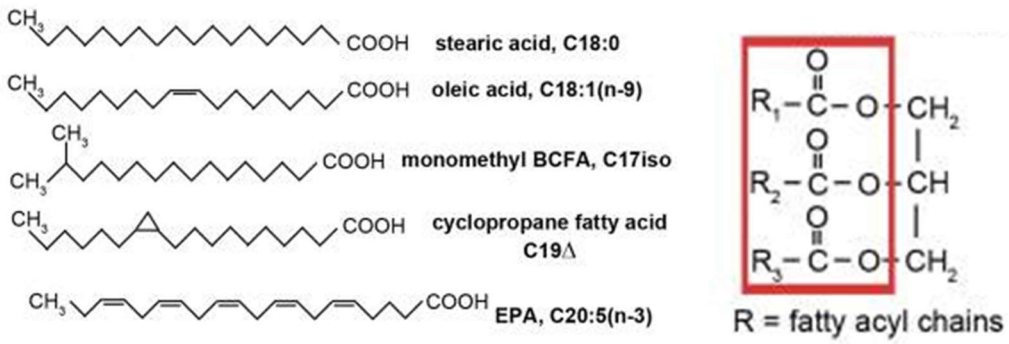

Figure 1.5 Abundant *C. elegans* fatty acids and triglyceride molecule
A) Structures of abundant *C. elegans* fatty acids. B) Structure of a triglyceride with the fatty acyl chains. Figure adapted from (Watts and Ristow, 2017).

1.4 Lipid metabolism

1.4.1 *C. elegans* lipid metabolism

In *C. elegans* the intestine is the main organ where food absorption, incorporation of nutrients into metabolic pathways, fat storage and utilization take place (Srinivasan, 2015). While *C. elegans* does not have adipocytes dedicated to fat storage like in mammals, they do store their fats as triglycerides (TAGs) in lipid droplets and yolk (Watts, 2009, Srinivasan, 2015). *C. elegans* synthesizes fatty acids *de novo* from acetyl-CoA (Coenzyme A), but also acquires them from its bacterial diet (Watts, 2009). Triglycerides are the main components of lipid droplets. They are localized in the intestine, epidermis, and germline of *C. elegans*. The processes of fatty acid synthesis, elongation, desaturation, as well as mitochondrial and peroxisomal ß-oxidation of fatty acids are highly conserved in *C. elegans* (Palgunow et al., 2012*)*.

As depicted in Figure 1.6, fatty acid *de novo* synthesis is driven by levels of acetyl-CoA. The needed carbon can originate from the glycolysis or ß-oxidation. The limiting step in fatty acid *de novo* synthesis is implemented by acetyl-CoA carboxylase (ACC). Acetyl-CoA carboxylase uses CO_2 to carboxylate acetyl-CoA to form malonyl-CoA. Malonyl-CoA is used for fatty acid *de novo* synthesis by fatty acid synthase (FAS) and the elongation of fatty acids (Witkowski et al., 2011). Malonyl-CoA levels control mitochondrial fatty acid β-oxidation by regulating carnitine palmitoyl transferase (CPT) activity. Fatty acid storage happens incrementally by conversion of fatty acyl-CoAs into phosphatidic acid, diacylglycerol and in the end triacylglycerols (Fig. 1.6). The ß-oxidation of fatty acids can fuel ATP synthesis (Ashrafi, 2007, Watts, 2009, Watts and Ristow, 2017).

C. elegans reproductive larvae, which are feeding and growing, consume nutrients, from which they utilize predominantly lipids and proteins and to some extent sugars (Erkut et al., 2016). *C. elegans* larvae metabolize these nutrients through glycolysis and the TCA cycle to generate energy. Carbohydrates themselves are broken down into acetyl-CoA and can be ultimately stored as fats (Ashrafi, 2007, Watts, 2009, Watts and Ristow, 2017). Glycolysis, a relevant energy providing process is highly conserved and well-characterized in *C. elegans* (Yilmaz and Walhout, 2016, Gebauer et al., 2016). It promotes the survival of nematodes for example under hypoxic states (LaMacchia et al., 2015).

In the non-growing state, the dauer larvae, switches into a gluconeogenic mode in which metabolism is shifted toward the production of sugars from non-carbohydrate sources. This mode depends on the full activity of the glyoxylate shunt (GS), which supports the production of trehalose, sugar consisting of two molecules of glucose, from acetate (Fig. 1.6) (Erkut et al., 2016, Watts, 2009, Watts and Ristow, 2017). While sucrose, lactose, and maltose are the most significant disaccharides in mammalian biology, trehalose is the only disaccharide that has been characterized in nematodes (Watts and Ristow, 2017)

Glucose is synthesized by gluconeogenic enzymes. The genome of *C. elegans* encodes enzymes for the glyoxylate pathway. Acetyl-CoA can be transformed into oxaloacetate and this passes into the gluconeogenesis pathway. Contrary to mammals, nematodes oxaloacetate can be used as a substrate for gluconeogenesis to produce carbohydrates and amino acids (Ashrafi, 2007, Watts, 2009, Watts and Ristow, 2017).

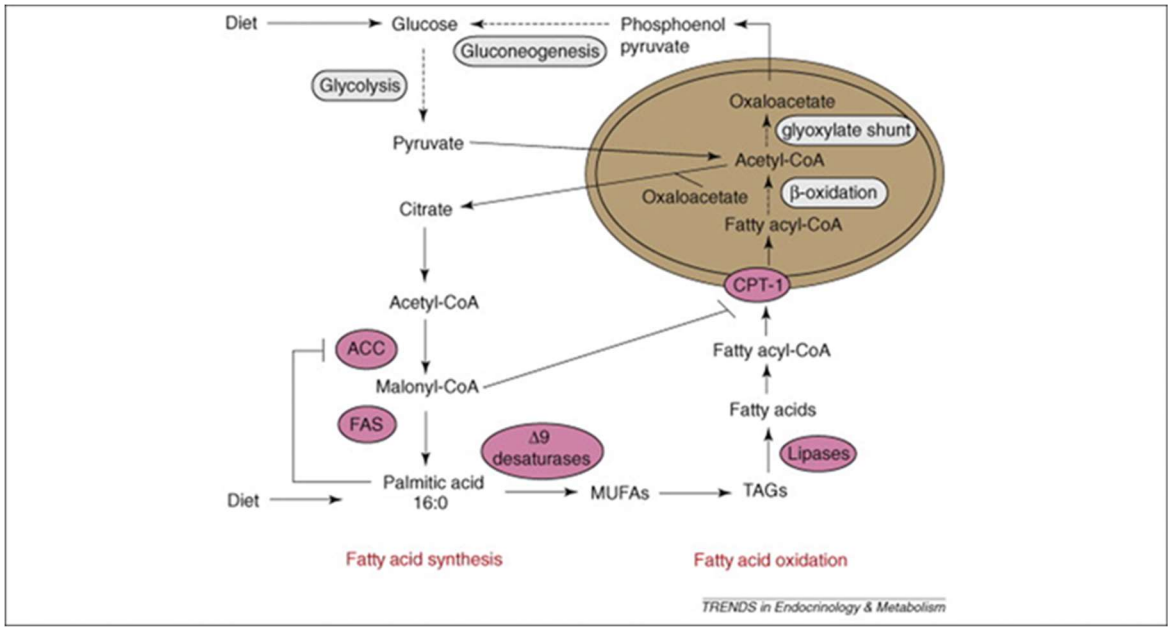

Figure 1.6 Lipid metabolism in *C. elegans*

Fatty acid synthesis requires acetyl-CoA from citrate that can be derived from glucose or fatty acids. Acetyl-CoA is carboxylated by ACC to yield malonyl-CoA. Malonyl-CoA functions as the fatty acid chain extender by FAS and regulates β-oxidation, through inhibition of CPT-1. Figure adapted from (Watts, 2009).

1.4.2 Lipid droplets general features

Lipid droplets (LDs) are organelles present in many different organisms including mammals, *Drosophila*, yeast, and *C. elegans*. LDs are sites where cellular fat storage and mobilization are controlled (Mak, 2012). The first observation of triglyceride (TAG) storage in cells was reported in a study of Altmann and Wilson in the 1890s (Farese and Walther, 2009, Walther et al., 2017), while in 1960, the biochemical reactions of the enzymatic synthesis of triglycerides were discovered by Kennedy and coworkers (Weiss et al., 1960). In mammals, fat is primarily stored in adipose tissue. Mammals have two types of adipose tissue, white and brown, where white adipose tissue functions as the main depot for fuel storage mammals (Ashrafi, 2007). Lipid droplets store energy in the form of TAGs and release free fatty acids by TAG degradation. Moreover, lipid droplets interact with other subcellular organelles such as endoplasmic reticulum, mitochondria, lysosome, endosome, and autophagosome (Barbosa et al., 2015, Welte, 2015, Yu and Li, 2017, Mak, 2012, Olzmann and Carvalho, 2019). The proliferation of white adipocytes and massive TAG storage in enlarged lipid droplets during adipocyte differentiation correlate with obesity in mammals (Faust et al., 1978, Rodeheffer et al., 2008).

As already mentioned, the lipid storage capacity of lipid droplets is determined by its volume and controlled by the balance between triglyceride synthesis and degradation. This regulation is important to enable normal biological functions. Deregulation of these processes, may lead to the development of metabolic diseases, such as obesity, diabetes, fatty liver, cardiovascular disease, neurogenerative disease and cancer (Welte, 2015, Walther et al., 2017). Lipid droplets have a unique structure and are composed of a neutral lipid core with triglycerides and sterol esters encapsulated by a monolayer of phospholipids and numerous related proteins as represented in Figure 1.7 (Yu and Li, 2017, Olzmann and Carvalho, 2019). Phosphatidylcholine (PC) represents the main phospholipids next to phosphatidylethanolamine (PE) and phosphatidylinositol (PI). PLIN1 is the first described lipid droplet protein, initially identified in mammals, where it plays a key role in regulating fasting-induced lipolysis (Yu and Li, 2017).

Thenceforth, several other types of LD- associated proteins were identified, such as enzymes involved in lipid droplet metabolism, neutral lipid synthesis and lipolysis (Yu and Li, 2017, Walther et al., 2017). In eukaryotes, lipid droplets are produced *de novo* from the endoplasmic reticulum, where most of the enzymes for triglycerides synthesis are localized.

Nascent lipid droplets bud out from the endoplasmic reticulum membrane and form cytosolic lipid droplets (Gao and Goodman, 2015, Barbosa et al., 2015).

Also, a majority of *C. elegans* intestinal fat is stored in lipid droplets. Lipid droplets comprise a much-advanced amount of TAGs compared to phospholipids. In worms, well-conserved proteins, acyl-CoA synthase-22 (ACS-22) and diacylglycerol acyltransferase 2 (DGAT-2), which are required for the generation of lipid droplets, form a complex at the transition point, where LDs bud off from the endoplasmic reticulum (Fig. 1.7). *C. elegans* lipid droplets are small, usually in the size range of 1–2.0 µm (Mak, 2012, Srinivasan, 2015, Olzmann and Carvalho, 2019, Vrablik et al., 2015, Watts and Ristow, 2017).

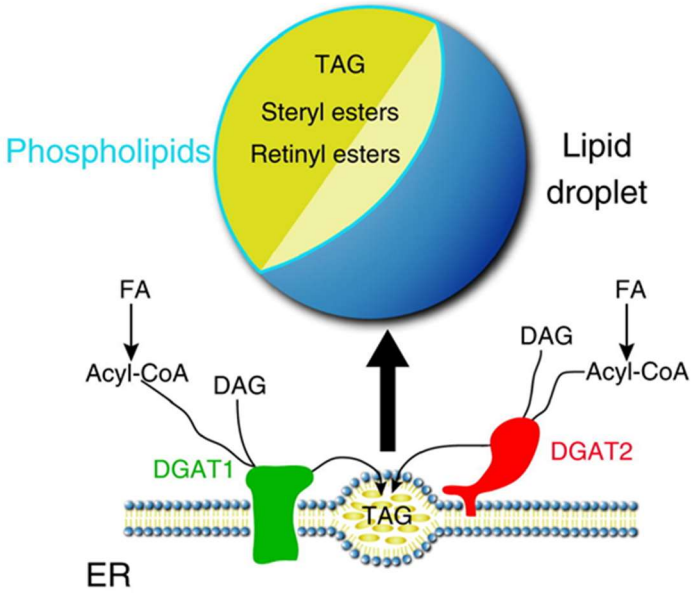

Figure 1.7 Lipid droplets

Lipid droplets consist of a core of neutral lipids like triglycerides, steryl esters, and retinyl esters, which is enclosed by a monolayer phospholipids and proteins. Lipid droplets bud off from the endoplasmic reticulum and the two enzymes DGAT1 and DGAT2 synthesize diacylglycerol. Triglycerides initially gather between the two membranes of the endoplasmic reticulum (ER). Figure adapted from (Welte, 2015).

1.4.3 Peroxisomes structure and function

Peroxisomes were first identified as organelles in mammalian cells in 1966 by de Duve (De Duve and Baudhuin, 1966). They are single membrane encircled organelles with a crystalline core of oxidative enzymes (Lodhi and Semenkovich, 2014). Peroxisomes alternate in their structure and stand from 0.1-0.5 µM in diameter (Lodhi and Semenkovich,

2014). Peroxisomes play an essential role in metabolic functions in mammalian cells, such as removal of reactive oxygen species, synthesis of bile acids, amino acid degradation, ß-oxidation of very-long-chain fatty acids, and α-oxidation of branched-chain fatty acids as summarized in Figure 1.8 (Lodhi and Semenkovich, 2014, Wanders et al., 2015).

The two major categories of peroxisomal functions are lipid metabolism and ROS metabolism. Both categories are interconnected and need cooperation with other organelles, such as mitochondria, endoplasmic reticulum (ER), lipid droplets and lysosomes (Lodhi and Semenkovich, 2014). The peroxisomal respiration produces H_2O_2 and this makes up to 35% of total H_2O_2 in mammalian tissues (Boveris et al., 1972). To deal with the harmful effect of ROS, peroxisomes have abundant amounts of a dense crystalline core of antioxidant enzymes, like catalases (Fig. 1.8). Catalases, found in most cell types, reduce H_2O_2 to water (Cipolla and Lodhi, 2017, Lodhi and Semenkovich, 2014). Besides H_2O_2, peroxisomes also produce superoxide and nitric oxide radicals (Fransen et al., 2017, Lismont et al., 2015, Antonenkov et al., 2010).

The importance of peroxisomes in human metabolism and development is seen in patients with the rare genetic human disease called the cerebrohepatorenal syndrome (CHRS), also called the Zellweger syndrome (ZS), which is a fatal autosomal recessive disorder (Brown et al., 1982). In this patients, peroxisomal biogenesis is completely or partially lost. Meaning patients lack multiple proteins required for the formation, proliferation, and maintenance of peroxisomes (Wanders et al., 2015, Brown et al., 1982, Wanders, 2004). Studies showed that peroxisomes also play a role in brain development and function since patients with defective peroxisomes develop neurogenerative diseases (Berger et al., 2016). Likewise, peroxisomal dysfunction has been related to many age-related diseases such as Type-II Diabetes, Alzheimer's and Parkinson's disease (Fransen et al., 2013).

Peroxisomal proteins contain one of two peroxisomal targeting signals, PTS1 or PTS2, which are recognized by specific receptors that allow them to enter the peroxisomal membrane (Wanders, 2004). Peroxisomal proteins are encoded by nuclear genes, and they are synthesized in the cytosol, and go through post-translational import (Deori et al., 2018). The PTS1 targeting signal is recognized in the cytosol by the receptor PEX5 (Apanasets et al., 2014). This receptor-protein complex is localized at the peroxisomal membrane and when docking at the peroxisomal membrane, PEX5 releases proteins into the peroxisome matrix (Apanasets et al., 2014). Afterwards, PEX5 is monoubiquitinated and is recycled back

to the cytosol (Apanasets et al., 2014, Deori et al., 2018). Thus, PEX5 turnover is crucial for an immaculate matrix protein import (Apanasets et al., 2014, Deori et al., 2018, Lismont et al., 2015, Lodhi and Semenkovich, 2014, Ma et al., 2013).

To accomplish their role in metabolism, peroxisomes require interactions with other subcellular organelles. For example, in adipocytes, peroxisomes are mostly small and localize close to lipid droplets (Lodhi and Semenkovich, 2014, Wanders et al., 2015). Already in 1982, a study by Moser and co-workers concluded that peroxisomes play a crucial role in the fatty acid ß-oxidation (Wanders, 2004, Brown et al., 1982). In humans, most of the β-oxidation occurs in mitochondria, but peroxisomes are essential for β-oxidation of very-long-chain fatty acids (VLCFA) and α-oxidation of branched-chain fatty acids (Yokota et al., 2002, Van Veldhoven and Baes, 2013, Olzmann and Carvalho, 2019).

Peroxisomes are exclusive sites of yeasts β-oxidation (Lodhi and Semenkovich, 2014). Peroxisomes in nematodes were first described by Aueron und Rothstein 1974. In gravid adult *C. elegans*, peroxisomes are mainly found in the gut and the pharyngeal gland (Van Veldhoven and Baes, 2013, Yokota et al., 2002). PRX-5 is a *C. elegans* ortholog of the previously described human PEX5, which takes over similar functions (Wang et al., 2013). Thieringer and coworkers showed that knockdown of *prx-5* leads to an early larval arrest at the L1 stage. Worms missing peroxisomes display a developmental blockade similarly to what is known from phenotypes of starvation-arrested nematodes (Thieringer et al., 2003).

Peroxisomes and mitochondria are intimately linked, and the interplay between the two organelles is important (Narayan et al., 2016). Mitochondria and peroxisomes both generate ROS. When the peroxisomal catalase has a defect, mitochondrial redox balance can be interrupted (Hwang et al., 2012, Ivashchenko et al., 2011). Peroxisomes are conserved across species and *C. elegans* constitutes to be a promising model organism to study peroxisomes.

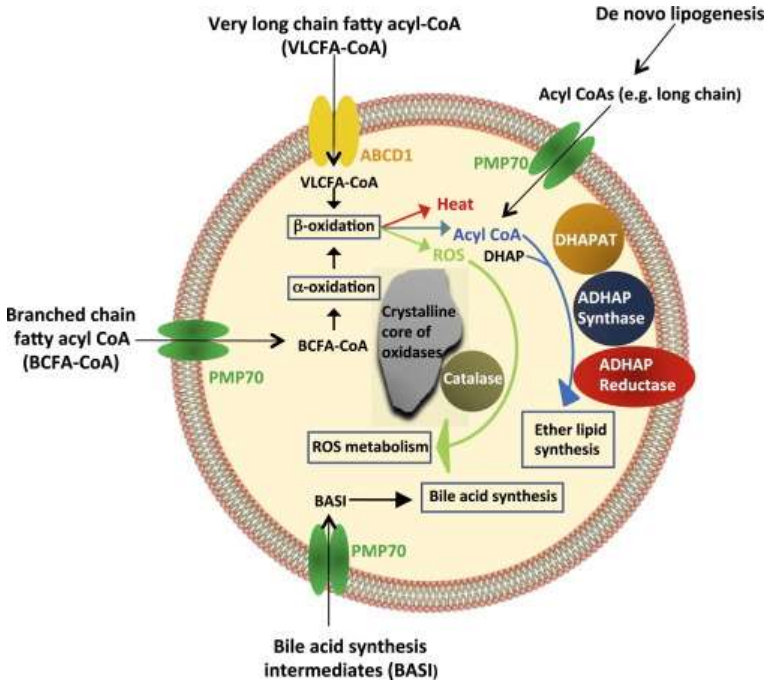

Figure 1.8 Peroxisome Structure and Function

Figure adapted from (Lodhi and Semenkovich, 2014).

1.4.4 Comparison of mitochondrial versus peroxisomal ß-oxidation

Fatty acid ß-oxidation (FAO) is a step-by-step mechanism by which fatty acids are catabolized in the cell in four-subsequent reactions (Fig. 1.9). Every ß-oxidation cycle is composed of the desaturation of fatty acyl-CoA esters between carbon 2 (C2) and carbon 3 (C3) resulting in two products: acyl-CoA which is two carbons shorter, and acetyl-CoA or propionyl. The next reaction involves the hydration of the formed 2-enoyl-CoA. The third reaction consists of the dehydrogenation of 3-hydroxylacyl-CoA, while the last and fourth step includes the thiolytic cleavage of 3-oxoacyl-CoA (Watts and Ristow, 2017).

Whereas reactions two to four are similar in both mitochondria and peroxisomes, the first step in peroxisomal FAO is catalyzed by FAD-dependent acyl-CoA oxidase (ACOX) (Fig 1.9) (Lodhi and Semenkovich, 2014, Fransen et al., 2017). Electrons from reduced FAD ($FADH_2$) are passed directly to molecular oxygen (O_2), thus generating heat and H_2O_2. In contrast, the first step in mitochondria is catalyzed by FAD-dependent acyl-CoA dehydrogenase (ACAD) and electrons from $FADH_2$ are transported to the respiratory chain through the electron transfer flavoprotein (ETF) and the ETF dehydrogenase (ETFDH) (Wanders, 2004, Fransen et al., 2017, Van Veldhoven and Baes, 2013).

Mitochondria and peroxisomes have different groups of enzymes for each step in the ß-oxidation (Wanders, 2004, Wanders et al., 2015). Hence, both organelles have altered substrate specificities. In mammals, the peroxisomal ß-oxidation predominantly breaks down very-long-chain fatty acids. Very-long-chain fatty acids (VLCF) are fatty acids which are > 22 carbons in length. Mitochondrial ß-oxidation is responsible mainly for long, medium and short-chain fatty acids (Watts and Ristow, 2017, Fransen et al., 2017).

Moreover, mitochondrial and peroxisomal ß-oxidation differ in their end products. Mitochondria oxidize their fatty acids to CO_2 and H_2O by the entrance of acetyl-CoA into the tricarboxylic acid cycle (TCA) and the reoxidation of NADH and $FADH_2$ through the respiratory chain and generate 2 ATP molecules. It has been proposed that products of peroxisomal ß-oxidation are shortened fatty acids that are then sent to mitochondria for full oxidation (Fransen et al., 2017, Watts, 2009, Watts and Ristow, 2017, Wanders, 2004, Wanders et al., 2015). Mitochondrial and peroxisomal β-oxidation systems also vary in terms of fatty acyl-CoA import from the cytosol. The uptake of fatty acyl-CoAs throughout the mitochondrial membrane needs a carnitine switch system. This carnitine switch system comprises of two carnitine palmitoyl transferases (CPT1 and CPT2) and the transporter protein carnitine-acylcarnitine translocase (CACT). CPT1 is located in the outer mitochondrial membrane, where it replaces CoA for carnitine in the fatty acid, resulting in fatty acid carnitine, which is moved across the inner mitochondrial membrane by CACT. Then inside the matrix, fatty acid carnitine is converted back to fatty acyl-CoA by CPT2. Importantly, carnitine does not seem to be essential for fatty acyl-CoA import into peroxisomes (Lodhi and Semenkovich, 2014).

However, peroxisomes need to reoxidize NADH to NAD^+ to continue the ß-oxidation, a process that can only be achieved in mitochondria (Fransen et al., 2017). Although the mechanism is not fully understood, it has been proposed to include specific NAD(H)-redox shuttle, a carrier system in the peroxisomal membrane that catalyzes the switch between NADH in the peroxisome and NAD^+ in the cytosol (Poirier et al., 2006). Indeed, a peroxisomal NAD(H)-redox shuttle has been reported in yeast (Baumgart et al., 1996). This NAD(H)-redox shuttle involves a malate-oxaloacetate based redox shuttle for reoxidation of peroxisomal NADH (Baumgart et al., 1996). In higher eukaryotes, no peroxisomal NAD(H)-redox shuttle has been identified, although some evidence, e.g. the presence of a lactate/pyruvate-based redox shuttle, suggest its existence (Baumgart et al., 1996).

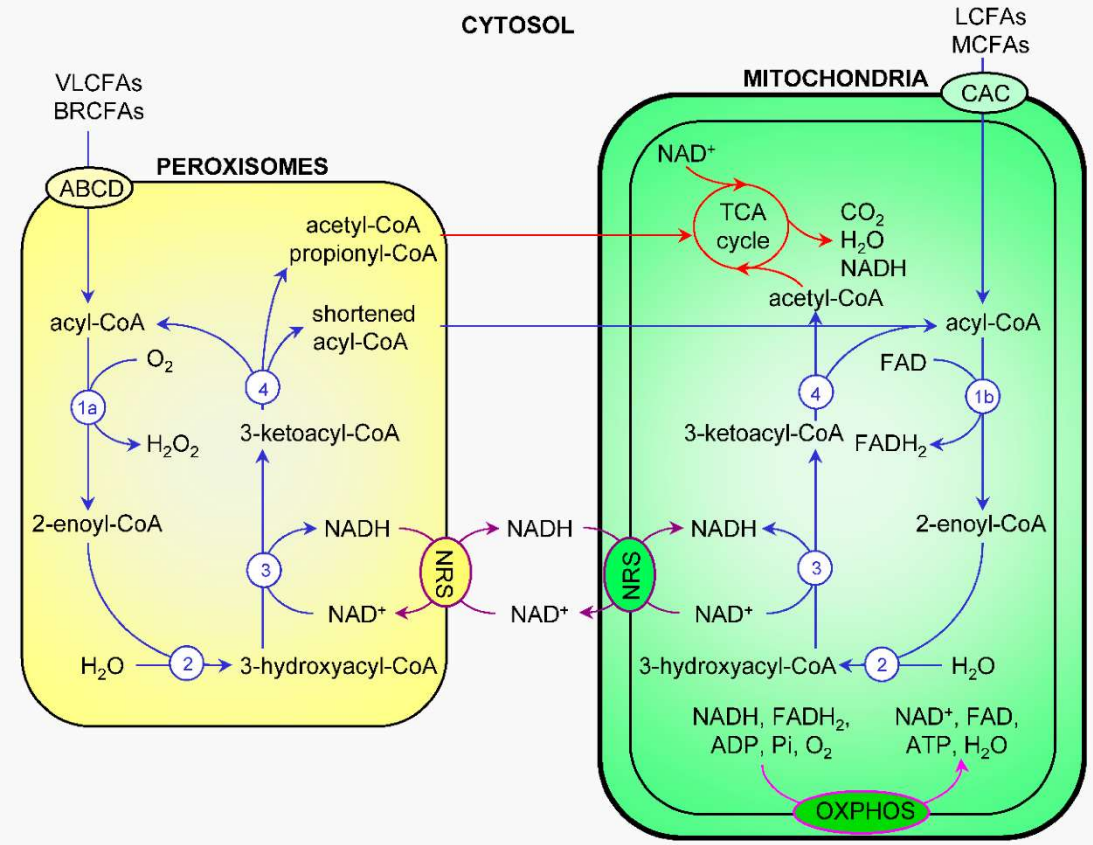

Figure 1.9 Interplay of mitochondrial and peroxisomal ß-oxidation
Figure adapted from (Fransen et al., 2017).

1.4.5 Lipid peroxidation

Lipid peroxidation describes a process, where free radicals attack lipids containing carbon-carbon double bonds, preferentially polyunsaturated fatty acids (Ayala et al., 2014, Conrad et al., 2018). These include linoleic, arachidonic, and docosahexaenoic acids. During the process of lipid peroxidation free radicals appropriate electrons from phospholipids, leading to their degradation (Gaschler and Stockwell, 2017).

Lipid peroxidation reaction consists of three key steps: 1. initiation, 2. propagation and 3. termination. It results in the formation of lipid peroxides or lipid oxidation products (LOPs) (Gaschler and Stockwell, 2017, Conrad et al., 2018). Firstly, initiation is the step where fatty acid radicals are produced. Initiators are H_2O_2 which gets converted into H_2O and lipid radicals. In cells, this is done using iron and it is called Fenton-reaction. Secondly, in the propagation step, the fatty acid radical reacts with molecular oxygen and produces a peroxyl-

fatty acid radical. This peroxyl-radical reacts with other lipids, starting a constant free radical lipid peroxidation chain reaction, so-called autooxidation (Porter, 1986, Gaschler and Stockwell, 2017). Both the hydroxyl and peroxyl radicals, can take over the hydrogen from the bis-allylic methylene of a membrane polyunsaturated fatty acid (PUFA), producing a resonance-stabilized, carbon-centered radical (Gaschler and Stockwell, 2017). This can react with molecular oxygen to form a lipid-peroxyl radical $ROO^{\cdot}$. This lipid-peroxyl radical can take over another hydrogen from different bis-allylic methylene, creating a lipid peroxide (ROOH) and another carbon-centered radical that reacts with oxygen (Gaschler and Stockwell, 2017). If the concentration of radicals is high enough for two radicals to react with each other, they will develop a new bond between. Finally, molecules that can donate electrons to radical compounds without themselves turning into a radical can stop radical propagation (Gaschler and Stockwell, 2017, Conrad et al., 2018, Su et al., 2019).

The primary function of antioxidants is a defense against uncontrolled lipid peroxidation and other oxidative damage. Aldehydes are the major class of lipid peroxide degradation products, with 4-Hydroxynonenal (4-HNE) and malondialdehyde (MDA) being the most well described (Gaschler and Stockwell, 2017, Yang et al., 2016). Peroxidation of membrane lipids is known to extensively alter the physical properties of lipid bilayers. In particular, the peroxidation alters lipid-lipid interactions, ion gradients, membrane fluidity, and membrane permeability (Catala and Diaz, 2016, Gaschler and Stockwell, 2017, Yang et al., 2016).

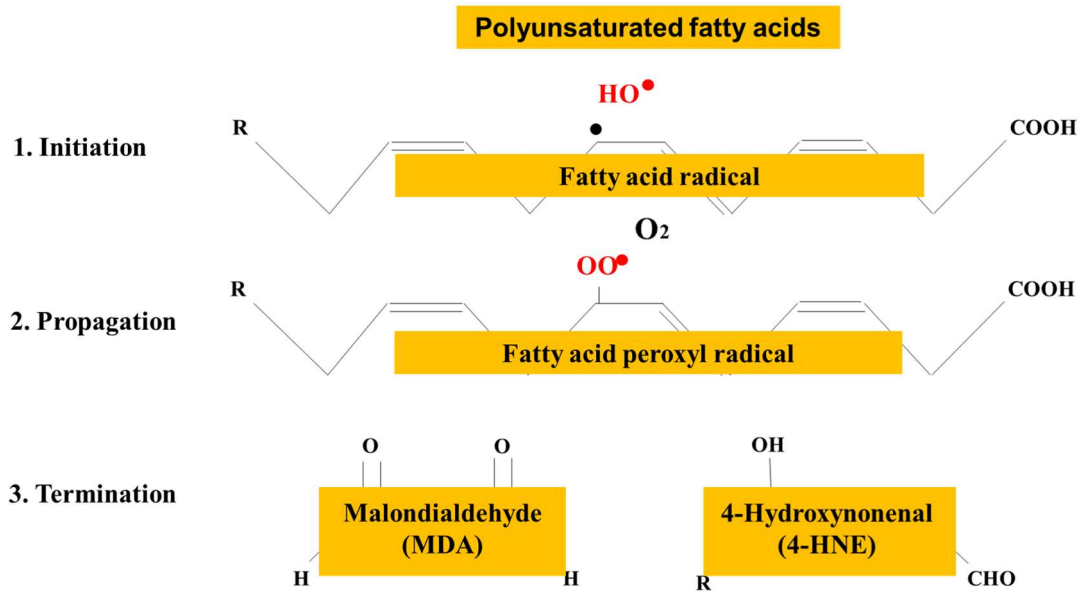

Figure 1.10 Steps of lipid peroxidation and end products
Figure adapted from (Gaschler and Stockwell, 2017).

1.4.6 Ferroptosis

Ferroptosis is an iron-dependent non-apoptotic mode of cell death characterized by the accumulation of lipid peroxides (Fig. 1.11) (Gao et al., 2016, Gao et al., 2019, Su et al., 2019, Li et al., 2020). Signs of ferroptosis differ from typical cell death, since the main characteristics of typical necrosis, like swelling of the cytoplasm and organelles and crack of the cell membrane are not present. Similarly, no characteristics of conventional apoptosis, such as cell shrinkage, chromatin condensation, the formation of apoptotic bodies and a breakup of the cytoskeleton are shown either (Gao et al., 2016, Yang and Stockwell, 2016, Li et al., 2020).

Ferroptosis also does not have the formation of autophagic vacuoles. Ferroptosis is caused by the loss of cellular redox homeostasis. Further, it appears that lipid ROS or peroxides instead of cytosolic ROS play more important roles in ferroptosis (Fig. 1.11) (Gao et al., 2019). Inactivation of glutathione peroxidase 4 (GPX4), an enzyme required for the clearance of lipid ROS, can induce ferroptosis even when cellular cysteine and intracellular glutathione (GSH) contents are normal. Importantly, it has been recently demonstrated that the intracellular metabolic pathway glutaminolysis also plays a crucial role in ferroptosis by promoting cellular ROS generation (Gao et al., 2016, Gao et al., 2019). It has been shown that during ferroptosis, mitochondria shrinks and shows increased membrane density and

reduction or relieving of mitochondrial cristae (Gao et al., 2016, Kagan et al., 2017, Li et al., 2020). From the biochemical side, if the GSH is depleted and there is a decreased activity of glutathione peroxidase 4 (GPX4), lipid peroxides cannot be metabolized by the GPX4-catalyzed reduction reaction, and Fe^{2+} oxidizes lipids in a Fenton-like manner, resulting in a large amounts of ROS, which further promotes ferroptosis (Yang et al., 2016, Yang and Stockwell, 2016, Perez et al., 2019). Ferroptosis mainly involves genetic changes in iron homeostasis and lipid peroxidation metabolism, but the specific regulatory mechanisms need to be further studied.

As mentioned before, polyunsaturated fatty acids (PUFAs) are sensitive to lipid peroxidation and are one of the essential elements for ferroptosis as shown in Figure 1.10 in the previous section (Yang and Stockwell, 2016, Li et al., 2020). Free PUFAs need to be esterified into membrane phospholipids and oxidized to convey the ferroptosis signal (Li et al., 2020). Vitamin E and coenzyme Q_{10} can interact with peroxyl radicals to produce peroxide. These oxidized lipids can be detoxified by glutathione and glutathione peroxidase 4 (GPX4) and additional elements of the cellular antioxidant defense system (Conrad et al., 2018).

In *C. elegans* ferroptosis is rarely described, but studies on numerous other organisms and conserved pathways present also in worms suggest a likely role.

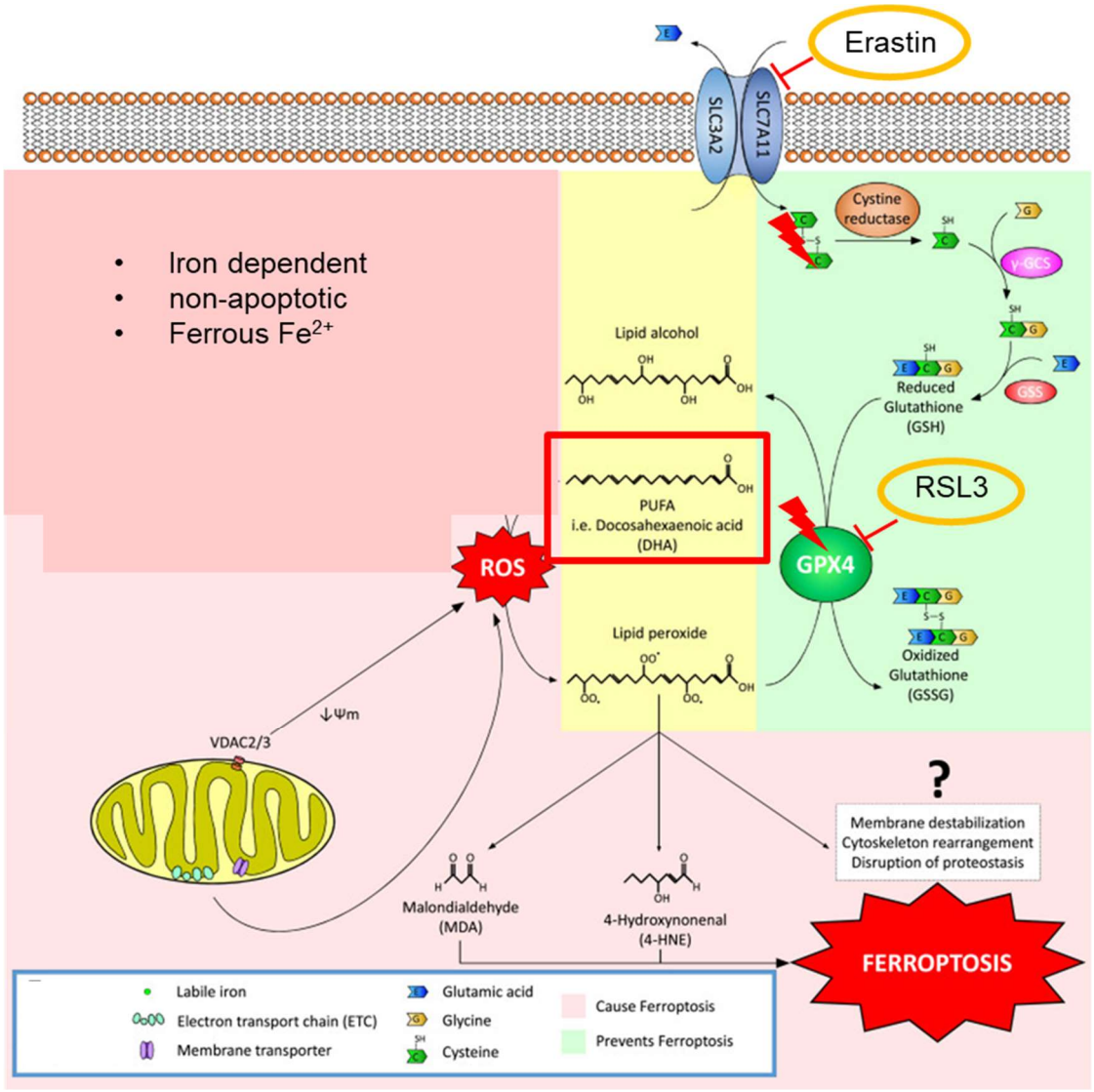

Figure 1.11 Scheme of ferroptosis cascade

Figure adapted from (Dodson et al., 2019).

1.5 Krüppel-like factor-1

Recently, we identified Krüppel-like factor 1 (KLF-1) as a major regulator of the longevity assurance caused by mitochondrial dysfunction in *C. elegans*. In the mammalian system, 17 different members of this family play a significant role in cell homeostasis, metabolism, and survival (McConnell and Yang, 2010, Zhang et al., 2011, Wu and Wang, 2013). Mammalian KLFs play central roles in lipid metabolism and they act as transcription key components, responsible for regulating adipocyte differentiation, adipogenesis, and obesity (Brey et al., 2009, Altun, 2009).

There is no precise mammalian homolog for *C. elegans* KLF-1. All three *C. elegans* KLFs, KLF-1, KLF-2, and KLF-3, reveal the highest similarity with members of mammalian KLFs in their C-terminal C_2H_2 zinc fingers, with a minor homology in the N-terminal region (Hashmi et al., 2008, Zhang et al., 2011, Brey et al., 2009). *C. elegans klf-1* is expressed mainly in the intestine and to a lesser extent in the hypodermis, and a minority of neurons detectable during larval and adult stages (Zhang et al., 2011). We have recently described KLF-1 as a mediator of a cytoprotective response that affects longevity induced by mild mitochondrial dysfunction (Herholz et al., 2019). KLF-1 activates genes involved in the xenobiotic detoxification program, namely cytochrome P450 oxidases (CYPs) and those are longevity-assurance factors of mitochondrial mutants (Herholz et al., 2019). We showed that the sudden increase in the number of dysfunctional mitochondria in *isp-1;ctb-1* mutant worms produces a signaling pulse of mtROS, which eases nuclear translocation and the activation of the KLF-1 mediated response (Herholz et al., 2019). Further, we demonstrated that the KLF-1 activation must be timed to day one of adulthood to support reproduction and the life-extending mitohormetic response, observed in "mit-mutants". The closest homologs of *C. elegans* KLF-1, such as KLF2, KLF4, and KLF5, are also sensitive to oxidative stress, and appear to have precisely timed functions in mammalian cardiomyocytes and vascular endothelium (Hsieh et al., 2017, Cullingford et al., 2008).

As mentioned earlier, our study also identified CYPs as direct effectors of the KLF-1 mediated response that promotes longevity (Herholz et al., 2019). In mammals, *cyp* expression is done by a complex regulation process containing four nuclear transcription factors, two different cofactors, and an intricate signaling cascade (Tralau and Luch, 2013). Interestingly, mammalian KLFs were also shown to bind the basic transcription element (BTE) in different *cyp* promoters. Therefore, some KLFs probably regulate CYP expression (Zhang et al., 1998). We also determined that both KLF-1 and CYPs are required for the activation of phase II detoxification genes (Herholz et al., 2019), the majority of enzymes belong to the glutathione metabolism (An and Blackwell, 2003).

The *C. elegans* transcription factor *klf-1* was initially described by Hashmi and coworkers in 2008. They investigated the role of KLF-1 in cell death, phagocytosis and fat regulation (Zhang et al., 2011, Hashmi et al., 2008). They reported that *klf-1* knockdown results in increased fat storage in worms, suggesting that loss-of-function of *klf-1* leads to disorganized fat metabolism, thus increased fat storage (Hashmi et al., 2008). They further observed that

older hermaphrodites showed a lower production of progeny and accumulation of apoptotic cells upon *klf-1* depletion (Hashmi et al., 2008). Additionally, they described that KLF-1 is not required for embryonic or germline development since germline, oocytes, and spermatheca were unaffected in *klf-1* RNAi worms (Hashmi et al., 2008). Another study reported that KLF-1 mediates longevity of *eat-2* mutant, a genetic model for caloric restriction-induced longevity in worms (Carrano et al., 2014). Moreover, they demonstrated that WWP-1, a HECT ubiquitin E3 ligase, ubiquitylates KLF-1, which in turn promotes dietary restriction-induced longevity. In this model, depletion of *klf-1* resulted in increased lipid accumulation (Carrano et al., 2014).

More recently, the role of KLF-2 and KLF-3 in *C. elegans* lipid metabolism, were also reported by a study of Ling and coworkers (Ling et al., 2017). They showed that KLF-3 is the main regulator of fatty acid synthesis, lipid secretion, and degradation (Ling et al., 2017). KLF-2 plays a comparable role in lipid metabolism but vary in quantitative and developmental pattern as compared to KLF-3. *Klf-2* expression was detected in the intestine, suggesting a possible KLF-2 role in lipid metabolism (Ling et al., 2017). Here, they demonstrated that calcium might be the most effective in regulating fat storage and *klf-2* expression, as high Ca^{2+} diet decreased *klf-2* expression, and resulted in reduced fat accumulation (Ling et al., 2017).

1.6 Objectives

As introduced above, lipids are essential components of all living organisms and the fatty acid metabolism is conserved across species. We recently identified KLF-1 as central transcription factor regulating longevity and beneficial effect of moderate mitochondrial dysfunction in *C. elegans*. Remarkably, lipid metabolism genes were one of the major KLF-1 targets in the long-lived mitochondrial *isp-1;ctb-1* mutant. Therefore, this study focused on the role of lipid metabolism in mitochondrial *isp-1;ctb*-1 mutants and raises the following questions:

1. Why do *isp-1;ctb-1* mutant worms have lower lipid levels and what are the major lipid metabolism pathways regulating this?

2. Is the change in lipid metabolism essential for the longevity of the *isp-1;ctb-1* mutants?

3. What is the role of mitochondria and peroxisomal interplay in lipid metabolism of the long-lived *isp-1;ctb-1* mutant animal?

2 Material and methods

2.1 *C. elegans* Methods

2.1.1 Strains and maintenance

Strains were grown at 20°C on nematode growth media agar plates (NGM) (0,25% bacto-peptone, 0,3 % NaCl, 1,7 % agar, 1mM CaCl2, 1mM MgSO4, 25mM KPI buffer pH 6,5 µg/ml cholesterol, nystatin 25 units/ml) spread with *Escherichia coli* (*E. coli*) OP50, unless otherwise stated and kept in air-permeable boxes (Brenner, 1974). The following strains (Table 1) were used in this study.

Table 1 List of strains with respective genotypes used in this study

Strain	Genotype
N2, Bristol	wild type
MQ989	*isp-1(qm150)IV;ctb-1(qm189)*
WBM170	*wbmEx57 [acs-2p::GFP + rol-6(su1006)].*
ATR4075	*isp-1(qm150)IV;ctb-1(qm189);wbmEX57[acs-2p::GFP + rol-6(su1006)]*
VS15	*hjIs8 [ges-1p::GFP-PTS1]*
NV6	*pgst-4::nls-gfp*
ATR1040	*isp-1;ctb-1;pgst-4::nls-gfp*
Grx	*prpl-17::Grx1-roGFP2*
ATR1045	*isp-1;ctb-1;prpl-17::GRX-1-roGFP*
HyPer	*prpl-17::HyPer*
ATR1054	*isp-1;ctb-1;prpl-17::HyPer*
ATR4081	*N2;pvha-6::klf-1-yfp integrated*
ATR4082	*isp-1;ctb-1 pvha-6::klf-1-yfp integrated*
RB675	*pmp-4(ok396) IV.*
RB859	*Y57A10C.6(ok693) II*
VS24	*kat-1(tm1037) II.*
RB1899	*F28F8.2(ok2457) V.*
ATR1022	*N2; atEx100 [pklf-1::gfp;rol-6(su1006)]*

2.1.2 Synchronization of *C. elegans*

For all experiments, gravid adult worms were synchronized by hypochlorite treatment to obtain homogeneous *C. elegans* populations. Worms were washed off the plates and collected in 7ml M9 (20mM KH_2PO_4, 40 mM Na_2HPO_4, 80 mM NaCl, 1mM $MgSO_4$). Bleaching solution, a mix of 1ml 5mM NaOH and 714µl hypochlorite solution 14%, was added. After 10 minutes incubation, by vortexing every 2 min, worms were spun down by centrifugation (3000 rpm 1 min). Eggs were washed 3 to 5 times by adding 4.5ml fresh M9 buffer and spun down by centrifugation, as mentioned before, to get rid of bleaching solution. After washing and centrifugation steps eggs were directly pipetted on NGM plates and incubated at 20°C.

2.1.3 RNAi treatment

In the year 1998, Fire and coworkers reported that injection of double-stranded RNA (dsRNA) into worms leads to exclusive degradation of the corresponding messenger RNA (mRNA), known as RNA interference (RNAi). In this study, a standard feeding RNAi protocol, with bacteria expressing the desired dsDNA, to produce knock-down phenotypes, were used as described previously (Kamath et al., 2003). All RNAi clones were obtained from Ahringer RNAi library and verified by sequencing before use (Kamath et al., 2003). All clones used for RNAi experiments were transformed into *E. coli* HT115 strain. Worms feeding on a bacterial clone, carrying the empty vector (L4440), were used as control. In brief, bacterial cultures were grown in Luria broth media until reaching OD_{595}=0.5. Isopropyl β-D-1-thiogalactopyranoside (IPTG) (Applichem, Darmstadt, Germany) was added to a concentration of 1mM to induce bacteria for three more hours by shaking at 37°C and seeded on NGM plates, additionally containing 100 µg/ml ampicillin, 25 µg/ml tetracycline, 1mM IPTG. After 1-2 days, eggs were placed on these NGM plates. That way worms were treated from hatching and phenotypes were observed from the first day of adulthood (D1).

Table 2 RNAi clones Ahringer RNAi library

Gene	Sequence	Location
klf-1	F56F11.3	III-1J15
acs-2	F28F8.2	V-10A16
acs-1	F46E10.1	V-4D12
acs-3	T08B1.6	V-14L24
prx-5	C34C6.6	II-6G16
cpt-1	Y46G5A.17	II-10D09
cpt-2	R07H5.2	IV-5P12

2.1.4 Lifespan assay

The purpose of the lifespan assay was to investigate the effect on lifespan of different RNAi treatments. Therefore, 100 worms of synchronized populations were used per condition and scored every second day. The first day of adulthood (D1) was defined as day 1 of lifespan. From that point on worms that escaped the plate, or died due to internal hatching or protrusions, were censored.

2.1.5 Oxygen consumption

Oxygen consumption rates were measured using an Oroboros Oxygraph 2k (Oroboros Instruments GmbH). In brief, 300 animals on the first day of adulthood were manually picked and transferred to non-seeded NGM plates. Worms were washed off the non-seeded NGM plates step by step with 500µl M9 and resuspend in 50µl 1M mitochondrial respiration buffer (MIB) and poured into the Oxygraph chamber containing 2ml of MIB. Oxygen consumption was measured at least 20 minutes at 20/25°C and repeated at least three times. Data were analyzed using DatLab7 software.

Table 3 Mitochondrial respiration buffer pH 7.2

Reagent	PM (g/mol)	Amount for 500ml
Sucrose	342.3	20.54g
KCl	75.5	1.89g
Tris-HCl	121.1	1.21g
EGTA	380.3	0.19g
KH_2PO_4	136.1	0.27g
$MgCl_2$	203.3	0.20g
BSA		50 mg for 50 ml

2.1.6 Movement assay

Worms were grown on respective RNAi plates. On day one of the adulthood worms were individually picked on non-seeded NGM plates and allowed to settle for a 1 min. Following this, the movement was scored as the number of body bends that a worm made moving forward or backward, for 3 minutes. Body bends are defined as the times a determined region (e.g. head or midbody) reaches the maximum bend during measurement. The data were presented as the number of body bends per minute.

2.1.7 Pharyngeal pumping

Worms were grown on respective RNAi plates. On day one of the adulthood worms were individually picked on seeded NGM plates. Pharyngeal pumping was scored as the number of pumping for 1 minute. At least 15 animals were counted per condition and data were presented as pumping per minute.

2.1.8 KLF-1 nuclear localization

KLF-1 nuclear localization was examined by using ATR4081 and ATR4082 strains. Animals were grown from eggs on RNAi plates and were imaged on the first day of adulthood. Activation was quantified as “low” when less than 2 nuclei per animal were stained, “medium” when 2–6 nuclei were stained, and “high” when more than 6 nuclei were observed. Each experiment was repeated at least three times on different days.

2.1.9 The *klf-1* expression under stress conditions

As previously described (Herholz et al., 2019) ATR1022 strain was used and grown until adulthood on L4440 RNAi NGM plates at 20°C and treated for osmotic stress by transferring worms to NGM plates containing 500mM NaCl kept for 20 hours. After 20 hours animals were washed off the plates using M9 buffer containing 300mM NaCl and transferred to L4440 RNAi NGM plates. Heat stress was induced by incubating worms at 35 °C for 9 hours. For oxidative stress, worms were grown from eggs until adulthood on 0.1mM paraquat throughout the development or young adults were either transferred to 16mM paraquat plates for 24 hours.

2.1.10 Determination of peroxisomal network

To visualize peroxisomes, the VS15 strain was used. Worms were grown until adulthood on L4440, *cyc-1* or *cco-1* RNAi NGM plates at 20°C and were imaged on the first day of adulthood. For Western blot experiments, worms were treated with either L4440, *cyc-1*, *cco-1*, antimycin A and hydrogen peroxide (H_2O_2) and proceeded as described in section 2.2.7 Western Blotting.

2.2 Molecular biology and biochemistry

2.2.1 Standard genotyping PCR

After crossings worms were genotyped. Single worms were collected in a PCR tube stripe, one worm per tube, in 10µl of worm lysis buffer (30 mM Tris pH 8, 8 mM EDTA, 100 mM NaCl, 0.7% NP40, 0.7% Tween 20, proteinase K 100 µg/ml). After that, worms were stored at -80°C for at least 10 min and activation and inactivation of proteinase K was performed by exposure to 60°C for one hour and followed by 15 minutes at 95°C in the Veriti 96-Well Thermal Cycler. Next, the lysis program (65°C for 1h, 90°C for 15 min) was run in the Veriti® 96-well Thermal Cycler (Thermo Fisher, USA). Dream Taq and respective primers (Table 4) were used for genotyping experiments in 20 µl reaction volume (2 µl DNA, 1µl forward primer, 1 µl reverse primer, 3.2µl 1.25mM dNTP mix, 2µl Dream Taq buffer, 0.1µl Dream Taq polymerase, water to 20µl). The amplified product was digested by BsmAI restriction enzyme. Therefore 10 µl of the digestion mix (0.5µl BsmAI Enzyme, 2µl cutsmart and 7.5µl water) and 10 µl of the PCR product were filled into a new tube and incubated for

4 hours at 55°C. The gel electrophoresis was used to separate the DNA by size and charge to identify the genotype of crossed worms.

Table 4 Primers used for genotyping

Allele	Primer	Restriction
isp(qm150)	Fw 5'-CAAATCGCGAACTTTTCTTCA-3'	BsmAI
	Rv 5'-AACGTCGTGCTCTTCCAACT-3'	

2.2.2 Gel electrophoreses

PCR products were then analyzed by 2% agarose (Roth, Germany) gel electrophoresis using Gene Ruler DNA Ladder Mix (Fermentas, Thermo Scientific, Braunschweig, Germany) and Ethidium bromide stain (Sigma Aldrich, USA). The gel electrophoresis was run with 135V for 30min and extraction Zymoclean Gel DNA Recovery Kit (Zymo Research, Germany) was used according to manufacturer's instructions.

2.2.3 Neutral lipids staining

BodiPY 498/503 (D2933, Thermo Fisher, Germany) was used to stain neutral lipids the major storage compartments, intestine and hypodermis, and in oocytes and embryos. Worms were grown till the first day of adulthood on different RNAi treatments. On the day of experiment D1 old worms were washed off the plates with M9 and washed additionally to remove bacteria. A mixture of 2x MRWB buffer and 2% PFA was added and worms were incubated for 1 hour by shaking at room temperature (RT). After 1-hour worms were washed twice with M9 buffer to get rid of the mixture. Subsequently, 999 µl M9 + 1µl of 5mM BodiPY 498/503 was mixed and 500µl was added and allowed to shake for 1 hour in the dark. Afterward, worms were extensively to remove the dye and 10µl was placed on a slide and imaged on the green channel immediately.

2.2.4 Lipid absorption assay

For lipid absorption assay BodiPY C12 500/510 (D3823, Thermo Fischer, Germany) was used to trace the fatty acid uptake. Therefore, one day in advance NGM plates were seeded with heat-inactivated bacteria. Bacteria were grown as described in chapter 2.1.3,

aliquoted in 1ml Eppendorf tubes and heat-inactivated at 65° for one hour by shaking. On the day of the experiment, 1ml M9 + 0.75µl of BodiPY C12 500/510 were mixed and 500µl of this mixture was seeded on top of the heat-inactivated bacteria. Plates were dried under the hood. Meanwhile, worms were washed off the plate, washed again to remove bacteria and placed on plates with BodiPY C12 500/510 dye. Plates were kept in the dark and worms were imaged after one, three and six hours. NaN_3 was used to paralyze the worms for imaging.

2.2.5 Lipid peroxidation

For lipid peroxidation, BodiPY C11 581/591 (D3861, Thermo Fischer, Germany) was used. One day in advance NGM plates were seeded with heat-inactivated bacteria. On the day of experiment 500µl of the fresh mixture of 5 ul BodiPY C11 + 1ml M9 were seeded on top of the heat-inactivated bacteria and dried under the hood. In the meantime, day one old worms were washed off the plates and washed twice to get rid of bacteria. Animals were placed on NGM plates with heat-inactivated bacteria and BodiPY C11 dye. Worms were stained 45 minutes in dark. At the stated time worms were washed extensively to remove the dye, 100µl M9 + 10 Levamisole were added and incubated by shaking in the dark for 15 minutes. Finally, 10µl of stained worms were placed on a slide and imaged by red and green channels immediately.

Table 5 RIPA buffer

Reagent	Concentration	Amount 500ml
Tris-HCl, ph7.4	50mM	25ml of 1M
NP-40	1%	5ml
Na-deoxycholate	0.5%	2.5g
SDS	0.1%	0.5g
NaCl	150mM	15ml of 5M
EDTA	2mM	2ml of 0.5M
NaF	50mM	1.05g

2.2.6 Triglyceride Assay Kit

Quantification of triglyceride was performed by using the Triglyceride Assay Kit as described in the EnzyChrom™ Triglyceride Assay Kit (Bioassay Systems) manufacturer's instructions. Briefly, synchronized 200–300 worms were collected on the first day of adulthood in M9 buffer and lysis buffer was added according to the pellet. Worm pellets were frozen in liquid nitrogen and thawed again to tissue lyse in six cycles followed by centrifugation at 11000rpm at 4°C. Supernatant was used for the quantification of triglycerides which were normalized to total protein content determined using Bradford assay (Bio-Rad).

2.2.7 Western blotting

As described in (Herholz et al., 2019) for the protein sample preparation worms were collected on the first day of adulthood from at least three full 9 cm plates with M9 buffer. Lysis buffer was added according to the pellet and worm pellets were frozen in liquid nitrogen. On the day of experiment worm pellets were thawed and tissue lysed in six cycles followed by centrifugation of cell debris at 11000 rpm at 4°C for 15 min. The supernatant was decanted to fresh Eppendorf tubes and kept on ice. Protein concentration was determined by Bradford (Sigma Aldrich) assay. Samples were diluted 1:5 and 10µl of the dilution + 250µl of Bradford solution were used to measure the protein concentration. SDS page was run by standard technique. In brief, protein samples were loaded in 10% SDS gel and run using a 1x Running buffer. First, the gel was running for 15 minutes at 75V and proceeded with 150V for 1hour, after samples entered the separating gel. PageRuler Prestained Protein Ladder (Thermo Scientific) was used as a size standard. Membrane transfer was done by using nitrocellulose membrane-like for standard procedures. For primary antibodies, the membrane was blocked with 5% milk or 5% ECL-solution in PBST and incubated overnight at 4°C followed the next day with secondary antibodies at room temperature for 1 hour. The development of the blots was performed by using ECL solution (ThermoFisher, 32106) to visualize protein bands. Western blotting was performed using primary antibodies against GFP (1:2000, provided by Jan Riemer), HSC70 (1:2000, Santa Cruz sc-7298) and 4-HNE (1:2000, Millipore, AB5605). Secondary antibodies used against anti-mouse (1:2000, Sigma-Aldrich, A4416), anti-rabbit (1:2000, Sigma-Aldrich, A6154) and anti-goat (1:7000, Sigma-Aldrich, AP106P).

Table 6 Recipe for two 10% Separating gels

Reagent	Amount
Acrylamide Bisacrylamide 40% (37.5:1)	4.5ml
Seperating Buffer	4.5ml
H_2O	8.9ml
Ammonium Persulfate (10%)	100µl
TEMED	10µl

Table 7 Separating buffer (1.5M Tris-HCl pH 8.6)

Reagent	Amount
Tris base	54.46g
ddH_2O	150 ml
Adjust pH 8.8 with HCl and add H2O up to 300ml	

Table 8 Recipe for two 4% Stacking gels

Reagent	Amount
Acrylamide Bisacrylamide 40% (37.5:1)	0.9ml
Stacking Buffer	1.9ml
H_2O	5.1ml
Ammonium Persulfate (10%)	100µl
TEMED	10µl

Table 9 Stacking buffer (0.5M Tris-HCl pH 6.8)

Reagent	Amount
Tris base	12g
ddH_2O	120ml
Adjust to pH 6.87 with HCl and add H_2Oup to 100ml	

Table 10 10x Running buffer

Reagent	Amount
Tris base	302g
Glycine	142g
SDS	10g
H_2O	up to 2L

Table 11 10x Transfer buffer

Reagent	Amount
Tris Base	30,3g
Glycine	144,1g
ddH2O	up to 1L
For 1x Transfer buffer mix 100ml of 10x Buffer with 200ml Methanol	

2.2.8 ROS measurements

Mitotracker Red CM-H2XRos was used. Worms were grown until one day of adulthood. The day before, NGM plates were seeded with heat-inactivated bacteria. On the day of the experiments, 200µl of 10µM dye solutions were added on top of the bacteria. Animals were then added to the plates and incubated for 1 h in the dark. After one-hour worms were extensively washed to remove the dye and placed on NGM plates without dye. Thereafter worms were imaged.

2.2.9 Oil-Red-O staining

Fat staining with Oil-Red-O in whole worms to determine neutral lipids amount. In brief, two days in advance 0.5g Oil-red-O powder was diluted in 100ml isopropanol and left on stirrer for at least two days. One day in advance 2x MRWB buffer was prepared. On the day of the experiment, Oil red was diluted to 60% with water and incubated for 1hour shaking. Meanwhile, day one old worms were washed off the plates with 1x PBS. After three more washing steps, approximal 120µl was left in the tube and 120µl MRWB buffer was added. Worms were incubated for 1 hour shaking at room temperature. After that worms

were washed with 1xPBS and 1ml of 60% Isopropanol was added and incubated for exactly 15 min at room temperature. Then 60% Isopropanol was removed, 1ml filtered Oil Red was added and worms were incubated overnight shaking in the dark. The next day, the dye was removed, 200µl of 1x PBS containing 0,01% Triton X-100 was added and worms were immediately imaged.

Table 12 2x MRWB buffer

Reagent	Concentration
KCl	160mM
NaCl	40mM
Na_2EGTA or EGTA pH 8.0	14mM
Spermidine-HCl	1mM
Spermine	0.4mM
Na-PIPES pH 7.4	30mM
Mercaptoethanol	0.2%
Paraformaldehyde (PFA)	2%

2.2.10 qPCR

Worms were collected from a 9cm plate and total RNA was isolated with Trizol (Invitrogen). DNAse treatment was performed using DNA-free™, DNAse and removal (Ambion, Life Technologies), according to the manufacturer's protocol. RNA was quantified by spectrophotometry and 0.8µg of total RNA was reversely transcribed using the High-Capacity cDNA Reverse Transcription Kit (Applied Biosystems). For each condition, five independent samples were prepared. qPCR was performed using the Step One Plus Real-Time PCR System (Applied Biosystems), with the following PCR conditions: 3 min at 95 °C, followed by 40 cycles of 5s at 95 °C and 15s at 60 °C. Amplified products were detected with SYBR Green (Brilliant III Ultra-Fast SYBR Green qPCR Master Mix, Agilent Technologies).

Table 13 Primers used for qPCR-based gene expression analysis

Genotype	Sequence 5'-3'	Application
acs-2	ATTTCGGGCTGAACAACAAC	qPCR
	GGACTTTGATGGGAAGACCA	
acs-1	GATGAACGATTCGGTGAGGT	qPCR
	GAGACGACTTGCTGGAGACC	

2.2.11 Lipidomics

Glycerophospholipid (GPL) and triacylglycerol (TAG) species in *C. elegans* were quantified by nano-electrospray ionization tandem mass spectrometry (Nano-ESI-MS/MS) with direct infusion of the lipid extract (Shotgun Lipidomics):
1,500 C. worms were homogenized in 400 µl of Milli-Q water using the Precellys 24 Homogenisator (Peqlab, Erlangen, Germany) at 6,500 rpm for 30 sec. The protein content of the homogenate was routinely determined using bicinchoninic acid. For the analysis of GPL species (PC, PE, PI, PS) aliquots of the homogenates being equivalent to 70 µg of protein were diluted to 500 µl with Milli-Q water. 1.875 ml of methanol/chloroform 2:1 (v/v) and internal standards (144 pmol PC 17:0-14:1, 143 pmol PE 17:0-14:1, 127 pmol PI 17:0-14:1, 136 pmol PS 17:0-14:1; Avanti Polar Lipids, Alabaster, AL, USA) were added. For the analysis of TAG species, separate homogenate aliquots equivalent to 70 µg of protein were used, to which 1.875 ml of chloroform/methanol/37 % hydrochloric acid 5:10:0.15 (v/v/v) and 30 µl of 4 µM d5-TG Internal Standard Mixture I (Avanti Polar Lipids) were added. Lipid extraction and Nano-ESI-MS/MS analysis of GPL species were performed as previously described (Kumar et al., 2015).The Nano-ESI-MS/MS analysis of TAG species is described in (Rashid et al., 2019).

2.3 Computer analyses and microscopy

2.3.1 Microscopy

Animals were immobilized on 2% agarose pads in 5 mM levamisole buffer in M9 and imaged using an AxioImager Z.1 epifluorescence microscope, equipped with a Hammamatsu camera (OrcaR2) and AxioVision software 4.8. Likewise, the CECAD

imaging facility was used to image animals with the Meta 710 Confocal Microscope (Zeiss). Images were analyzed using Fiji/ImageJ (National Institutes of Health).

2.3.2 Statistical analyses and graphical representation

A two-tailed unpaired Student's t-test was used to determine statistical significance. Error bars represent standard error of the mean (SEM). All p values below 0.05 were considered significant: p*<0.05, p**<0.01, p***<0.001; p****<0.0001. All statistical analyses and generation of graphs were performed in GraphPad Prism 8. (GraphPad Software, USA).

3 Results

3.1 Expression of KLF-1 in *C. elegans*

3.1.1 The *klf-1* expression increases specifically upon oxidative stress and upon other types of stresses

We have previously shown that *klf-1* knockdown normalizes the lifespan of the long-lived *isp-1;ctb-1* mitochondrial mutant (Herholz et al., 2019). Since many long-lived mutants show resistance to various stresses, we wanted to understand how KLF-1 behaves under different stress conditions. Firstly, we investigated whether the *klf-1* expression changes when worms are exposed to different stresses. For this purpose, we used a strain expressing *gfp* under the *klf-1* promoter (Fig. 3.1), which shows the highest activity in the gut, muscle, and few neurons. We exposed young adults (D1 – adult day 1) to the following stresses: a) osmotic, where worms were transferred to higher concentration of NaCl of 500mM; b) heat stress, where worms are shifted from the culturing temperature of 20°C to 35°C for 9 hours; c) paraquat which has been shown to increase reactive oxygen species (ROS) levels and thus induce oxidative stress (Wang et al., 2014). While high concentrations of paraquat, such as 16 mM used here is toxic for the worms, treatment with a low concentration (0.1mM) has been previously shown to increase the lifespan (Yang and Hekimi, 2010, Schaar et al., 2015). Our results clearly show that *klf-1* expression is affected by heat shock and oxidative stress. Even more, the expression level on paraquat seems to be dosage dependent. This in accordance to our previous data (Herholz et al., 2019), where the levels of *klf-1* increase in the mitochondrial *isp-1;ctb-1* mutant due to increased ROS production as seen in Fig. 3.1 A.

Next, we investigated the role of KLF-1 in the response of animals to different stresses. To this end, the survival of worms during a heat shock or osmotic stress were evaluated (Fig 3.1 B and C). The *klf-1* knockdown did not affect the survival of wild type and *isp-1;ctb-1* mutants upon heat stress (Fig. 3.1 B). While *isp-1;ctb-1* mutants were more tolerant to osmotic stress, compared to wild type worms (Fig.3.1 C), the survival on high concentration NaCl significantly decreased when *klf-1* was depleted (Fig. 3.1 C). Together, these data suggest that KLF-1 has a role in protection against osmotic stress.

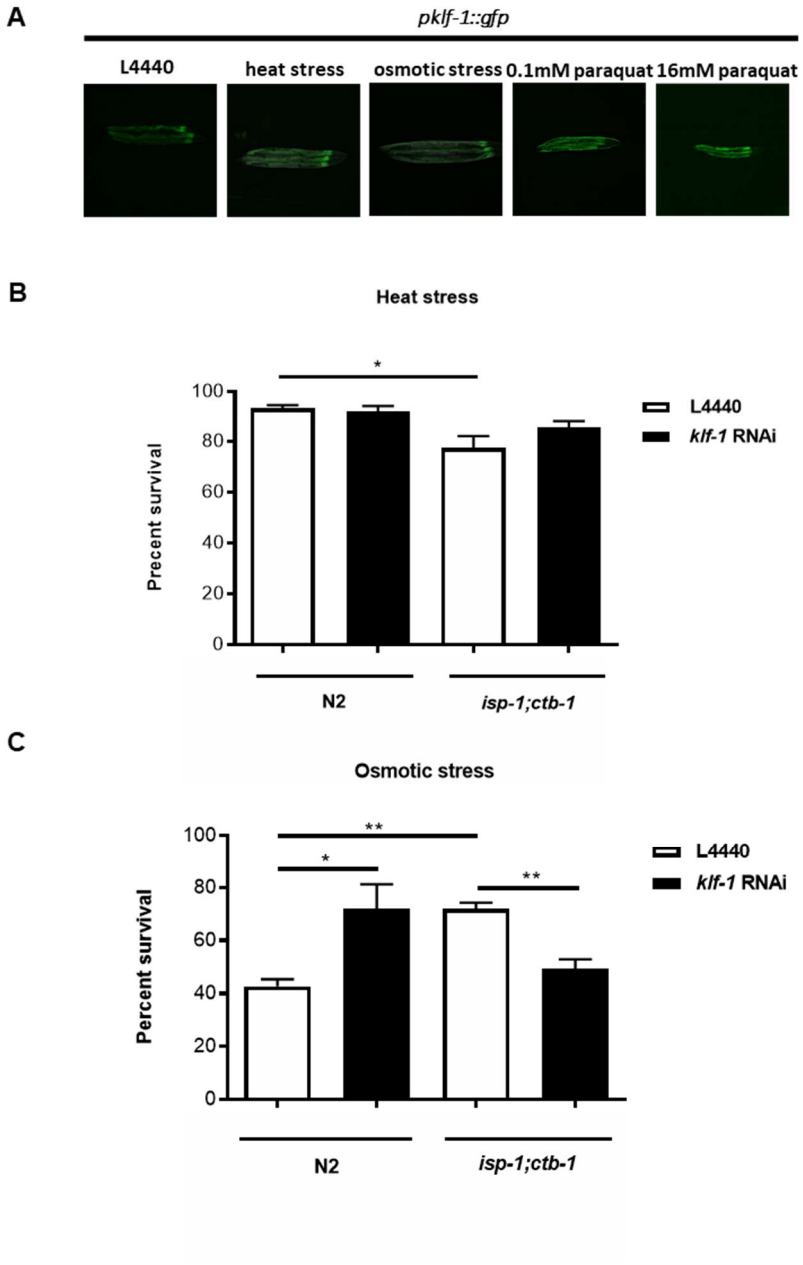

Figure 3.1 Oxidative stress increases expression of *klf-1*

A) Fluorescent images of the strain p*klf-1*::gfp;rol-6(su1006) expressing *gfp* under the *klf-1* promoter. Young adults were exposed to osmotic and heat stress or 16 mM paraquat. For 0.1 mM paraquat, animals were treated with the drug during the larval development and imaged on the first day of adulthood. Images were quantified by the percentage of survival. B) Quantification of survival of worms under heat stress. C) Quantification of survival of worms under osmotic stress. Bars represent mean ±SEM (p*<0.05, p<0.01, student's T-test).**

3.2 Investigation of Triglycerides and the role of KLF-1

3.2.1 KLF-1 regulates Triglyceride levels in *C. elegans*

KLF-1 was proposed to be a regulator of lipid metabolism, as loss of its function results in lipid accumulation (Hashmi et al., 2008). As mentioned earlier, we showed that KLF-1 is a mediator of a cytoprotective response that commands longevity forced by reduced mitochondrial function and increases in mitochondrial ROS production (Herholz et al., 2019). KLF-1 promotes genes involved in the xenobiotic detoxification program, specifically cytochrome P450 oxidases, which act as longevity-assurance factors of mitochondrial mutants. As another group of KLF-1 regulated targets, we identified multiple genes involved in lipid metabolism (Herholz et al., 2019). A role of KLF-1 as a regulator of the lipid metabolism has previously been suggested by Hashmi and coworkers (Hashmi et al., 2008). We thus aimed to further investigate the lipid metabolism in the long-lived *isp-1;ctb-1* mutant.

Firstly, we assessed the lipid levels in *isp-1;ctb-1* mutants, by staining the worms with Oil-Red O, a stain that preferentially stains neutral lipids, such as triglycerides (TAGs). *isp-1;ctb-1* mutants showed low neutral lipid levels that are fully corrected by *klf-1* knockdown (Fig. 3.2 A). The effect of *klf-1* deficiency increased lipid levels in both wild type and *isp-1;ctb-1*, further strengthening KLF-1 involvement in the lipid metabolism (Fig. 3.2 A). To confirm these results, we next determined levels of lipids extracted from wild type and *isp-1;ctb-1* mutants in control conditions, and upon *klf-1* depletion, using the Triglyceride Assay Kit on day one of adulthood animals (Fig. 3.2 B). Here, the triglyceride levels in *isp-1;ctb-1* mutant were congruent with the results in the Oil-Red O staining experiment (Fig. 3.2 A). Upon *klf-1* knockdown, the lipid levels also came back to those in wild type N2 (Fig. 3.2 B). Conspicuously, the lipids levels in wild type N2 upon *klf-1* depletion showed upregulation when assayed with Oil-Red O staining, while we detected mild decrease when using triglyceride assay kit (Fig. 3.2 B). The reason for this discrepancy could be in that Oil-Red O stains all neutral lipids, while the assay kit stains only triglycerides. Alternatively, Oil-Red-O is used on the whole worms, while for the triglyceride assay kit lipids need to first get extracted.

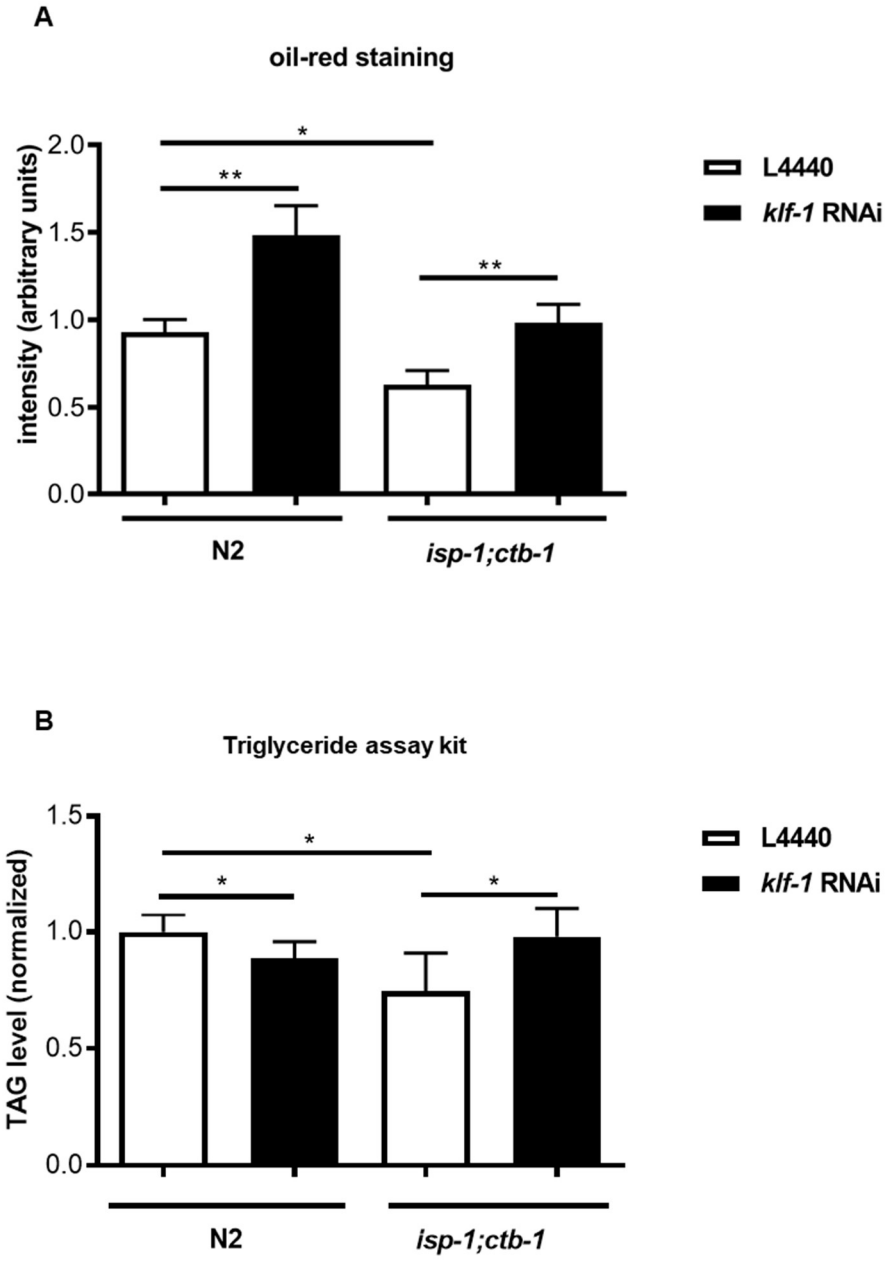

Figure 3.2 KLF-1 regulates lipid metabolism in *C. elegans*

Wild type worms N2 and *isp-1(qm150);ctb-1(qm189)* mutants treated with RNAi targeting *klf-1* gene. On day one of the adulthood worms were either stained with A) Oil-red O or used for B) Triglyceride assay kit to determine lipid levels. Results shown are means ±SEM (p*<0.05, p<0.01 Students T-test) for three independent biological replicates. Data are normalized to the current control. Together with Dr. Marija Herholz.**

3.2.2 Mitochondrial *isp-1;ctb-1* mutants have fewer triglyceride levels, but elevated phospholipids

Since neutral lipid levels were lower, we wanted to understand the global changes in lipid composition in *isp-1;ctb-1* mutant. Therefore, we analyzed the lipid profiles of wild type N2 and *isp-1;ctb-1* mutant on the first day of adulthood (D1). This was performed by nano-electrospray ionization tandem mass spectrometry with a direct infusion of the lipid extract. Figure 3.3 depicts a summary of triglycerides and phospholipids found in wild type N2 compared to *isp-1;ctb-1* mutant (Fig. 3.3 A). Fatty acids are abbreviated X:Y, where X represents the number of carbon atoms, and Y represents the number of double bonds (Fig. 3.3 A). Long-chain fatty acids detected have a size of C14 to C20 or higher.

Our results show that the most common fatty acids present in both wild type N2 and *isp-1;ctb-1* mutants are C17:1, known as heptadecenoic acid and 18:2, known as linoleic acid (Fig 3.3 A). In agreement with Oil-Red O staining and triglyceride assay kit data, the *isp-1;ctb-1* mutant had overall fewer triglyceride levels (Fig. 3.3 A). Unexpectedly, the *isp-1;ctb-1* mutant showed a massive increase in phospholipid levels as seen in Figure 3.3B.

All five classes of phospholipids: phosphatidylcholine (PC), phosphatidylethanolamine (PE), phosphatidylinositol (PI) and phosphatidylserine (PS) were significantly increased. High upregulation of phospholipids could be explained by an increase in the total amount of organellar membranes. Indeed, we have shown that *isp-1;ctb-1* mutants increase overall mitochondrial mass to compensate for respiration deficiency (Herholz et al., 2019).

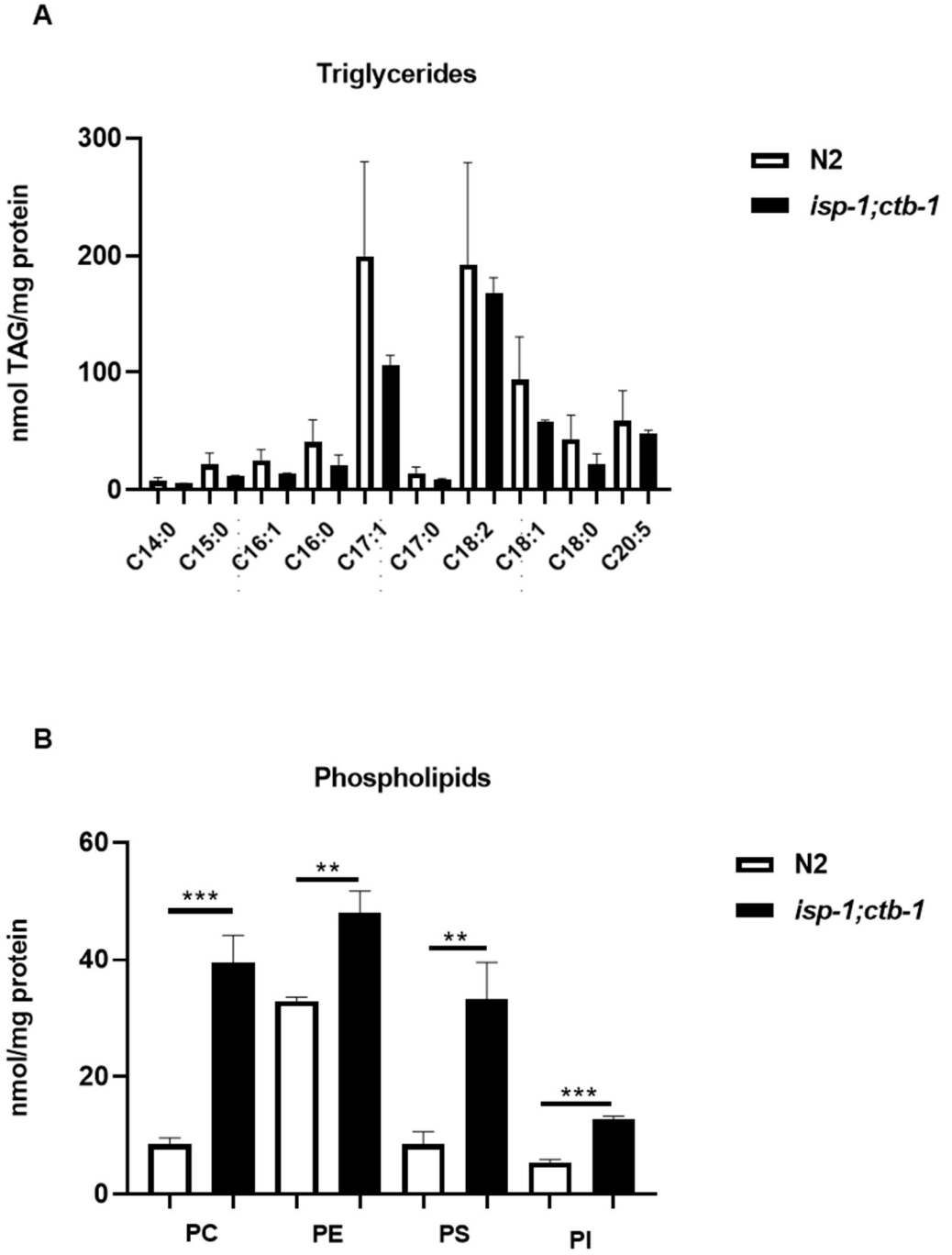

Figure 3.3 The *isp-1(qm150);ctb-1(qm189)* mutant has less triglycerides levels, but increased amounts of phospholipids A) Triglyceride levels and B) Phospholipid levels. Investigated by mass spectrometry. 15000 worms per condition were used. Bars represent mean ±SEM (p<0.01, p***<0.001, Student's T-test). Experiments were performed together with Susanne Brodesser (CECAD, Lipidomics facility).**

3.3 Uptake of fatty acids and KLF-1

3.3.1 Pharyngeal pumping and food intake are decreased in *isp-1;ctb-1* mutants

The decreased amount of lipids in the mitochondrial mutant can either come from a decrease in the nutrient uptake and/or increased utilization of lipids. To distinguish between the two, we first assayed the feeding behavior of the mitochondrial mutant. In the nematode, feeding occurs via rhythmic contractions, pumping of the pharynx, the feeding organ (Trojanowski et al., 2016). A decrease in the pumping rate would lead to a decrease in the food intake, such as in *eat-2(ad1116)* mutant, which is commonly used as a model for dietary restriction (Lakowski and Hekimi, 1998). Thus, we counted the rate of pharyngeal pumping on 15 animals of each genotype on the first day of adulthood. Worms were observed on the NGM agar plate and the rhythmic contractions were counted for one minute. We found that wild type N2 animals pumped 170 times per minute, whereas the *isp-1:ctb-1* mutant animals just pumped 100 times per minute (Fig. 3.4 A). Thus, the pharyngeal pumping was significantly decreased in *isp-1;ctb-1* mutants. Remarkably, upon *klf-1* RNAi, pharyngeal pumping of *isp-1;ctb-1* mutant is mildly, but significantly improved (Fig. 3.4 A). This data indicates that KLF-1 suppresses pharyngeal pumping in the *isp-1;ctb-1* mitochondrial mutant, but since the effect of KLF-1 on pharyngeal pumping is only mild, it cannot explain the differences seen in the lipid levels.

To further investigate this, we fed worms with GFP-expressing bacteria. This allows us to better visualize the feeding of the worms. Gravid adult worms of wild type N2 and *isp-1;ctb-1* mutants were plated on seeded NGM plates with a confluent lawn of GFP-expressing bacteria. Animals were allowed to feed for 15 min and after that worms were put on a slide and anesthetized with NaN_3. Images of a whole worm using a GFP filter were taken. A significant decrease in uptake of GFP-expressing bacteria in the *isp-1;ctb-1* mutant was observed (Fig. 3.4 B).

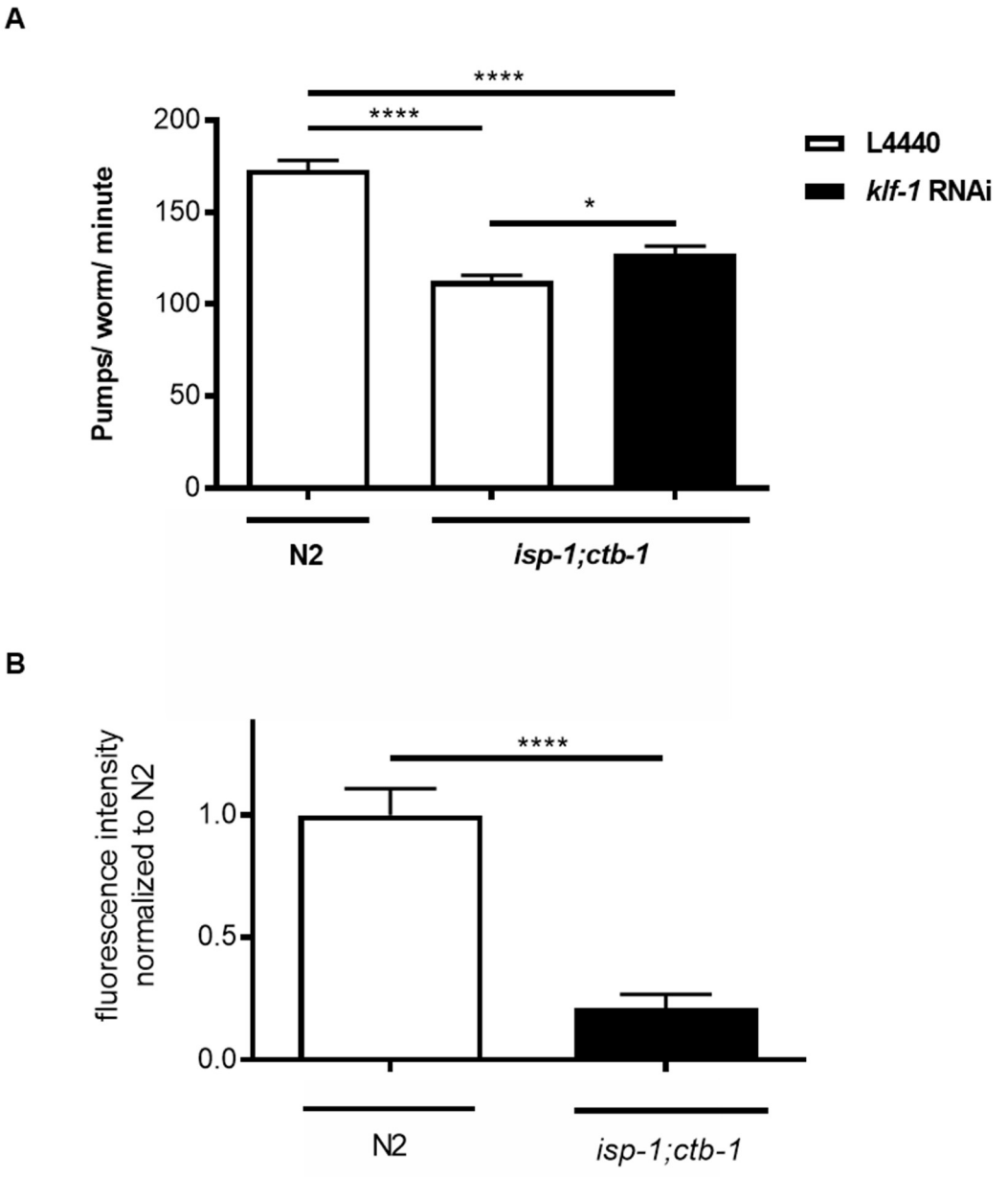

Figure 3.4 Pharyngeal pumping and food intake is decreased in *isp-1;ctb-1* mitochondrial mutant
A) Pumps per minute were counted for wild type N2 and *isp-1(qm150);ctb-1(qm189)* mutants on day one of adulthood. Worms were grown on NGM plates with either control L4440 or *klf-1* RNAi.
B) Wild type N2 and *isp-1(qm150);ctb-1(qm189)* mutants were feed with OP50 bacterial strain expressing GFP. Worms were imaged by AxioImager Z.1 epifluorescence microscope and images were analyzed by ImageJ. N=15 animals were counted per condition. Bars represent mean ±SEM (p*<0.05; p*<0.001; p****<0.0001, Student's T-test).**

3.3.2 The *isp-1;ctb-1* mitochondrial mutant shows delayed uptake of fatty acids

Next, we determined the uptake of fatty acids. Here, BodiPY C12, a fluorescent fatty acid analog has been used to follow lipid trafficking for six hours. Animals were grown until the first day of adulthood and were moved from RNAi NGM plates to fresh plates, containing the fluorescent dye BodiPY C12. The fluorescence of worms was measured after one, two, three and six hours.

The *isp-1;ctb-1* mutants initially (1 – 3h) showed a delayed uptake of fatty acids (Fig. 3.5). However, after six hours *isp-1;ctb-1* mutants on control conditions reached the lipid uptake level like wild type N2 worms (Fig.3.5). Upon *klf-1* depletion, the uptake of fatty acids increases immediately after one and two hours in the *isp-1;ctb-1* mutant animals (Fig. 3.5). These data indicate that the presence of KLF-1 suppresses the uptake of fatty acids in *isp-1;ctb-1* mutant animals.

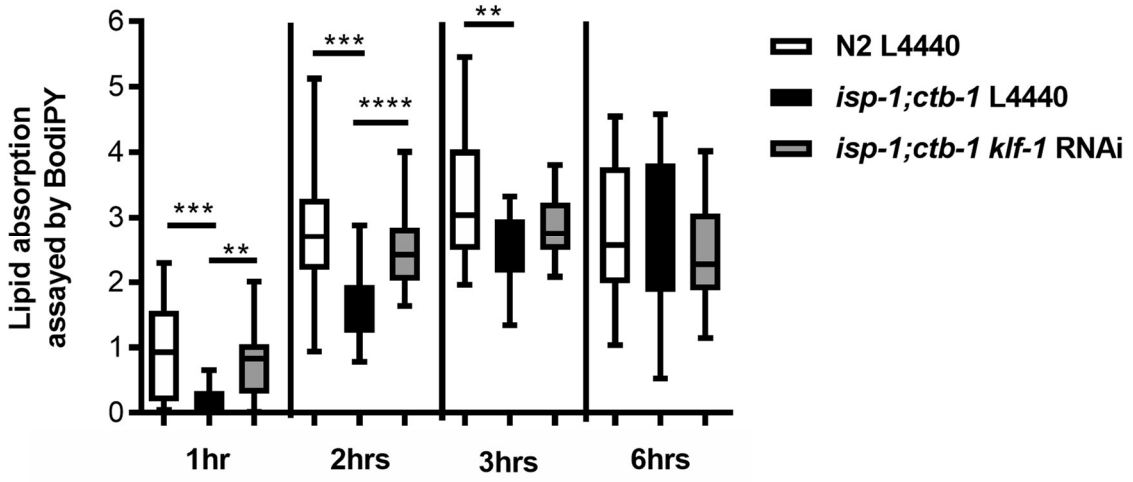

Figure 3.5 Lipid absorption assay using BodiPY C12 fluorescent fatty acid analog
Wild type N2 and *isp-1(qm150);ctb-1(qm189)* mutants were grown on NGM plates with either L4440 or *klf-1* RNAi. Uptake of fatty acids was analyzed by feeding worms with specific dye BodiPY C12 and images were taken by AxioImager Z.1 epifluorescence microscope with a magnification of 5x. Images were analyzed using ImageJ. Bar represents mean ±SEM (p<0.01, p***<0.001; p****<0.0001 Student's T-test).**

3.4 Gene expression in *isp-1;ctb-1* mitochondrial mutant upon *klf-1* depletion

3.4.1 Microarray data of mitochondrial-and peroxisomal ß-oxidation genes

As mentioned earlier, we previously performed a microarray analysis of the *isp-1;ctb-1* mutant animals at day five of adulthood. Next to the detoxification pathway, the second most changed pathway was lipid metabolism. Expression of many of these genes was changed in the KLF-1 dependent manner (Herholz et al., 2019). Figure 3.6 lists the genes involved in both mitochondrial and peroxisomal FAO in *isp-1;ctb-1* mutant normalized to wild type levels upon *klf-1* knockdown. One of the genes whose expression was mostly altered are two acyl-CoA synthetases that prime fatty acids for peroxisomal and mitochondrial FAO, ACS-1 and ACS-2 respectively (Fig. 3.6 A and B). Their expression changed in the KLF-1 dependent manner. Acyl-CoA synthases catalyze the conversion of free fatty acids to acyl-CoA derivates as a step preceding fatty acid oxidation in both mitochondria and peroxisomes.

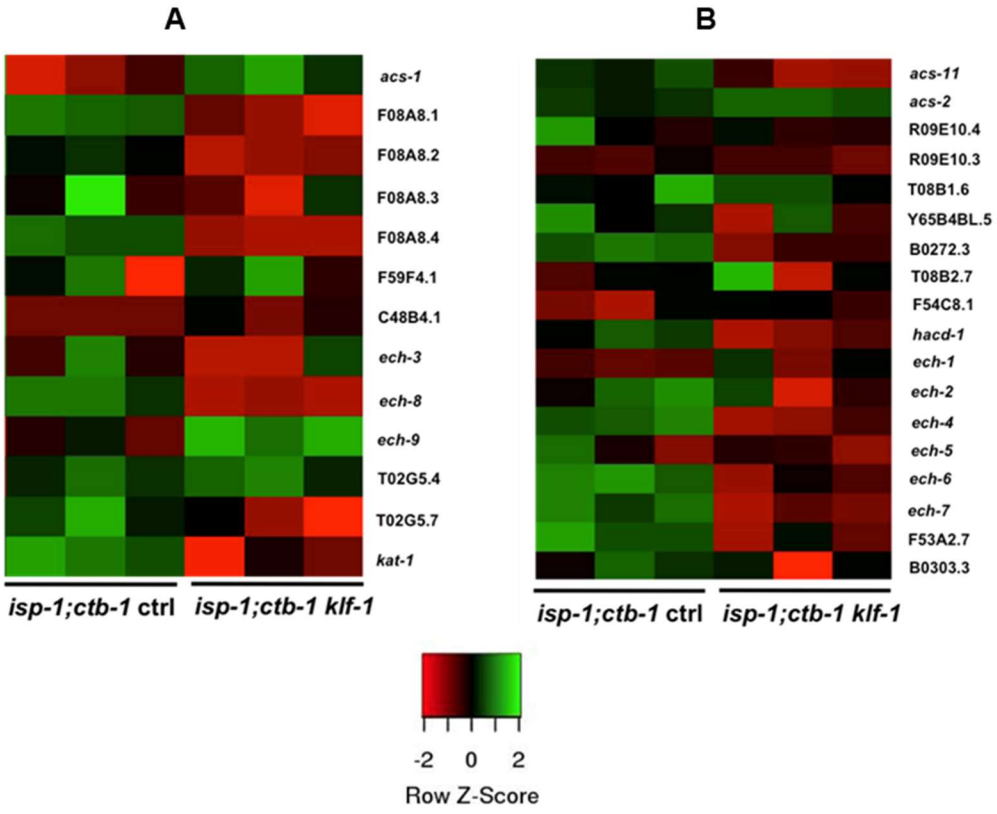

Figure 3.6 Microarray data of *isp-1(qm150);ctb-1(qm189)* mutants upon control or *klf-1* RNAi
Microarray data of *isp-1(qm150);ctb-1(qm189)* mutants on day five of adulthood. A) presents microarray data of the peroxisomal ß-oxidation (left) and B) presents microarray data of the mitochondrial ß-oxidation (right). Red represents which genes are downregulated. Additional analysis of microarray data from (Herholz et al., 2019).

3.4.2 Acyl-CoA synthases *acs-2* and *acs-1* are upregulated in mitochondrial *isp-1;ctb-1* mutant

In agreement with microarray data, our qPCR data indicate that genes encoding for mitochondrial and peroxisomal acyl-CoA synthase *acs-2* and *acs-1* respectively, are highly overexpressed in the *isp-1;ctb-1* mitochondrial mutant in comparison to wild type N2, on day one of adulthood (Fig 3.7 A and B). In wild type N2 worms, *acs-2* is almost not expressed at all, on day one of adulthood. Only after *klf-1* depletion, the expression of *acs-2* in wild type N2 animals was observed (Fig. 3.7A). The expression of *acs-1* decreases upon *klf-1* knockdown, in wild type N2 worms compared to control conditions (Fig. 3.7B).

KLF-1 deficiency impairs the expression of *acs-2* and *acs-1* in *isp-1;ctb-1* mitochondrial mutant. In wild type N2 animals *klf-1* knockdown enhances the expression of *acs-2* but reduces the expression of *acs-1*. In conclusion, these data suggest that mitochondrial mutants increase the expression of genes involved in FAO, in a KLF-1 dependent manner. However, the CHIP-seq data did not identify *acs-1* and *acs-2* as direct targets of the KLF-1 (Herholz et al., 2019). Thus, it still remains unclear whether KLF-1 directly or indirectly regulates the expression of these genes.

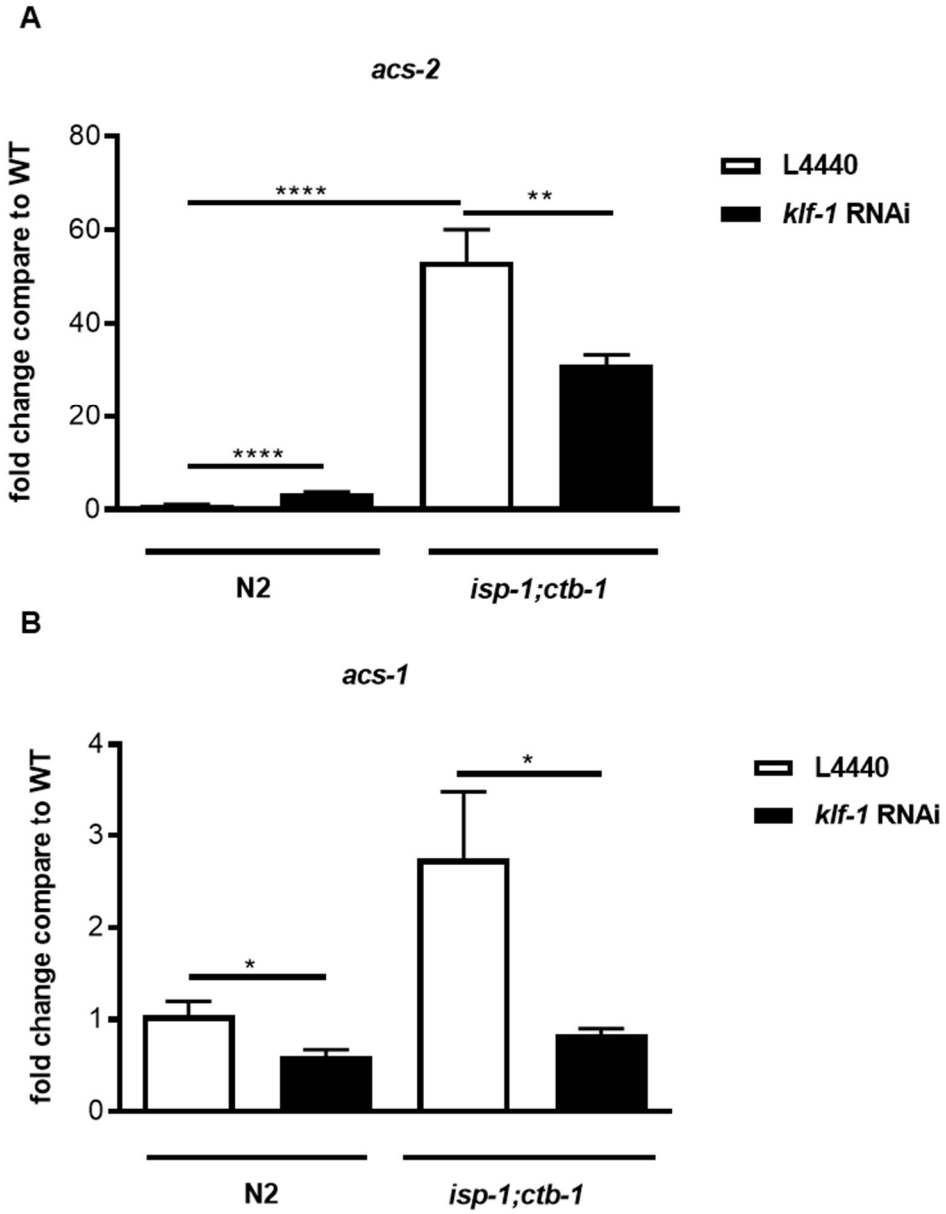

Figure 3.7 Expression levels of mitochondrial *acs-2* and peroxisomal *acs-1* gene
The expression levels measured by qPCR of A) mitochondrial ß-oxidation gene *acs-2* and B) peroxisomal ß-oxidation gene *acs-1* in *isp-1(qm150);ctb-1(qm189)* mutant on day one of adulthood. Worms were treated either with control L4440 or *klf-1* RNAi. Bars represent mean ±SEM (p*<0.05, p<0.01, p****<0.0001, Student's T-test).**

3.5 Behavioral parameters upon depletion of *acs-2* and *acs-1*

3.5.1 Pharyngeal pumping improves after *acs-2* depletion in *isp-1;ctb-1* mutant animals

To understand if priming of fatty acids for mitochondria and peroxisomes was of equal importance for longevity and fitness in mitochondrial mutants, we concentrated on acyl-CoA synthetases ACS-2 and ACS-1. Initially, we investigated behavioral parameters upon deletion of *acs-2* and *acs-1* genes, in wild type N2 and mitochondrial *isp-1;ctb-1* mutant animals. Firstly, we measured pharyngeal pumping of wild type N2 and *isp-1;ctb-1* mutant animals treated with either control, or *acs-2* and *acs-1* RNAi on day one of adulthood.

Overall, Figure 3.8 shows that pharyngeal pumping is significantly improved upon *acs-2* knockdown in both strains. This means that for *isp-1;ctb-1* mutant animals, the pharyngeal pumping rate upon *acs-2* depletion comes back to wild type control levels (Fig. 3.8). The knockdown of *acs-1* decreased the pumping rate in wild type N2, while the pharyngeal pumping rate, of *isp-1;ctb-1* mutant animals, stayed unaffected (Fig. 3.8). These data suggest that the peroxisomal acyl-CoA synthetase, *acs-1*, is not essential for the pharyngeal pumping in our mitochondrial mutant.

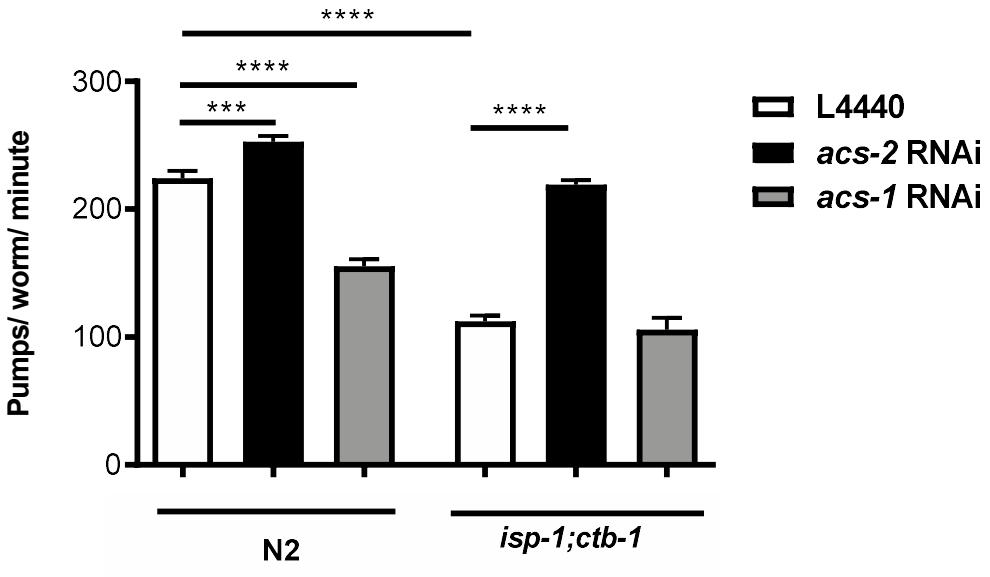

Figure 3.8 Pharyngeal pumping is increased in the mitochondrial *isp-1;ctb-1* mutant upon *asc-2* depletion
Pumps per minute were counted for wild type N2 and *isp-1(qm150);ctb-1(qm189)* mutants on day one of adulthood. Worms were grown on NGM plates with either control L4440 or *acs-2* or *acs-1* RNAi. 10 animals were counted per condition. Bars represent mean ±SEM (p*<0.001; p****<0.0001, Student's T-test).**

3.5.2 Uptake of fatty acids upon *acs-3* knockdown is increased

Next, we wanted to see how the effect of *acs-1* and *acs-2* on pharyngeal pumping reflects on the fatty acid uptake. It has been already reported that acyl-CoA synthases are crucial for lipid synthesis and breakdown. It has been previously shown by Mullaney and co-workers, that *acs-3* increases the intestinal uptake of fatty acid and thus is crucial for lipid synthesis and breakdown (Mullaney et al., 2010). Thus, we decided to use *acs-3* depletion as a positive control for fatty acid uptake. On day one of adulthood, worms were imaged after one, three and six hours of feeding with BodiPY C12. Wild type N2 worms reach their maximum uptake after six hours of feeding (Fig. 3.9). As shown before, the *isp-1;ctb-1* mutant in control condition has a lower uptake and reached its maximum also after six hours (Fig. 3.9).

The *acs-3* knockdown repaired the fatty acid uptake of *isp-1;ctb-1* mutants during the first hour. This advantage is lost after three hours already and reached the same uptake rate as *isp-1;ctb-1* control conditions (Fig. 3.9). Upon *acs-2* depletion, we could not observe any significant difference to *isp-1;ctb-1* control conditions, despite the increased pharyngeal pumping. On the other hand, upon *acs-1* depletion *isp-1;ctb-1* mutant worms have a significantly decreased uptake of fatty acids after the dedicated time points (Fig. 3.9). The effect of *acs-3* on fatty acid uptake clearly uncouples the decreased fatty acid uptake in mitochondrial *isp-1;ctb-1* mutant from pharyngeal pumping. These data also strongly implicate ACS-1 in this process.

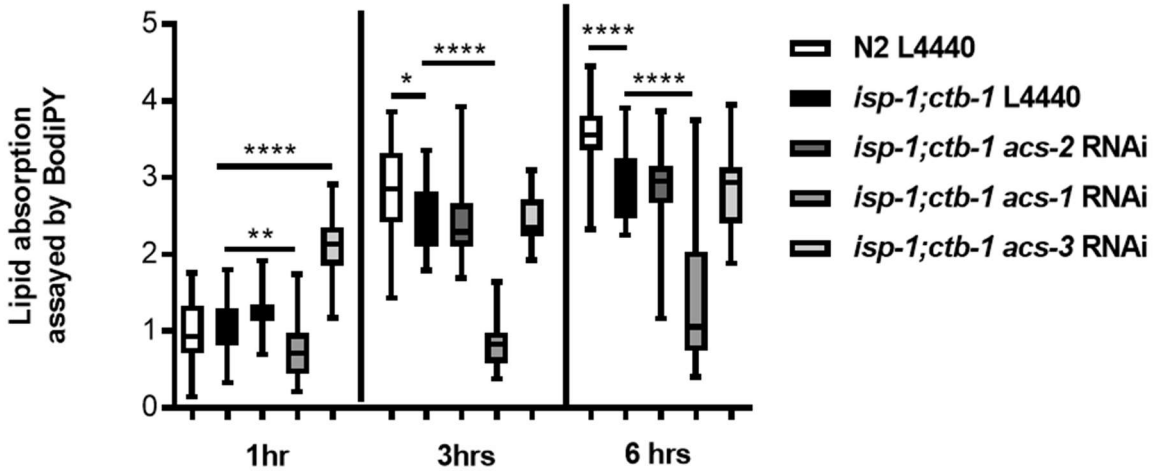

Figure 3.9 Lipid absorption assay using BodiPY C12 fluorescent fatty acid analog upon ACS knockdowns
Wild type N2 and *isp-1(qm150);ctb-1(qm189)* mutants were grown on NGM plates with either L4440 or *acs-2*, *acs-1*, and *acs-3* RNAi. Uptake of fatty acids was analyzed by feeding worms with specific dye BodiPY C12 and images were taken by AxioImager Z.1 epifluorescence microscope with a magnification of 5x. Images were analyzed using ImageJ. Bar represents mean ±SEM (p*<0.05, p<0.01, p***<0.001; p****<0.0001 Student's T-test).**

3.5.3 Respiration deteriorates after depletion of peroxisomal genes

Next, we determined metabolic and behavioral parameters of wild type N2 and *isp-1;ctb-1* mutant animals upon *acs-2* and *acs-1* depletion. Figure 3.10 compares respiration and movement of wild type N2 and *isp-1;ctb-1* mutant animals, upon knockdown of mitochondrial- and peroxisomal ß-oxidation genes *acs-2* and *acs-1* on day one of adulthood. Surprisingly, when blocking enzymes that prime fatty acids for mitochondrial ß-oxidation by knocking down acs-2, basal respiration and movement increased in both wild type N2 and isp-1;ctb-1 mutant animals compared to control conditions (Fig 3.10 A). Likewise, the movement of both strains increased significantly (Fig. 3.10 A).

Contrary, depletion of acs-1 leads to impaired respiration and movement in isp-1;ctb-1 mutant animals, while wild type N2 worms remain not affected at all (Fig. 3.10B). To further confirm peroxisomal effect on these parameters, we depleted prx-5, encoding a protein that is important for the import of peroxisomal proteins. This decreased respiration in both wild type N2 and isp-1;ctb-1 mitochondrial mutant animals (Fig. 3.10 C). Here however, the movement of either worm strain was not affected (Fig 3.10 C).

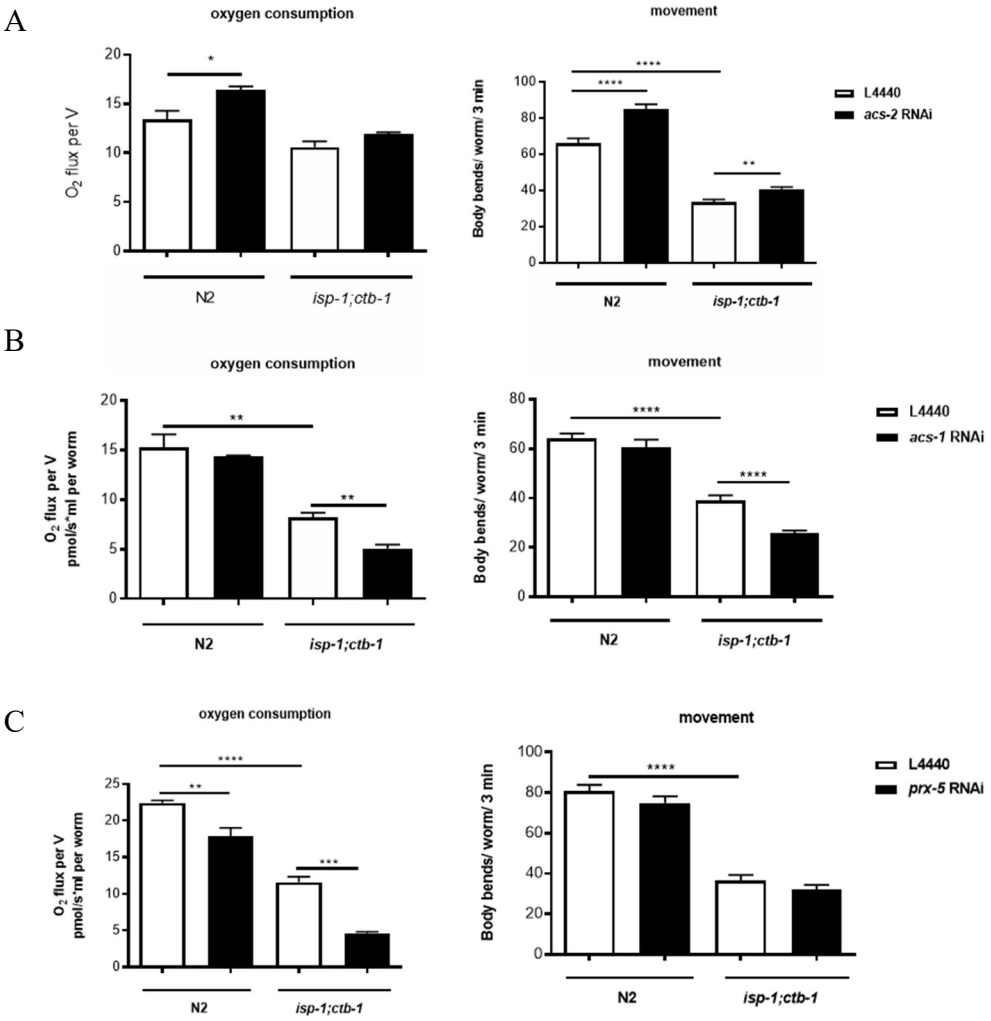

Figure 3.10 Knockdown of peroxisomal genes decrease respiration and movement
Wild type N2 and *isp-1(qm150);ctb-1(qm189)* mutants were treated with RNAi targeting either L4440 or *acs-2*, *acs-1* or *prx-5* gene. 300 animals were assayed per condition for basal respiration and 10 animals were assayed per condition for movement. Oxygen consumption and movement were analyzed on the first day of adulthood (D1). Bars represent mean ± SEM (p*<0.05, p<0.0, p***<0.001; p****<0.0001, Student's test).**

Taken together, depletion of mitochondrial *acs-2* resulted in improved basal respiration and movement, an indicator of health status, of wild type N2 and *isp-1;ctb-1* mutant animals. In contrast, depletion of peroxisomal genes, resulted in a massive decrease of basal respiration in *isp-1;ctb-1* mutant animals and worms move slower and look sicker. These data indicate that mitochondrial mutant worms need intact peroxisomal function for maintaining normal function and fitness.

3.5.4 The *acs-3* depletion results in increased respiration of mitochondrial *isp-1;ctb-1* mutant animals

Since lipid metabolism is strongly coupled to overall energy status, we wanted to see to which extent the increased fatty acid uptake changes observed upon *acs-3* knockdown could affect the metabolic and behavioral parameters of wild type N2 and *isp-1;ctb-1* mutant animals. Firstly, we measured the respiration rate in control conditions and upon *acs-3* knockdown. As expected, *isp-1;ctb-1* mutant animals had decreased respiration in basal conditions that was normalized upon *acs-3* depletion. (Fig 3.11 A). The knockdown of *acs-3* did not have an impact on the wild type N2 animals (Fig. 3.11 A). Remarkably, the lower movement rates in *isp-1;ctb-1* mutant animals remained unchanged, whereas RNAi of *acs-3* leads to raised body bends in the wild type N2 worms (Fig. 3.11 B).

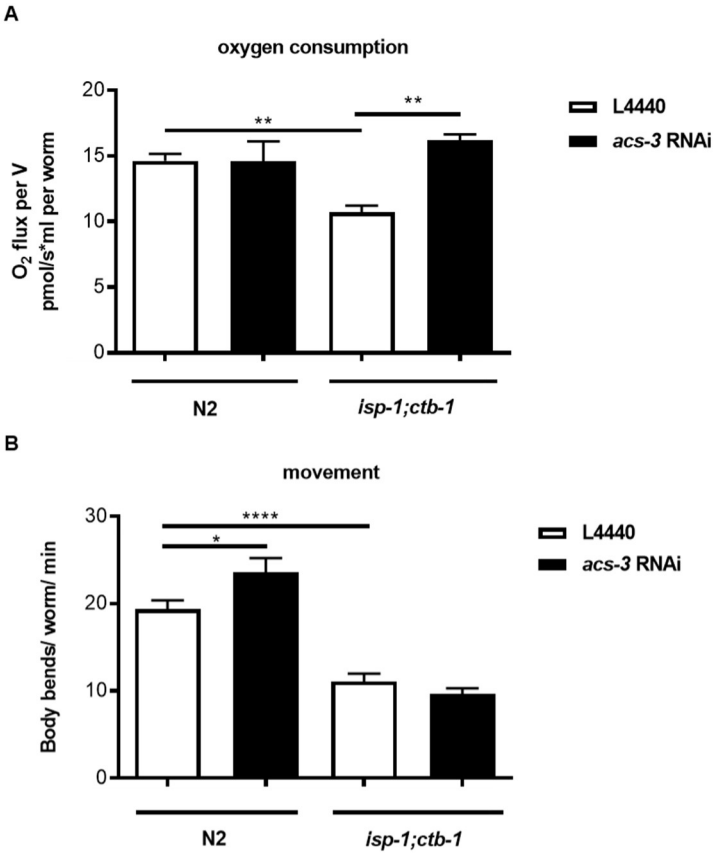

Figure 3.11 Oxygen consumption measurements and movement assay upon *acs-3* knockdown
Wild type N2 and *isp-1(qm150);ctb-1(qm189)* mutants were treated with RNAi targeting *acs-3* gene. Three times 300 animals were assayed per condition for basal respiration and 10 animals were assayed per condition for movement. A) Oxygen consumption and B) movement were analyzed on the first day of adulthood (D1). Bars represent mean ± SEM (p*<0.05, p<0.01, p****<0.0001 Student's test).**

These results indicate that the movement defect could be uncoupled from the mitochondrial respiration rate in *isp-1; ctb-1* mutant animals, questioning our current understanding of cause-consequence in "mit-mutants". However, they should also be taken with caution, as the respiration rate decrease observed in this analysis was not as strong as previously detected, suggesting potential issues with the strain or the analysis, hence should be repeated.

3.5.5 Depletion of peroxisomal genes mediate the longevity of mitochondrial *isp-1;ctb-1* mutant animals

Next, we elucidated the role of Acyl-CoAs ACS-2 and ACS-1 in longevity assurance, of mitochondrial *isp-1;ctb-1* mutant animals compared to wild type N2. In addition to *acs-1*, we included the knockdown of *prx-5* which is required for peroxisomal import (Thieringer et al., 2003). Chlorpromazine (CPZ), a peroxisomal ß-oxidation inhibitor was also used (Weeks et al., 2018). Our results show that peroxisomal genes depletion and CPZ treatment suppressed the long-lived phenotype in the *isp-1;ctb-1* mitochondrial mutant, but do not affect wild type lifespan (Fig. 3.12).

In contrast, the depletion of mitochondrial acyl-CoA synthetase ACS-2 did not show any effect on wild type N2 or *isp-1;ctb-1* mitochondrial mutant lifespan. Therefore, these results demonstrate that peroxisomal lipid metabolism is essential for longevity in mitochondrial mutant animals.

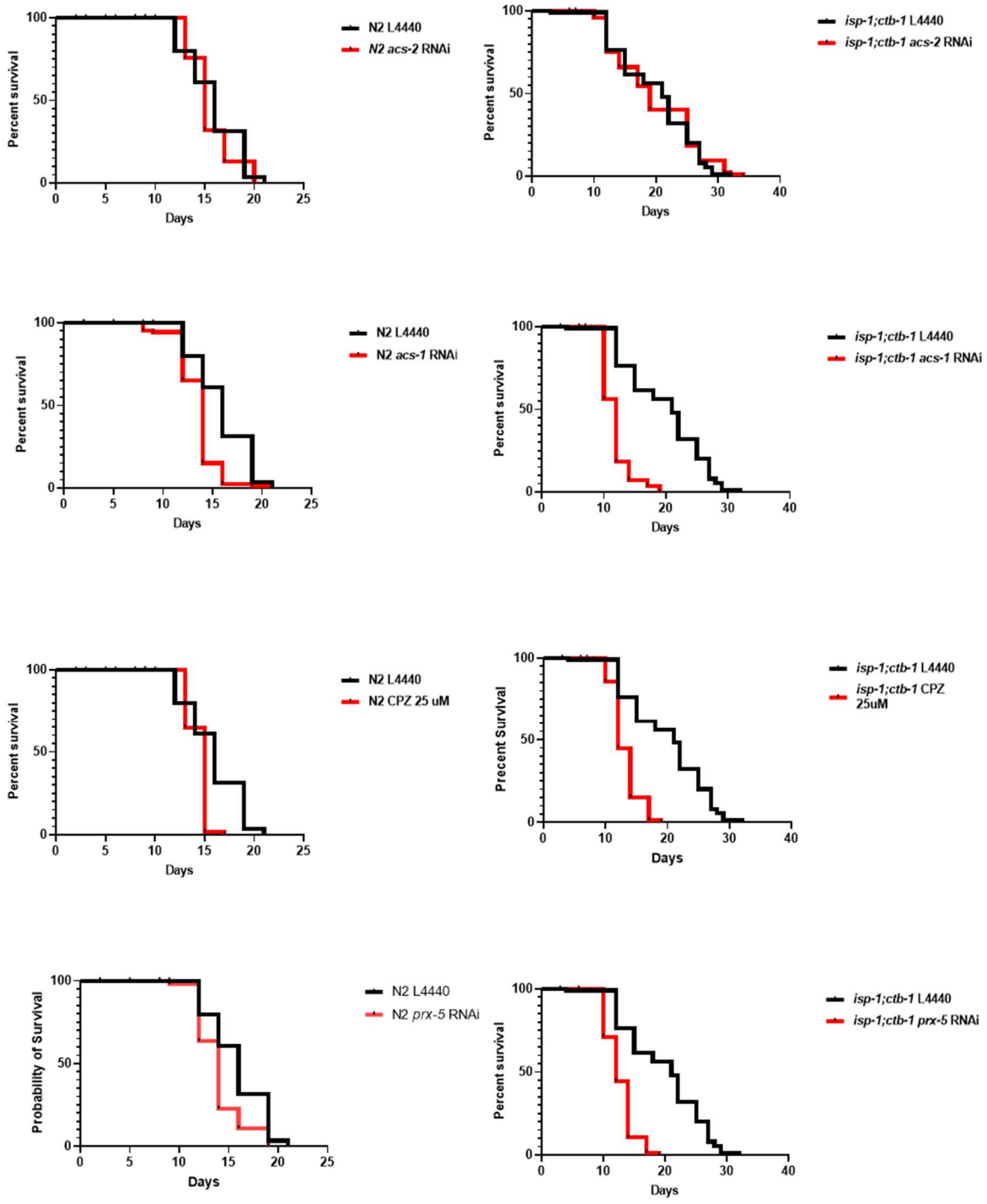

Figure 3.12 Peroxisomal genes suppress the longevity of *isp-1(qm150);ctb-1(qm189)* mutant without affecting the lifespan of the wild type worms. Lifespan curves of wild-type animals (left) and *isp-1(qm150);ctb-1(qm189)* mutant (right) grown their whole life on control L4440 or *acs-2*, *acs-1* and *prx-5* RNAi plates or plates containing 25µM chlorpromazine (CPZ). 100 worms were counted per condition at 25°C.

3.5.6 Depletion of mitochondrial carnitine acyltransferase 1 (CPT-1) improves respiration in mitochondrial *isp-1;ctb-1* mutant

To further elucidate the role of mitochondrial beta-oxidation on the fitness of mitochondrial mutant, we investigated CPT-2 and CPT-1, carnitine palmitoyl transferases which catalyzes the step in long-chain fatty acid import from the cytoplasm into the mitochondrial matrix for further ß-oxidation, and KAT-1, a 3-Ketoacyl-coA thiolase, which catalyzes the last step of mitochondrial fatty acid oxidation (Berdichevsky et al., 2010, Sebastián et al., 2009, Violante et al., 2010).

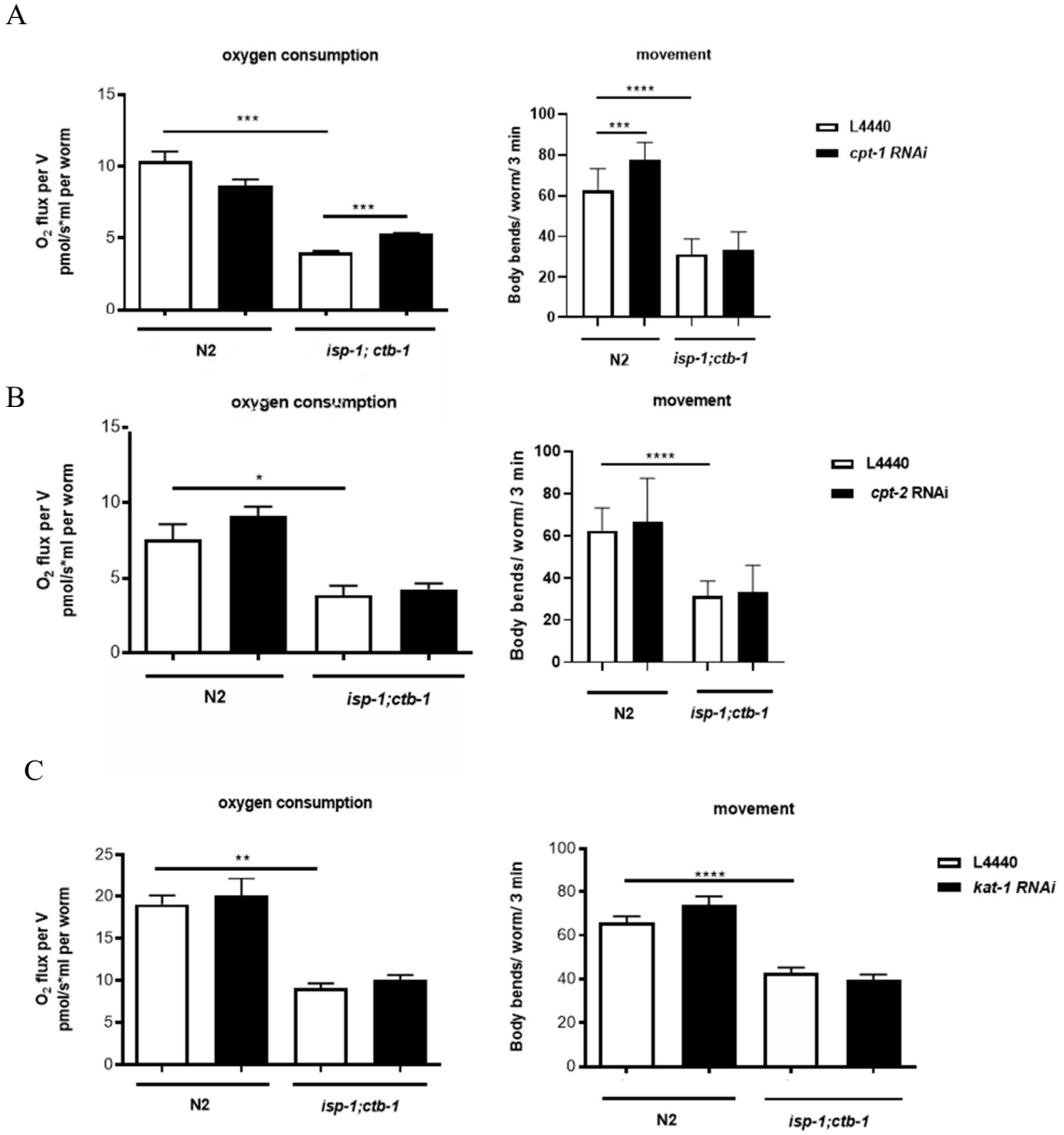

Figure 3.13 Respiration and movement are not affected upon depletion of mitochondrial ß-oxidation genes.

Wild type N2 and *isp-1(qm150);ctb-1(qm189)* mutants were treated with RNAi targeting either L4440 or *cpt-1*, *cpt-2* or *kat-1* gene. 300 animals were assayed per condition for basal respiration and 10 animals were assayed per condition for movement. Oxygen consumption and movement were analyzed on the first day of adulthood. Bars represent mean ± SEM (p*<0.05, p<0.0, p***<0.001; p****<0.0001, Student's test).**

We checked for metabolic and behavioral parameters in wild type N2 and *isp-1;ctb-1* mitochondrial mutant worms on day one of adulthood. Remarkable, if genes encoding proteins involved in mitochondrial ß-oxidation are knocked down, respiration and movement partially increase, or stayed unchanged in wild type N2 and *isp-1;ctb-1* mutant animals (Fig.3.13). The depletion of *cpt-1* leads to enhanced basal respiration in *isp-1;ctb-1* mutant animals. The wild type N2 stays unaffected but shows improved body bends in the movement assay, while the movement of *isp-1;ctb-1* remains constant (Fig. 3.13 A).

The same applies to knockdown of *kat-1*, no changes are detected in the basal respiration and movement of wild type N2 and *isp-1;ctb-1* mitochondrial mutant (Fig. 3.13 C). This in agreement with our previous results obtained upon *acs-2* depletion, suggesting that downregulation of mitochondrial fatty acid oxidation has a beneficial effect on *isp-1;ctb-1* mutant animals (Fig. 3.13 B).

3.5.7 ACS-2 enhances and ACS-1 depreciates triglyceride levels in mitochondrial *isp-1;ctb-1* mutant animals

Next, we quantified triglyceride levels of wild type worms N2 and *isp-1;ctb-1* mutant animals on control (L4440), or plates containing RNAi targeting either *acs-2*, and *acs-1* gene. Figure 3.14 shows that in *isp-1;ctb-1* mutant worms the triglyceride levels increased significantly after the depletion of *acs-2*. Intriguingly, *acs-1* RNAi shows the opposite effect and leads to a further decrease in triglycerides levels. These results go hand in hand with the lower take up of fatty acids (Fig. 3.9). Wild type N2 did not show any difference in all tested conditions (Fig. 3.14).

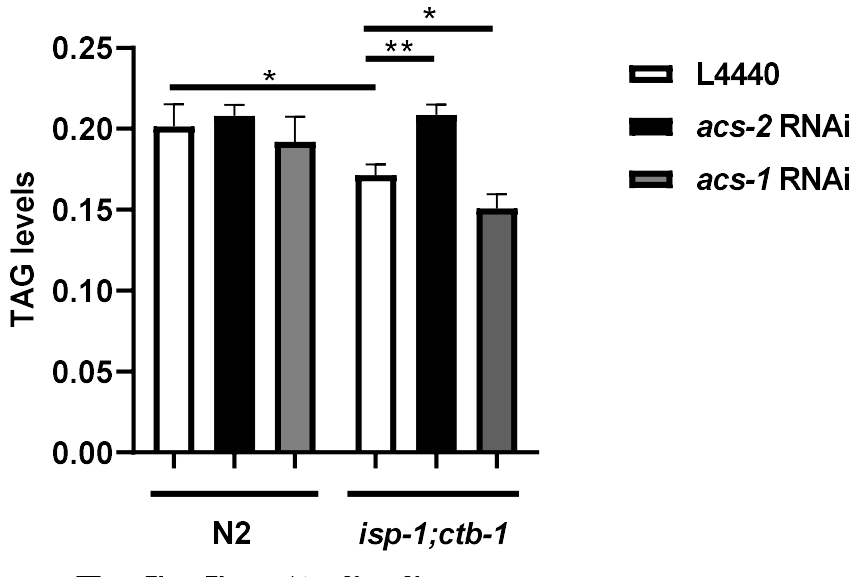

Figure 3.14 Mitochondrial *isp-1;ctb-1* mutants reveal decreased TAG levels upon *acs-1* depletion
Wild type N2 and *isp-1(qm150);ctb-1(qm189)* mutants were treated with RNAi targeting L4440 or *acs-2* or *acs-1* gene. On day one of adulthood Enzychrome™ Triglyceride assay kit was used to determine triglyceride levels. 1000 worms per condition were used. Bars represent mean ± SEM (p*<0.05, p<0.01, Student's T-test).**

3.6 Investigation of behavioral parameters in peroxisomal mutant animals

3.6.1 Respiration decreases in peroxisomal mutant *pmp-4(ok396)* and *daf-22(ok693)*

Thus far, our results reveal that knocking down peroxisomal genes in mitochondrial *isp-1;ctb-1* mutant resulted in a shorter lifespan, decreased respiration and movement. To further dissect the peroxisomal role in the context of mitochondrial dysfunction, we used mutant strains: *pmp-4*(ok396) (peroxisomal membrane protein) and *daf-22*(ok693) (peroxisomal ß-oxidation protein). Here we again tested metabolic and behavioral parameters to determine if reciprocally, also peroxisomal mutants depend on mitochondrial function.

Therefore, we treated our peroxisomal *pmp-4* and *daf-22* mutants with RNAi targeting the *cyc-1* gene. *Cyc-1* encodes the cytochrome c reductase, a component of complex III of the electron transport chain and its depletion increases longevity in *C. elegans* (Cristina et al., 2009). This is important to understand if the effect of peroxisomal fatty acid oxidation is universal for mitochondria dysfunction or is specific for our *isp-1,ctb-1* mutant strain.

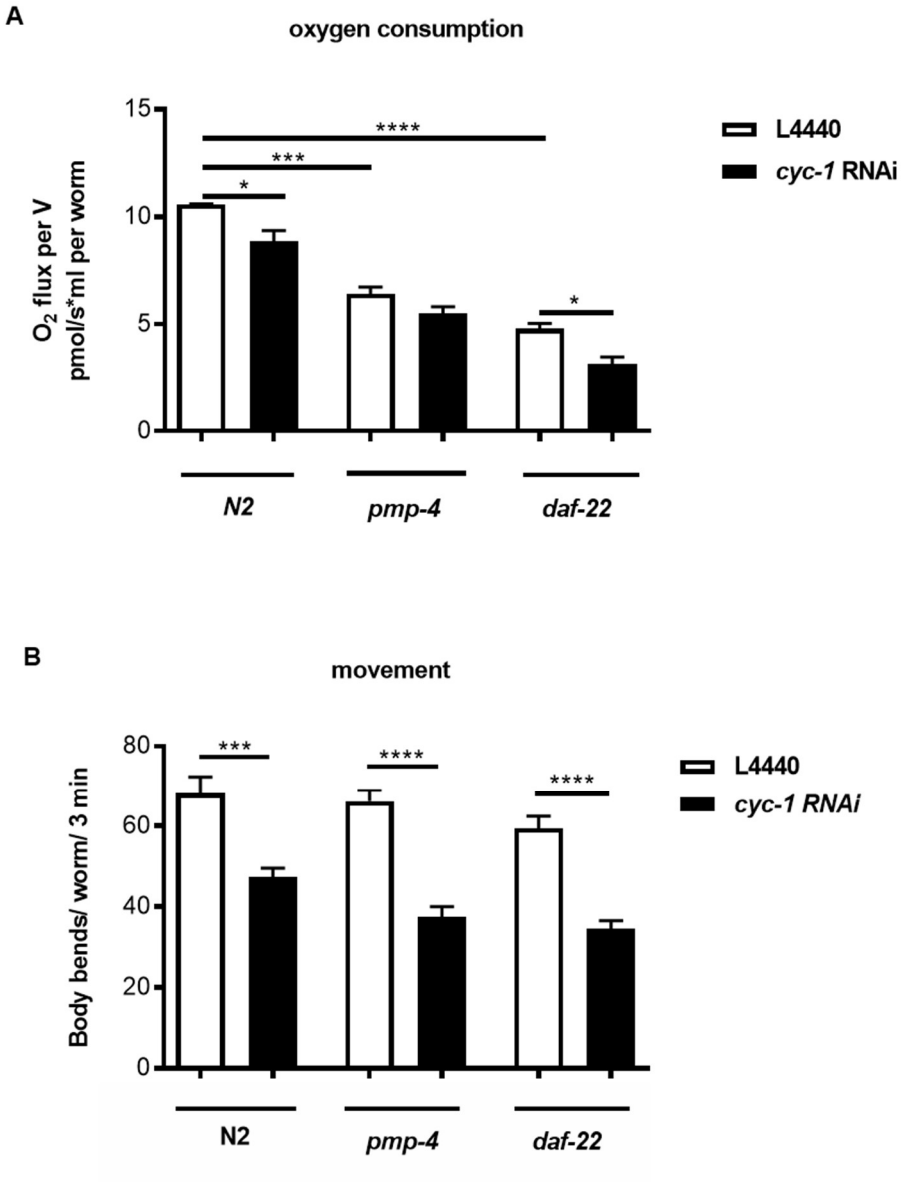

Figure 3.15 Oxygen consumption and movement of peroxisomal *pmp-4(ok396)* and *daf-22(ok693)* mutants
Wild type N2 and *pmp-4(ok396)* and *daf-22(ok693)* mutants were treated with RNAi targeting either L4440 or *cyc-1* gene. 300 animals were assayed per condition for basal respiration and 10 animals were assayed per condition for movement. A) Oxygen consumption and B) movement were analyzed on the first day of adulthood (D1). Bars represent mean ± SEM (p*<0.05, p*<0.001; p****<0.0001, Student's test).**

Interestingly, basal respiration was significantly and strongly impaired in peroxisomal *pmp-4* and *daf-22* mutants compared to wild type N2 worms even in control conditions (Fig. 3.15 A). The depletion of *cyc-1* has influenced the basal respiration of both wild type N2 and peroxisomal *daf-22* mutant significantly, while *pmp-4* peroxisomal mutant just displays a mild, not significant decrease in basal respiration (Fig. 3.15 A). The decrease in

the respiration was not reflected in the change of movement in both strains on the first day of adulthood (Fig. 3.15 B). However, upon *cyc-1* RNAi the movement rate declined strongly in all strains, as shown in Figure 3.15 B.

3.7 Determination of peroxisomal dynamics

3.7.1 Peroxisomal mass in intestinal cells is increased after depletion of mitochondrial electron transport chain genes *cyc-1* and *cco-1*

We next sought to further understand the importance of peroxisomes in mitochondrial dysfunction. To visualize peroxisomes, we used a strain expressing *gfp* with a peroxisomal targeting sequence PTS1, under gut specific *ges-1* promotor. This strain has been shown to be useful in observing and estimating the changes in peroxisomal network upon different external and internal stimuli (Weir et al., 2017). To examine the changes in peroxisomal dynamics upon mitochondrial dysfunction, worms were treated with either L4440 or RNAi targeting mitochondrial electron transport chain *cyc-1* (UQCR4 subunit of complex III – cytochrome C reductase) and *cco-1* (COX5B subunit of complex IV – cytochrome C oxidase) genes. Additionally, worms were exposed to Antimycin A (inhibitor of complex III).

In Figure 3.16 A images of the different conditions are shown. Although size of peroxisomal vesicle did not change significantly upon different conditions we detected a significant increase in the peroxisomal numbers, shown as the number of vesicles, in long-lived models of mitochondrial dysfunction triggered by *cyc-1*- and *cco-1* depletion (Fig. 3.16 B). Mitochondrial dysfunction caused by treatment with complex III inhibitor antimycin A, also increased peroxisomal amount (Fig. 3.16 B).

Further confirmation of these results came from the analysis of GFP levels on the Western blot. Worms were again treated either with L4440, *cyc-1*, *cco-1*, antimycin A and this time also with hydrogen peroxide (H_2O_2). Interestingly, Western blot analysis did not show any change in the GFP levels upon either drug treatment (Fig. 3.16 C). When genes of mitochondrial electron transport chain *cyc-1* and *cco-1* were depleted, we detected a stronger GFP signal (Fig. 3.16 C), suggesting a link between mitochondrial dysfunction and changes in peroxisomal dynamics.

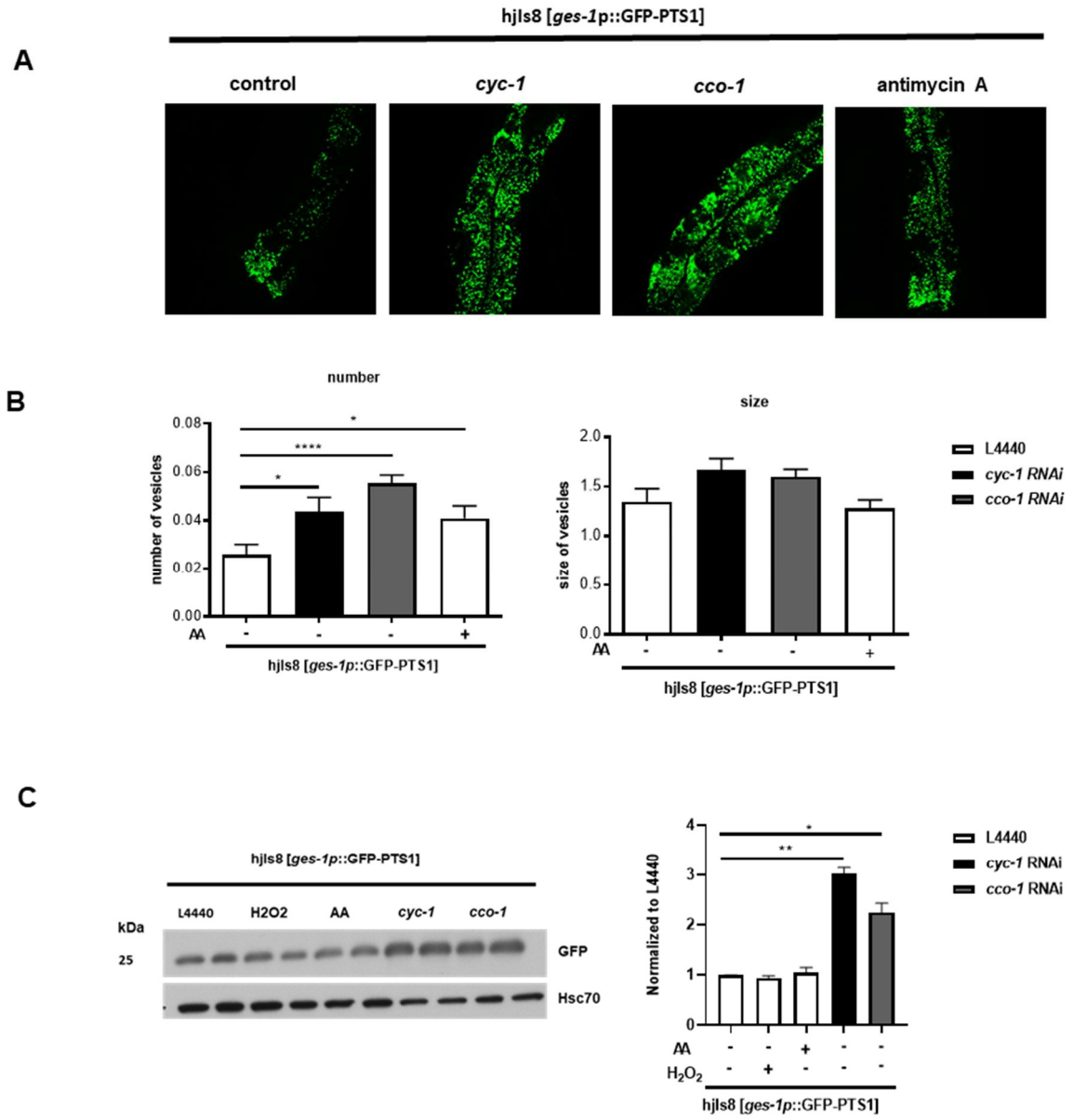

Figure 3.16 Number and size of peroxisomes in *C. elegans* intestinal cells

A) Representative fluorescent images of a strain expressing *gfp* under the *ges-1* promoter. Animals were treated with either L4440 or RNAi targeting *cyc-1* and *cco-1* gene or Antimycin A and imaged by Meta 710 confocal microscope (Zeiss) with a 20x objective on the first day of adulthood. B) Quantification of the number and size of peroxisomes in intestinal cells and C) protein levels of GFP in intestinal cells in *C. elegans*. The number and size of peroxisomes and blots were analyzed by ImageJ. Bars represent mean ±SEM (p*<0.05, p<0.01, p****<0.0001, Student's T-test).**

3.8 Determining the lipid droplet mass

3.8.1 Number and size of lipid droplets decline after *acs-1* depletion

The major storage compartments of lipid droplets are intestine, hypodermis, oocytes, and embryos in *C. elegans*. In Fig. 3.17 A , we quantified lipid droplets after depleting mitochondrial and peroxisomal acyl-CoA synthase *acs-2* and *acs-1,* respectively. In wild type N2 and *isp-1;ctb-1* mutant animals, we determined number and size of lipid droplets by BodiPY 493/503 staining.

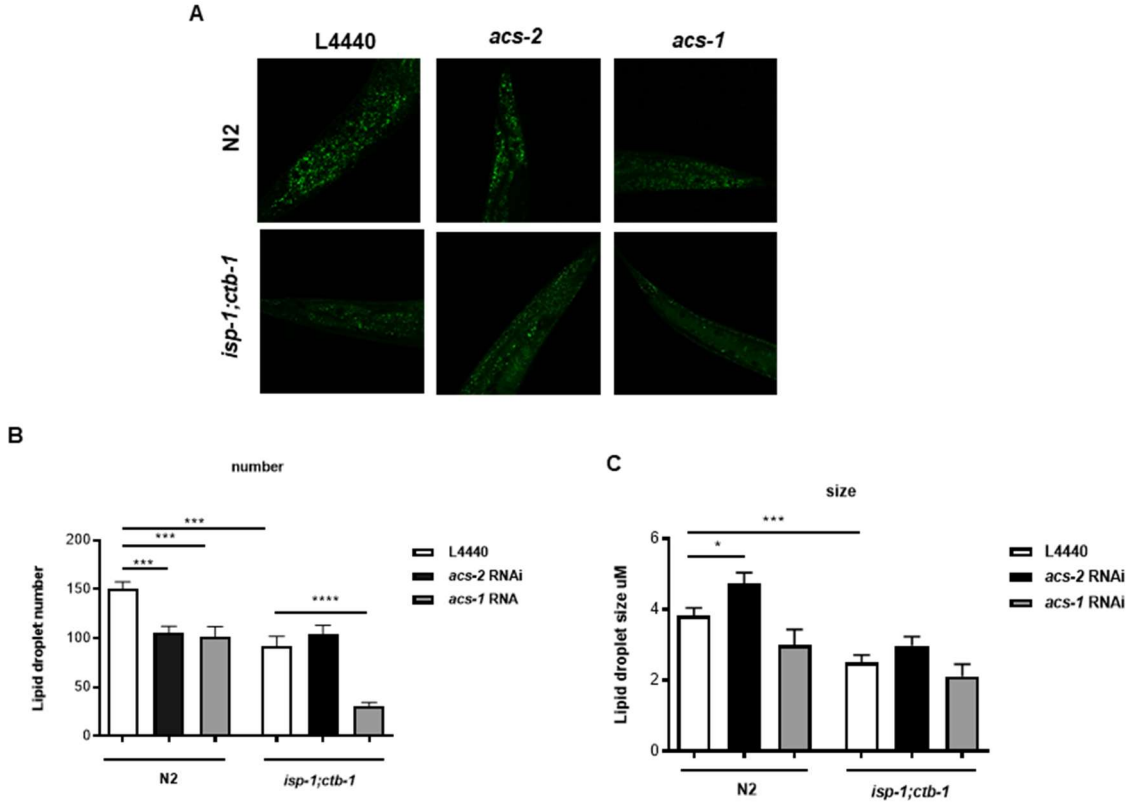

Figure 3.17 Lipid droplets number and size upon *acs-2* and *acs-1* knockdown.
Wild type N2 and *isp-1(qm150);ctb-1(qm189)* mutants were treated with either L4440 control or RNAi targeting *acs-2* and *acs-1* gene and A) imaged by Meta 710 confocal microscope (Zeiss) with a 20x objective.
B) Quantification of the number and C) the size of lipid droplets were analyzed by ImageJ. Bars represent mean ±SEM (p*<0.05, p*<0.001; p****<0.0001, Student's T-test)**

As expected, *isp-1;ctb-1* mutant animals had a smaller amount of lipid droplets compared to wild type N2 (Fig. 3.17 B). In wild type N2 worms, depletion of either *acs-1* or *acs-2* resulted in 30% decrease in the number of lipid droplets, although the size was differentially affected by either RNAi treatment. (Fig. 3.17B). In the *isp-1;ctb-1* mutant depletion of *acs-2* resulted

in mild, but not significant change in the number of lipid droplets (Fig 3.17 B). Blocking of *acs-1* lead to a dramatic, 75% loss of the number of lipid droplets in *isp-1;ctb-1* mitochondrial mutant animals (Fig 3.17 B). The size of lipid droplets was not significantly affected in *isp-1;ctb-1* mitochondrial mutant by depletion of either enzyme (Fig 3.17 B and C). Taken together, our results show that the acyl-CoA synthetase ACS-1 is important for *C. elegans* to generate lipid droplets.

3.8.2 Lipid droplets number and size increase upon *acs-3* depletion

To understand if the increased lipid uptake affects levels of lipids in tissues, we used BodiPY 493/503 to stain lipid droplets in wild type N2 and mitochondrial *isp-1;ctb-1* mutant animals, to investigate the number and size of vesicles. After treatment with either control L4440 or RNAi targeting *klf-1* or *acs-3* gene, animals were imaged by Meta 710 confocal microscopy, on day one of adulthood. Representative images are seen in Figure 3.18 A. We observed more and larger lipid droplets in *isp-1;ctb-1* mutant worms upon *klf-1* and *acs-3* knockdown (Fig 3.18 B).

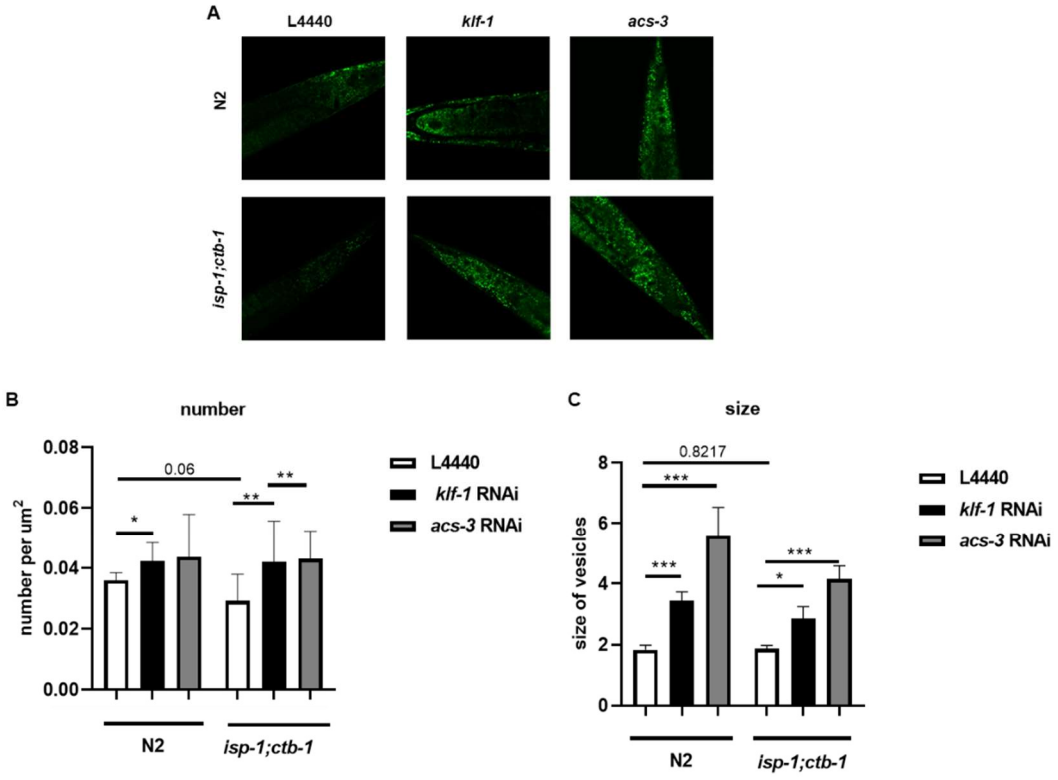

Figure 3.18 The *acs-3* depletion affects lipid droplets number and size

Wild type N2 and *isp-1(qm150);ctb-1(qm189)* mutants were treated with RNAi targeting *klf-1* and *acs-3* gene and A) imaged on day one of adulthood by Meta 710 confocal microscope (Zeiss) with 20x objective. B) The number of lipid droplets per animal and C) the size of vesicles per animal were analyzed by ImageJ. Bars represent mean ±SEM (p*<0.05, p<0.01, Student's T-test).**

The number of lipid droplets of wild type N2 animals significantly changed upon *klf-1* and their size increased upon both *klf-1* and *acs-3* depletion (Fig. 3.18 B and C).
These results provide a strong argument that higher lipid uptake upon depletion of ACS-3 increases size and number of LDs in both, wild type N2 animals and *isp-1;ctb-1* mutant animals and leave open question if ACS-3 might play further role in the regulation of lipid droplet morphology.

3.8.3 *Acs-3* enhances triglyceride levels in mitochondrial *isp-1;ctb-1* mutant animals

We could further confirm our previous results (Fig. 3.18), using the Triglyceride Assay Kit (Fig. 3.19). Taken all together, knockdown of both *acs-3* or *acs-2* improved number and size of the lipid droplets, as well as the uptake of fatty acids in the mitochondrial *isp-1;ctb-1* mutant.

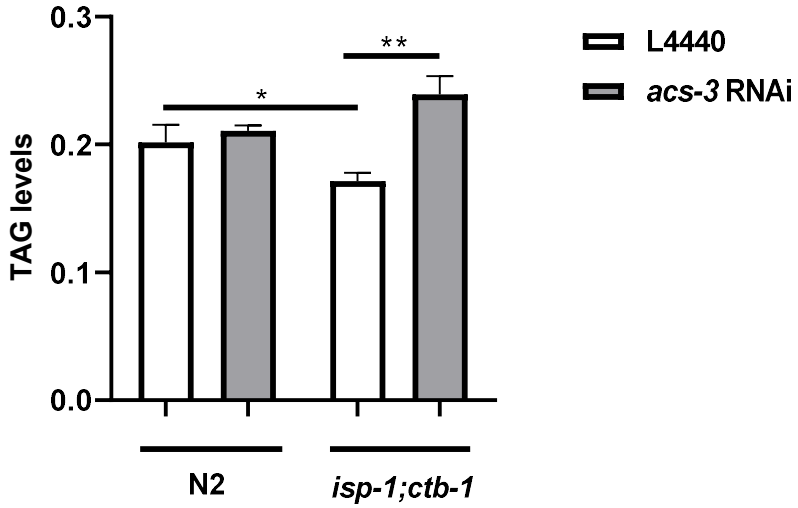

Figure 3.19 Knockdown of *acs-3* leads to increased triglyceride levels in *isp1;ctb-1* mitochondrial mutants

Wild type N2 and *isp-1(qm150);ctb-1(qm189)* mutants were treated with RNAi targeting either L4440 or *acs-3* gene. On day one of adulthood Enzychrome™ Triglyceride Assay kit was performed to determine Triglyceride levels. 1000 worms were used for each condition. Bars represent mean ±SEM (p*<0.05, p<0.01, Student's T-test).**

However, this effect seems to be specific for the mitochondrial mutant, since the same phenotype was not observed in the wild type N2 animals (Fig. 3.19).

3.9 Quantification of the level of lipid peroxidation

3.9.1 Depletion of *acs-2* and *acs-1* leads to elevated lipid peroxidation in mitochondrial *isp-1;ctb-1* mutant worms

Reactive oxygen species (ROS) are produced by normal physiological processes and play important roles in cell signaling and tissue homeostasis (Su et al., 2019). ROS damage various cellular components like lipids, proteins, and DNA, and are involved in cancer, cardiovascular disease, neurodegenerative disorders and aging (Su et al., 2019).

The *isp-1;ctb-1* mutant animals have increased mitochondrial ROS (mtROS) levels due to their deficiency in complex III, which causes a decreased electron flow through respiratory complex III. Excessive ROS can lead to oxidative damage, that further leads to peroxidation, mainly of membrane lipids, through a process named lipid peroxidation (Kwiecien et al., 2014).

To monitor lipid peroxidation levels, we used BodiPY C11 dye and stained wild type N2 and *isp-1;ctb-1* mutant animals after treatment with either L4440 control or with RNAi targeting *acs-2* and *acs-1* genes on day one of adulthood. Images were taken by Meta 710 confocal microscope (Zeiss) (Fig 3.20 A). The ratio between green- and red channel were used to quantify oxidized lipids. Depletion of *acs-2* and especially *acs-1* lead to a massive upregulation of oxidized lipids, in *isp-1;ctb-1* mutant animals (Fig. 3.20 B).

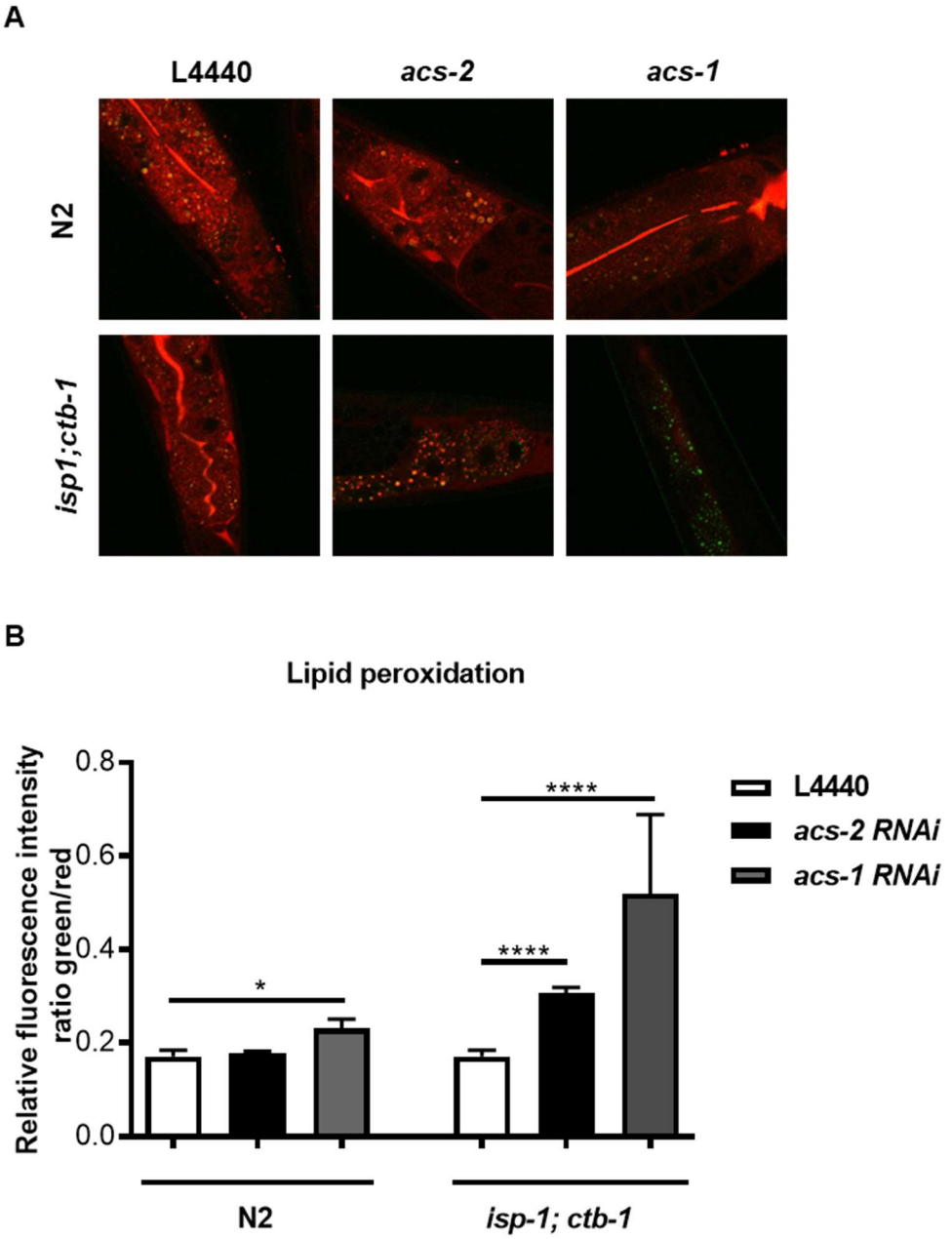

Figure 3.20 Lipid peroxidation increases in *isp-1(qm150);ctb-1(qm189)* mutant upon *acs-1* RNAi
Wild type N2 and *isp-1(qm150);ctb-1(qm189)* mutants were treated with RNAi targeting either L4440 or *acs-2*, *acs-1* gene. On the first day of adulthood worms were feeding with the fluorescence dye BodiPY C11 for one hour in the dark and A) Representative images by Meta 710 confocal microscope (Zeiss) with a 20x objective.
B) The quantification of the ratio between green and the red channel was determined by using ImageJ.
Bars represent mean ±SEM (p*<0.05, p**<0.0001, Student's T-test).**

3.9.2 Peroxisomal mutant animals show elevated lipid peroxidation after *cyc-1* depletion

We show that in particular depletion of peroxisomal acyl-CoA synthase *acs-1* resulted in massive upregulation of oxidized lipids, in *isp-1;ctb-1* mutant animals. To investigate if peroxisomal dysfunction on its own leads to increased lipid peroxidation we repeated the staining for lipid peroxidation in our mutants *pmp-4(ok396)* and *daf-22(ok693)* and wild type N2 upon in control conditions or *cyc-1* depletion. While the peroxisomal mutant animals do not show any increase in lipid peroxidation on its own, the depletion of *cyc-1* revealed the strong upregulation of oxidized lipids in both, peroxisomal mutant animals, but also wild type N2 (Fig. 3.21).

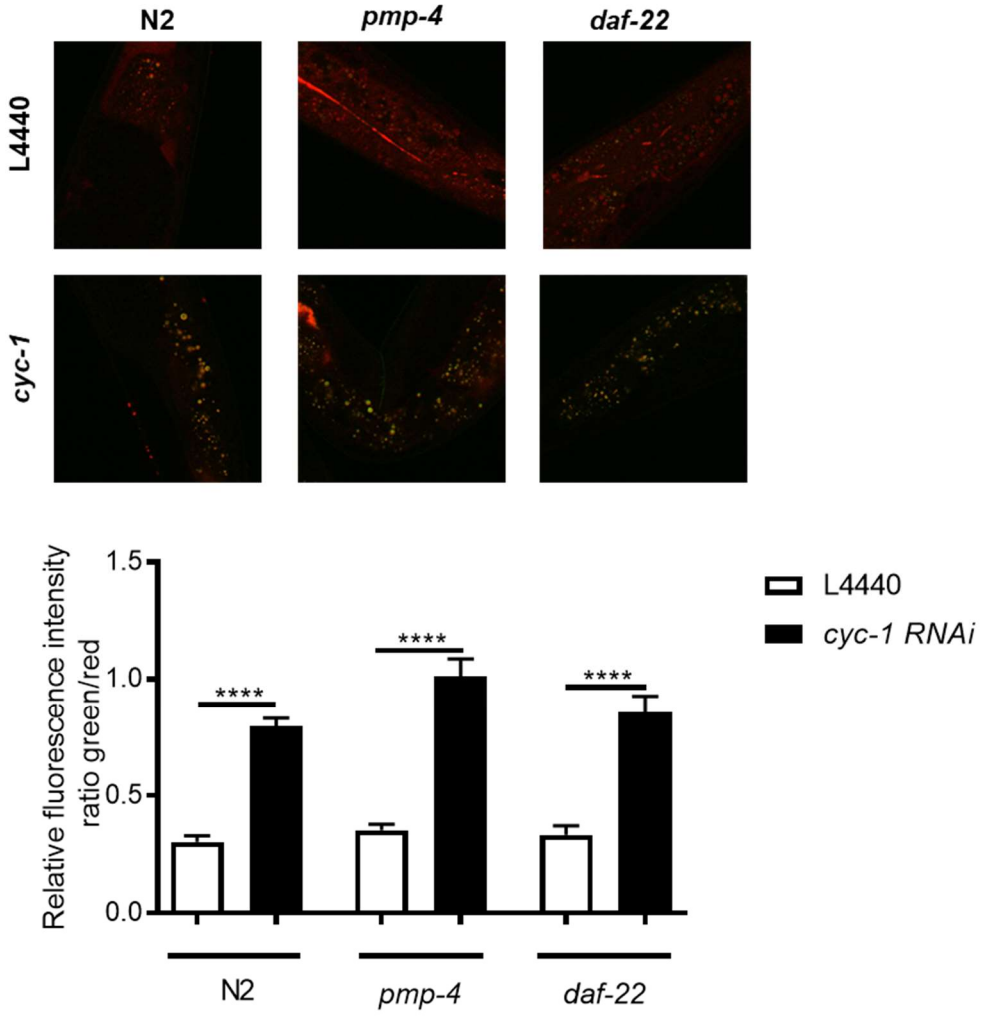

Figure 3.21 Lipid peroxidation in peroxisomal mutants *pmp-4(ok396)* and *daf-22(ok693)*

Wild type N2 and peroxisomal mutants *pmp-4* and *daf-22* were treated with RNAi either targeting the L4440 or *cyc-1* gene. On day one of the adulthood worms were feeding with the fluorescence dye BodiPY C11 and were imaged by Meta 710 confocal microscope (Zeiss) with a 20x objective. The quantification of the ratio between green and the red channel was determined by using ImageJ. Bars represent mean ±SEM (p**<0.0001, Student's T-test).**

3.9.3 4-Hydroxynonenal levels are not changed in *isp-1;ctb*-1 mutant animals

Aldehydes like 4-hydroxynonenal (4-HNE) and malondialdehyde (MDA), are the major class of lipid peroxide degradation products (Kwiecien et al., 2014). The 4-HNE levels were detected by Western blotting in wild type N2 and *isp-1;ctb-1* mutant animals, in control conditions, and upon treatment with *acs-2* and *acs-1* RNAi (Fig. 3.22). Although the Western blot analysis suggested that there might be an increase in 4-HNE signal upon deletion of *acs-1,* in both wild type N2 and *isp-1;ctb-1* mutant animals (Fig. 3.22 A) further quantification did not confirmed this initial observation (Fig. 3.22 B).

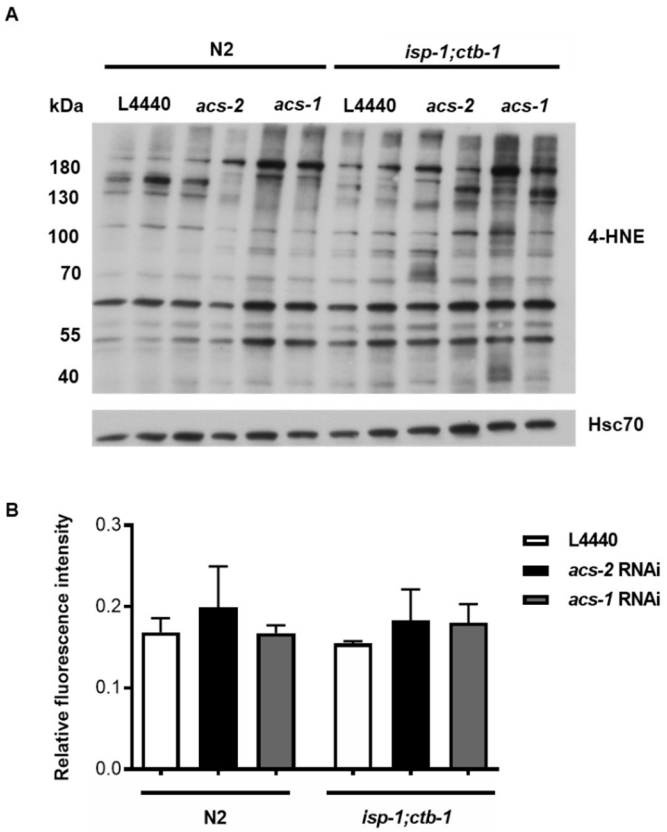

Figure 3.22 4-Hydroxynonenal levels in wild type N2 and *isp-1(qm150);ctb-1(qm189)* mutant
Wild type N2 and *isp-1(qm150);ctb-1(qm189) mutants* were treated with either L4440 or RNAi targeting *acs-2* and *acs-1* gene. On day one of adulthood protein pattern was analyzed by ImageJ. A) 4-HNE protein levels determined by western blot. B) Quantification of protein levels. Bars represent mean ±SEM.

3.9.4 Enhanced 4-Hydroxynonenal levels in peroxisomal mutant animals

To investigate level of 4-HNE in peroxisomal FAO mutants we again used the *pmp-4(ok396)* and *daf-22(ok693)* mutant animals. Worms were treated with either control L4440 or RNAi targeting *cyc-1* gene, and proteins were isolated at day one of adulthood. This analysis showed elevated 4-HNE levels in peroxisomal mutant animals already in control conditions (Fig. 3.23 A). The *cyc-1* depletion caused further increase in 4-HNE levels in all strains, with stronger effect in peroxisomal mutant animals (Fig. 3.23 A). Since we just ran two samples per condition to visualize it on one blot, we could not do proper statistics, but the blot reflect the trend seen in the 4-HNE protein pattern (Fig. 3.23 B).

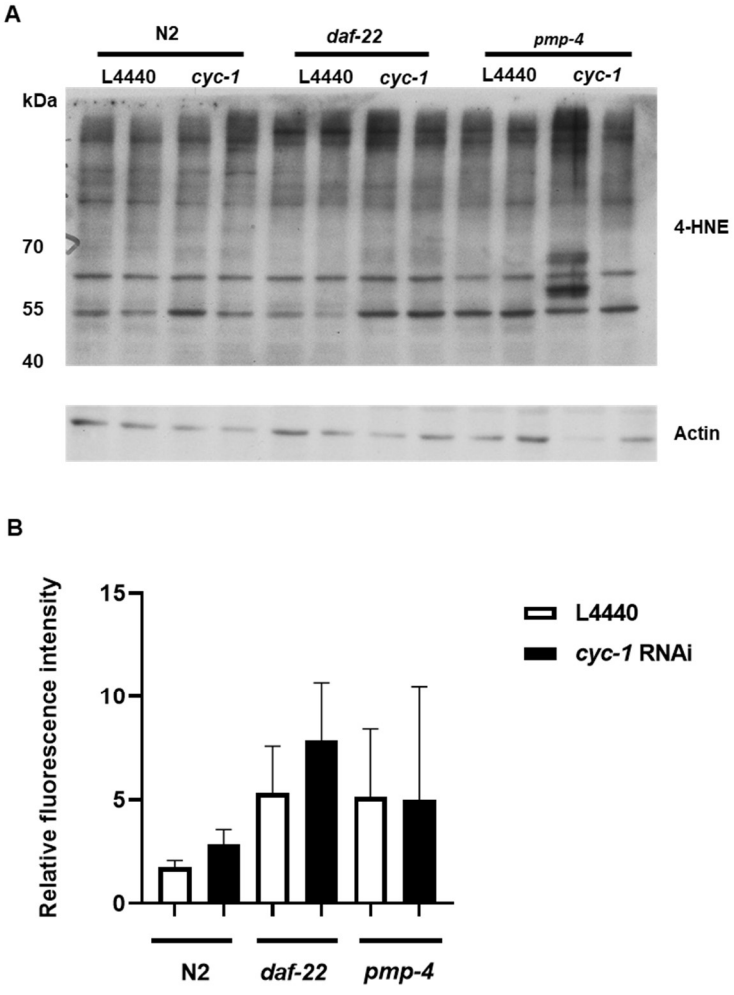

Figure 3.23 4-Hydroxynonenal levels in wild type N2 and peroxisomal mutants *pmp-4(ok396)* and *daf-22(ok693)*
Wild type N2 and peroxisomal *pmp-4(ok396)* and *daf-22(ok693)* mutants were grown on NGM plates containing RNAi targeting L4440 or *cyc-1* gene. On day one of adulthood protein levels were analyzed by ImageJ.
A) 4-HNE protein pattern by western blot. Actin was used as a control. B) Quantification of pattern levels. Bars represents mean ±SEM.

3.9.5 Vitamin E reverses upregulation of oxidized lipids in mitochondrial *isp-1;ctb-1* mutant animals

Previous studies described that a soluble form of antioxidant Vitamin E, called α-tocopherol, protects against H_2O_2 induced lipid peroxidation (Kwiecien et al., 2014). Therefore, we tested this by growing wild type N2 and *isp1;ctb-1* mutant worms on NGM plates containing 200ul/ml Vitamin E. Young adult worms at first day of adulthood were grown in either control conditions or upon RNAi against *acs-1*, stained with the lipid peroxidation sensor BodiPY C11. Animals were imaged by confocal microscope and lipid peroxidation levels were quantified by ImageJ software. Our results confirm that the depletion of *acs-1* leads to the substantial upregulation of oxidized lipids that can be fully corrected by addition of Vitamin E (Fig. 3.24)

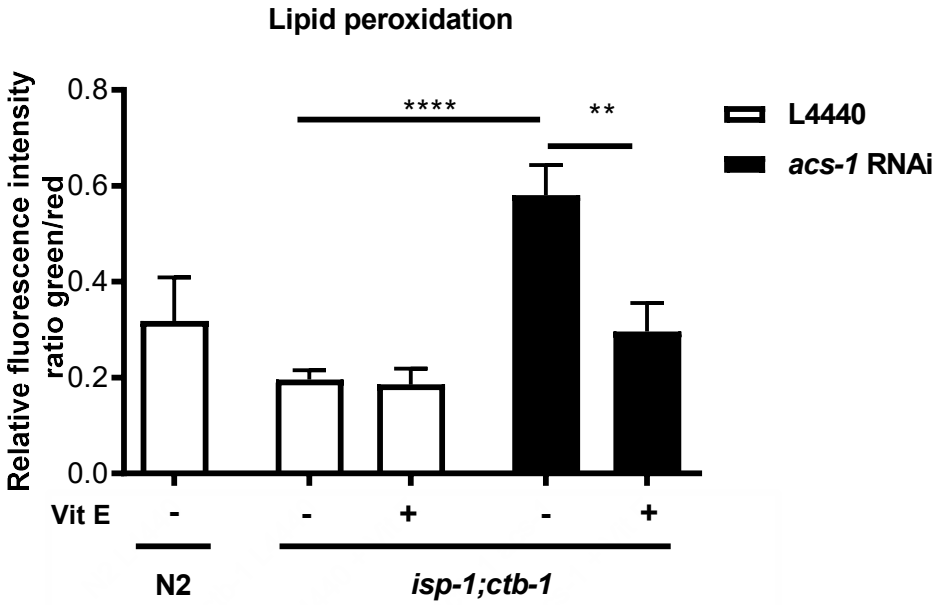

Figure 3.24 Lipid peroxidation upon Vitamin E treatment

Wild type N2 and *isp-1(qm150);ctb-1(qm189)* mutants were grown on NGM plates containing RNAi targeting L4440 or *acs-1* gene ± 200 ul/ ml Vitamin E. On day one of the adulthood worms were feeding with the fluorescent dye BodiPY C11 and were imaged by Meta 710 confocal microscope (Zeiss) with a 20x objective.

The ratio between green and the red channel was determined by using ImageJ. Bars represent mean ±SEM (p<0.01, p****<0.0001), Student's T-test.**

3.10 Investigation of oxidative damage

3.10.1 *isp-1;ctb-1* mutant shows specific ROS increase upon *acs-2* depletion

To test if increased level of lipid peroxidation is a product of increased ROS production we first tested if *acs-1* or *acs-2* depletion influence ROS production in *isp-1;ctb-1* mutant animals.

MitoTracker Red CMH2XROS is a reduced, nonfluorescent dye that fluoresces upon oxidation. We used this dye as a marker for mitochondrial ROS (mtROS) production. Day one old wild type and *isp-1;ctb-1* animals were used and stained. As we previously reported (Herholz et al., 2019), due to hormetic effect of KLF-1 activation, *isp-1;ctb-1* worms show decreased ROS levels (although in this case not significant due to high variation in control animals) (Figure 3.25). Remarkably, upon depletion of *acs-2*, *isp-1;ctb-1* mutants showed increased mtROS levels, while *acs-1* showed no effect (Fig. 3.25).

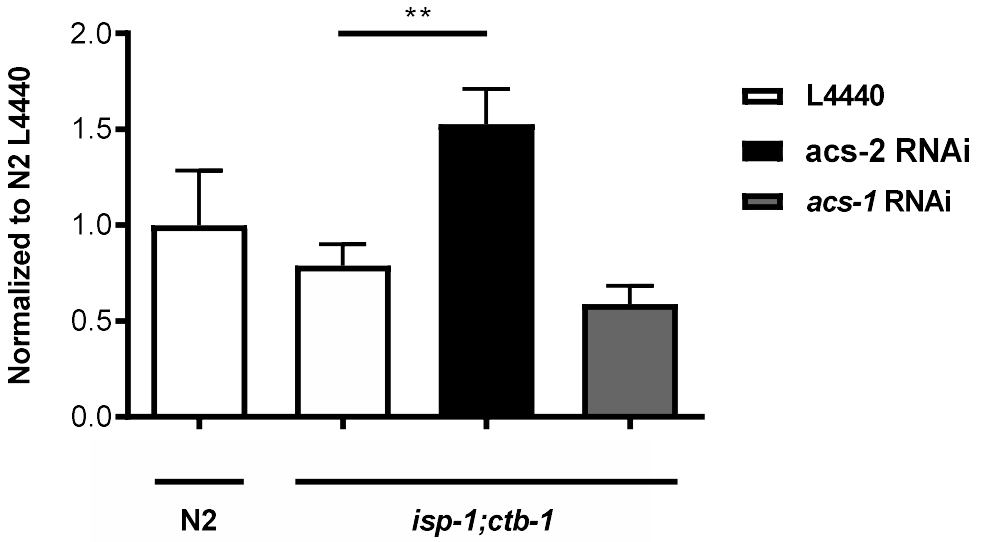

Figure 3.25 Mitochondrial ROS increases upon *acs-2* RNAi
Wild type N2 and *isp-1(qm150);ctb-1(qm189)* mutants were grown on NGM plates containing RNAi targeting L4440 or *acs-1* gene. On day one of the adulthood worms were fed with bacteria containing the dye Mitotracker red CM-H(2)XROS and imaged by AxioImager.Z1 (Zeiss) on a 5x objective. Bars represent mean ±SEM (p<0.01, Student's T-test).**

3.10.2 ACS-1 does not affect mitochondrial *isp-1;ctb-1* mutants cytosolic H_2O_2 and redox potential

We further determined the origin of the oxidative stress signal. Back and coworkers established *Caenorhabditis elegans* strains carrying the genetically encoded fluorescent biosensors HyPer for the detection of hydrogen peroxide (H_2O_2) and Grx1-roGFP2 for detection of the glutathione redox potential (Back et al., 2012). Hyper is a peroxide specific sensor protein. When Hyper interacts with H_2O_2, it passes through a conformational change resulting in a ratio matric shift (Back et al., 2012). If there is an increase in peroxide levels, one can monitor the oxidation/reduction ratio and quantify the cytosolic H_2O_2 production. Worms were grown on NGM plates containing RNAi targeting the L4440 or *acs-1* gene. On day one of the adulthood animals were imaged by Meta 710 confocal microscope (Zeiss) with a 20x objective. We observed that in the *isp-1;ctb-1* mutant animals compared to wild type N2 worms show reduced levels of cytosolic H_2O_2 in control conditions (Fig. 3.27A). This appears to be ACS-1 independent.

For the glutathione redox potential, we used the Grx1-roGFP2 reporter. As mentioned Grx1-roGFP2 is a radiometric biosensor that specifically detects GSH redox potential. On the other hand, Glutathione is an antioxidant peptide and several GSH-linked antioxidant enzymes catalyze the reduction of H_2O_2 by using Glutathione as the donor (Back et al., 2012). However, we found that oxidized/ reduced ratio was increased in *isp-1;ctb-1* mutant animals compared to wild type N2 (Fig. 3.26 B). We could not notice a change in reduced levels of cytosolic H_2O_2 nor differences in the GSH redox potential levels in the mitochondrial *isp-1;ctb-1* mutant after depletion of peroxisomal acyl-CoA synthase 1. These suggest, that even though GSH redox potential levels in the mitochondrial *isp-1;ctb-1* mutant are changed, this seems to be *acs-1* independent.

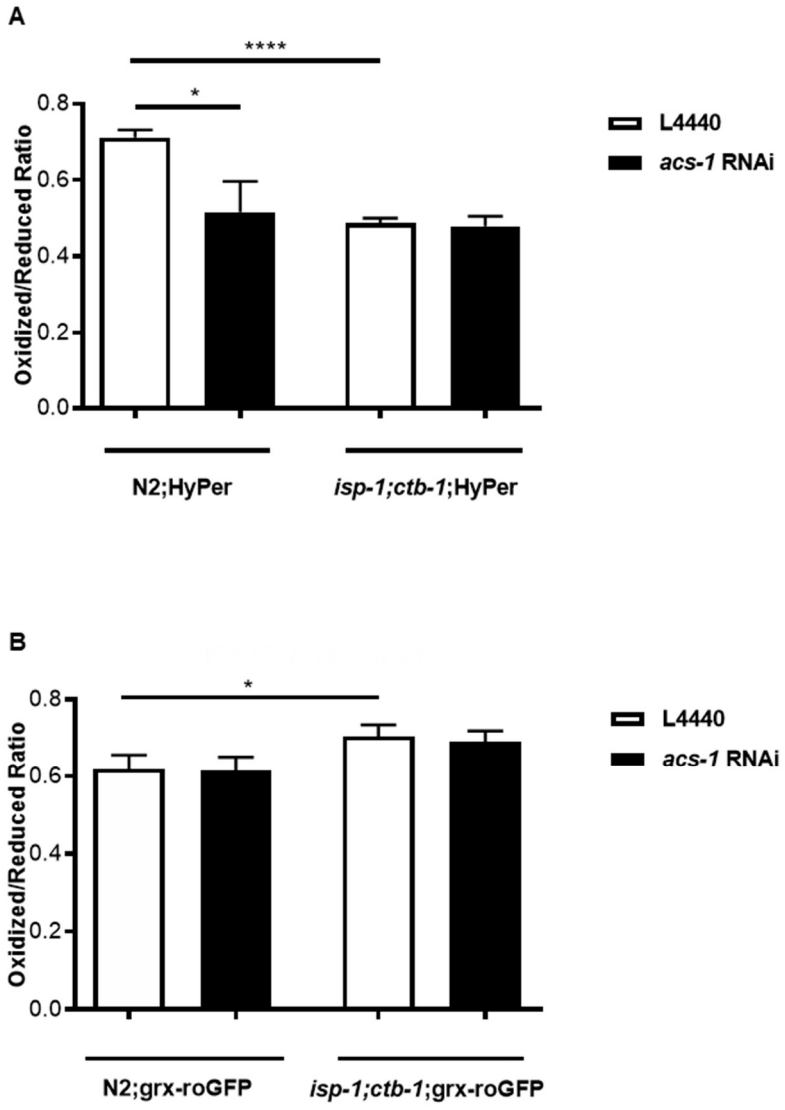

Figure 3.26 ***Isp-1(qm150);ctb-1(qm189)*** **mutants reveal a decrease in cytosolic H_2O_2, but increased redox imbalance Worms were grown on NGM plates containing RNAi targeting L4440 or** ***acs-1*** **gene A) Wild type N2 and** ***isp-1(qm150);ctb-1(qm189)*** **mutant expressing HyPer were imaged at day one of adulthood and levels were analyzed by the change in fluorescence between oxidized and reduced HyPer.**
B) Glutathione redox potential was assessed by Grx-roGFP in wild type N2 ***and isp-1(qm150);ctb-1(qm189)*** **mutant on the first day of adulthood. Both strains were imaged by Meta 710 confocal microscope (Zeiss) with a 10x objective. Bars represent mean ±SEM (p*<0.05, p***<0.001; Student's T-test).**

3.10.3 ACS-1 depletion results in high translocation of KLF-1 to the nucleus

We recently showed that KLF-1 activation is mediated by redox signaling (Herholz et al., 2019). Under normal conditions, most of KLF-1 is localized in the cytosol, and upon increased mitochondrial ROS it translocates into the nucleus (Herholz et al., 2019). Here, we used *C. elegans* strain with KLF-1-YFP, expressed under gut-specific *vha-6* promoter, to follow nuclear localization of KLF-1. As we previously showed (Herholz et al., 2019), in the *isp-1;ctb-1* mutant we observed persistent KLF-1 localization at day one of adulthood compared to wild type N2 under control conditions (Fig 3.27). Remarkably, depletion of *acs-1* leads to a further increase in already high nuclear localization of KLF-1 in the *isp-1;ctb-1* mutant (Fig.3.27).

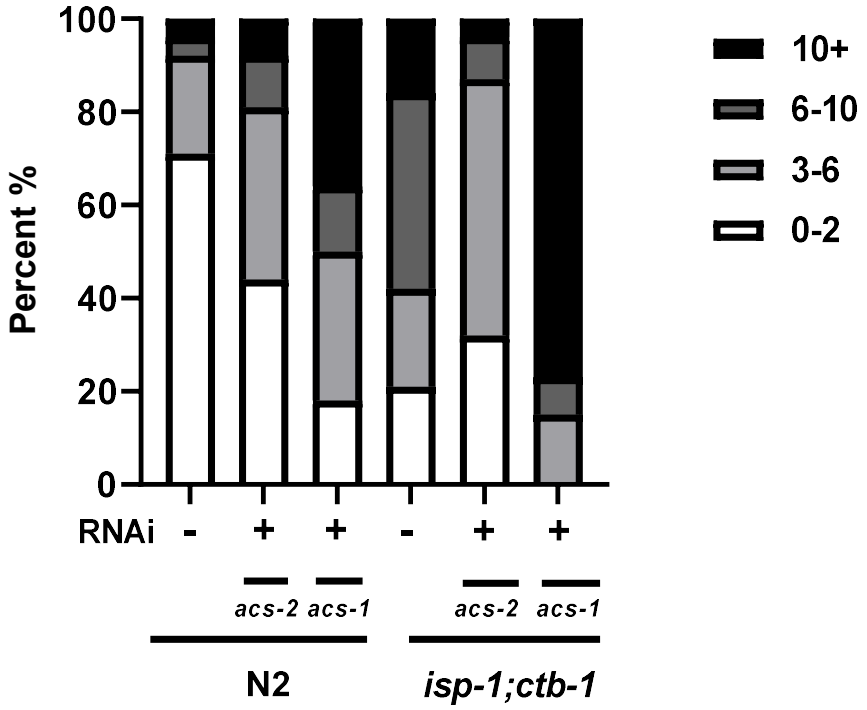

Figure 3.27 Nuclear Localization of KLF-1

Nuclear localization of *pklf-1::klf-1-yfp* in wild type worms N2 and *isp-1(qm150);ctb-1(qm189)* mutants feeding bacteria carrying the L4440 or targeting *acs-2* and *acs-1* gene. Animals were assayed based on KLF-1 nuclear localization as follows: "low" as less than 2 nuclei, "medium" 3–10 nuclei, and "high" where all nuclei were stained. Animals were imaged on day one of adulthood.

This goes in hand with other findings of this study showing that *acs-1* depletion in *isp-1;ctb-1* mutant leads to decreased longevity, respiration, body movement, and a massive increase in lipid peroxidation. In agreement with other results on the beneficial effect of *acs-2* depletion on *isp-1;ctb-1* mutants, we observed decreased KLF-1 translocation to the nucleus (Fig 3.27). In wild type worms, depletion of both *acs-1* and *acs-2* lead to higher KLF-1 translocation to the nucleus suggesting that multiple stressors might activate this transcription factor (Fig 3.27).

4 Discussion

4.1 KLF-1 in regulating lipid metabolism in *C. elegans*

In this study, we presented strong evidence that KLF-1 regulates lipid metabolism in *C. elegans*. This is in agreement with previous observation by Hashmi and coworkers, who reported that *klf-1* silencing by RNA interference (RNAi) results in an increase in fat storage in control worms, suggesting that loss-of-function of this gene might disturb the normal fat metabolism and thus increase the fat storage (Hashmi et al., 2008). We showed that a strong decrease in the level of neutral lipids in the *isp-1,ctb-1* mutant is fully corrected upon *klf-1* knockdown, confirming the findings that KLF-1 regulates neutral lipid levels in *C. elegans* (Fig. 3.2). KLF-1 is mainly expressed in the gastrointestinal tract of the worms, a tissue that is also the main site of lipid storage and metabolism of *C. elegans*, even though some expression could be discovered in hypodermal and neuronal cells (Brock et al., 2006). KLF proteins are highly conserved among mammals from human to mouse, with many KLFs also having homologs in *Gallus gallus* (chicken), *Danio rerio* (zebrafish), and *Xenopus laevis* (frog) (McConnell and Yang, 2010). Eight mammalian KLFs including KLF2 to KLF7, KLF11, and KLF15 have been reported to have a specific role in adipogenesis (Zhang et al., 2011). KLF2, KLF6, and KLF15 are expressed in the pancreas, adipose tissue, liver, and muscle (McConnell and Yang, 2010). KLF2 and KLF3 were reported to inhibit adipocyte differentiation since mice lacking KLF2 or KL3 are more willing to differentiate into adipocytes (McConnell and Yang, 2010, Hashmi et al., 2011, Zhang et al., 2011, Zhang et al., 2013). For example, both KLF4 and KLF5 bind to a variety of co-factors and transcription factors and form complexes that are essential for the differentiation of fat cells and can promote obesity (Brey et al., 2009, McConnell and Yang, 2010). The knockdown of *klf6* has been reported to prevent adipogenesis (McConnell and Yang, 2010, Hashmi et al., 2011). In the case of KLF15, it has been described that it regulates adipogenesis and energy metabolism in the liver, skeletal muscle, and adipocytes. It contributes to the transcriptional activation of mitochondrial acyl-CoA synthetase 2 in skeletal muscle and liver (McConnell and Yang, 2010, Hashmi et al., 2011, Zhang et al., 2011, Hashmi et al., 2013).

The *C. elegans* genome encodes three members of KLFs including *klf-1* (*F56F11.3)*, *klf-2* (F53F8.1) and *klf-3* (F54H5.4), all of which show high similarity with members of

mammalian KLFs (Brey et al., 2009). *C. elegans* KLFs share the highest sequence similarity with mammalian KLFs in their C-terminal C_2H_2 zinc-fingers, but differ in their N-terminal sites (Hashmi et al., 2015). Beside *klf-1,* the other two members of KLFs in *C. elegans klf-2* (F53F8.1) and *klf-3* (F54H5.4), were also reported to regulate lipid metabolism (Zhang et al., 2011, Ling et al., 2017). However, our previous results argue that in mitochondrial mutants, KLF-1, and not KLF-2 and KLF-3 play a role in longevity assurance (Herholz et al., 2019).

The role of lipid levels in *C. elegans* longevity was mainly studied in the context of the insulin signaling pathway regulated by the DAF-16/FoxO transcription factor (Ackerman and Gems, 2012). Remarkably, mitochondrial mutants or worms under dietary restriction, have less fat, but insulin-signaling mutants and germline-lacking animals contain far more, yet all of these animals are long-lived. This indicates that there is no easy explanation for the correlation between lifespan and lipid content.

One of the questions we wanted to address is: why the mitochondrial *isp-1;ctb-1* mutant exhibits less neutral lipids? Firstly, we investigated global changes in the lipid composition in *isp-1;ctb-1* mutant animals. A general decrease in the level of triacylglycerides (TAGs) and an extraordinary increase in the amount of all phospholipids (PLs) was detected in mitochondrial *isp-1;ctb-1* mutant animals (Fig 3.3). We further focused on triglyceride levels and investigated the effect of KLF-1 on food intake and the usage of triglycerides to understand the mechanism behind decreased lipid content. Although *isp-1;ctb-1* mutant animals exhibited delayed uptake of dietary fatty acids, the overall levels were the same and not affected by the *klf-1* depletion (Fig. 3.5).

Other studies reported that KLFs are involved in fatty acid biosynthesis, lipid secretion, beta-oxidation, insulin signaling, and mitochondrial proliferation, but the accurate mechanistic pathways behind it are still not fully understood (Hashmi et al., 2013, Hashmi et al., 2015). Mammalian KLFs have major roles in lipid metabolism (Hashmi et al., 2015). As introduced in *C. elegans* KLF-3 is the main regulator of fatty acid synthesis, lipid secretion, and degradation, while KLF-2 shows a comparable role in lipid metabolism, but vary in quantitative and developmental pattern as compared to KLF-3 (Zhang et al., 2011, Ling et al., 2017). KLF-3 controls β-oxidation of fatty acids and modification. The depletion of *klf-3* results in a fat phenotype characterized by extreme fat deposition and large lipid droplet formation in *C. elegans* intestine (Zhang et al., 2011). The *klf-2* expression was identified in

the intestine, suggesting a possible KLF-2 role in lipid metabolism (Ling et al., 2017). Together with our results, there is strong evidence for a key role of KLFs in general and in *C. elegans* lipid metabolism.

4.2 Role of peroxisomes in mitochondrial *isp-1;ctb-1* mutants

As we did not observe the difference in the overall lipid intake in the *isp-1;ctb-1* mutant we further focused on the usage of fatty acids. We investigated ß-oxidation next, and our qPCR and microarray data revealed two different acyl-CoA synthetases as the most upregulated, making them promising-candidates to examine further. Exceptionally, the most upregulated genes involved in lipid metabolism encode ACS-1 and ACS-2, acyl-CoA synthases expected to prime fatty acids for peroxisomal and mitochondrial FAO, respectively. They catalyze the conversion of free fatty acids to acyl-CoA derivates as a step preceding FAO in both mitochondria and peroxisomes. Interestingly, loss of *acs-1* led to full repression of longevity phenotype in *isp-1;ctb-1* mutant animals, with only a minor effect on the longevity of wild type worms. Further approval for the role of peroxisomes came from experiments displaying the depletion of *prx-5*, the peroxisomal biogenesis factor 5, and treatment with chlorpromazine, a drug that blocks peroxisomal biogenesis, results in a comparable damaging effect on the longevity of *isp-1;ctb-1* mutant animals (Fig 3.12).

These results thus identified peroxisomal lipid metabolism as fundamental for longevity assurance in mitochondrial *isp-1;ctb-1* mutant animals. Peroxisomes fulfill numerous crucial lipid metabolic functions such as fatty acid beta-oxidation; ether phospholipid biosynthesis, and fatty acid α-oxidation (Watkins and Ellis, 2012, Wanders et al., 2010). Almost all these functions require that an acyl group, either fatty acid or the acyl side chain of a steroid derivative, be thioesterified to coenzyme A (CoA) for subsequent reactions to continue (Watkins and Ellis, 2012). This " initiation" reaction, catalyzed by enzymes belonging to the acyl-CoA synthetase family, is therefore central for cellular lipid metabolism. However, in spite of the relevant understanding of peroxisomal metabolic pathways, little is known about the specific peroxisomal acyl-CoA synthetases that participate in these pathways (Watkins and Ellis, 2012). The results of this study identified ACS-1, to be essential for the longevity of mitochondrial *isp-1;ctb-1* mutant animals. We also showed that PRX-5, a putative

peroxisomal membrane protein involved in protein import has a similar role in suppression of increased lifespan in *isp-1;ctb-1* mutants.

We show that both ACS-1 and PRX-5 are important to sustain respiration in mitochondrial *isp-1;ctb-1* mutant worms. Our further results demonstrate that ACS-1 has a vital role in *isp-1;ctb-1* mutant animals. Notably, depletion of *acs-1*, but not *acs-2* decreased overall respiration and body movements. Additionally, ACS-1 plays a major role in the suppression of increased lifespan and likewise, it has an impact on the uptake of the fatty acids. The uptake of fatty acid was slowed down in mitochondrial *isp-1;ctb-1* mutant animals in control conditions and is further aggravated after *acs-1* depletion (Fig.3.9). These all highlight the importance of peroxisomes for *isp-1;ctb-1* mutant worms to generate lipid droplets (Fig. 3.17). However, the exact effect that suppression of *acs-1* has on lipid metabolism, specifically on TAG levels and lipid droplet size, is currently unclear.

The increase in *acs-1* levels is not exclusive for *isp-1;ctb-1* mutant animals. It was also observed in our other long-lived models of mitochondrial dysfunction, such as upon *cyc-1* and *cco-1* RNAi, who also show increased KLF-1 activation. The increase in *acs-1* levels in worms upon *cyc-1* and *cco-1* depletion was accompanied by a strong increase in levels of peroxisomes and the state of the fused network (Fig. 3.16). Additionally, mitochondrial dysfunction caused by treatment with complex III inhibitor and pro-oxidant antimycin A also increased peroxisomal biogenesis, intending a connection between mitochondrial ROS production and peroxisomal biogenesis (Fig. 3.16).

Our data highlight the crosstalk between mitochondria and peroxisomes, especially regarding lipid metabolism and shared fatty acid oxidation as central to a response beneficial for organismal survival. Accordingly, peroxisomal- and mitochondrial lipid metabolism affect each other (Fransen et al., 2017). For example, defects in peroxisome function lead to accumulation, of very-long-chain-fatty-acids (VLCFA), like seen in Zellweger syndrome patients, which can directly or indirectly lead to mitochondrial dysfunction (Lismont et al., 2015). Treatment of several cell types, like astrocytes or oligodendrocytes, with carboxylates like phytanic acid and pristanic acid, which arise due to peroxisomal dysfunction in α- or β-oxidation, has been reported to provoke mitochondrial depolarization, respiratory chain dysfunction, oxidative stress and loss of cytochrome c (Schonfeld et al., 2011, Reiser et al., 2006, Baarine et al., 2012). Vice versa, studies on skeletal muscle reported that impaired mitochondrial FAO results in an enhanced peroxisomal FAO (Wicks et al., 2015).

Also, mitochondrial and peroxisomal ß-oxidation allocate co-substrates which can again, directly, or indirectly alter metabolic activities, among each other. The best example represents the last step of peroxisomal ß-oxidation because NADH formed in peroxisomes needs to be reoxidized to NAD^+ and this solely takes place in mitochondria (Wanders et al., 2015). Other studies reported, that defects in peroxisomal biogenesis, peroxisomal fatty acid metabolism, and peroxisomal antioxidant capacity have harmful effects on mitochondrial function (Pascual-Ahuir et al., 2017). Importantly, these failings induce functional mitochondrial alterations such as abnormal cristae, depleted membrane potential, and respiration rates, increased ROS productions, reduced fatty acids oxidation, DNA alterations and an increase in the mass of several organs like brain, liver or kidney (Deori et al., 2018, Cipolla and Lodhi, 2017, Pascual-Ahuir et al., 2017, Fransen et al., 2017, Baumgart et al., 2001). However, both organelles show the ability to share information from one to the other through the distribution of biological messengers such as lipids, ROS or other metabolites (Fransen et al., 2017). Taken together, *isp-1;ctb-1* mutant worms, which have a deficiency in complex III of the electron transport chain, need implicitly functional peroxisomes for lipid metabolism and are not able to deal with deficiencies in the function of this organelle, as mimicked by depletion of *acs-1* or *prx-5*.

4.3 Lipid peroxidation in mitochondrial *isp-1;ctb-1* mutants

The depletion of *acs-1* in *isp-1;ctb-1* mutant animals lead to a mild increase in overall neutral lipid levels, but we observed an increase of oxidized lipids accompanied by massive upregulation of GST-4, a major antioxidant enzyme in *C. elegans* with glutathione transferase activity. Our data indicate that loss of ACS-1 in *isp-1;ctb-1* mutant worms induces further massive lipid peroxidation, including the accumulation of 4-Hydroxynonenal (4-HNE), one of the end products of lipid peroxidation (Fig. 3.20 and 3.22). Remarkably, we did not observe changes in overall O^{2-} or H_2O_2 production rates, showing that increased lipid peroxidation might be the main consequence of decreased peroxisomal fatty acid oxidation.

As already mentioned, peroxisomes are crucial for immaculate functioning of the eukaryotic cell. Aside from breaking down fatty acids, the reactive oxygen species metabolism is the most important function of peroxisomes, since alterations in peroxisomes result in fatal

oxidative damage (Schrader and Fahimi, 2006). Peroxisomes are also provided with multiple enzymatic and non-enzymatic antioxidant defense systems that scavenge harmful H_2O_2 and free radicals, like mitochondria (Antonenkov et al., 2010, Lismont et al., 2015). The most specified peroxisomal antioxidant enzyme is catalase. Catalase can eliminate H_2O_2 in a catalatic and peroxidative manner (Antonenkov et al., 2010, Lismont et al., 2015). Upon oxidative stress, PEX5 the receptor for PTS-1-containing proteins, was observed to lose its ability to reutilize and accumulate on the membrane, a feature necessary for an optimal peroxisomal protein import (Cipolla and Lodhi, 2017, Deori et al., 2018, Apanasets et al., 2014, Ma et al., 2013). ROS generated by peroxisomes changes the oxidative state of mitochondria and results in mitochondrial fragmentation and cell death (Wang et al., 2013, Ivashchenko et al., 2011, Pascual-Ahuir et al., 2017). In the previous chapter phytanic acid was mentioned, which accumulates in patients with α-oxidation defects, causes an increase in cytosolic $Ca^{2+,}$ mitochondrial depolarization and ROS generation, and leads to cell death within a few hours (Reiser et al., 2006, Schonfeld et al., 2011). Studies on isolated mitochondria from rat brain and heart show that phytanic acid also enhances the production of $O_2^{\bullet-}$ in mitochondria resulting in lower mitochondrial GSH and NADH levels, a decreased membrane potential and oxidative modification of lipids and proteins (Schonfeld et al., 2011). Compared to phytanic acid, pristanic acid has even a stronger cytotoxic effect due to a more intense mitochondrial depolarization and stronger production of ROS that leads to swelling of mitochondria due to impairment of the mPTP (Lismont et al., 2015).

Regarding our results, ferroptosis might be relevant in our mitochondrial *isp-1;ctb-1* mutant animals. Our data confirm that the depletion of *acs-1* leads to the extensive upregulation of oxidized lipids that can be fully corrected by addition of Vitamin E. Increased lipid peroxidation and insufficient capability to reduce lipid peroxides, result in the initiation of ferroptosis, a regulated cell death program genetically and biochemically distinct from apoptosis and necrosis (Conrad et al., 2018, Yang et al., 2016, Yang and Stockwell, 2016, Su et al., 2019).

4.4 *acs-1* suppresses KLF-1 translocation into the nucleus

Recently, we reported that KLF-1 activates genes involved in the xenobiotic detoxification program and identified cytochrome P450 oxidases, the KLF-1 main effectors, as longevity-assurance factors of mitochondrial mutants (Herholz et al., 2019). The cytochrome P450 oxidases represent, a large family of NADPH-dependent mono-oxygenases that are mostly involved in the metabolism of fatty acids and lipid signaling and oxidation (Riddick et al., 2013, Aarnio et al., 2011). The CYP-35A protein family is widely expressed in the *C. elegans* intestine, which is the major site of fat storage (Imanikia et al., 2015). Moreover, it has been reported that inactivation of *cyp-35* results in a moderated accumulation of intestinal fat, hence implying that CYPs are involved in lipid storage (Aarnio et al., 2011, Imanikia et al., 2015, Riddick et al., 2013).

We previously showed that KLF-1 is not involved in the transcription regulation of catalases, which are major H_2O_2 metabolizing enzymes, but that it translocate into the nucleus upon increased oxidative stress (Herholz et al., 2019). It is reported that upon improved oxidative stress due to peroxisomal deficiency, caused by an imbalance between production and accumulation of ROS, and the inability to detoxify the reactive products, an overload of reactive oxygen species, particularly H_2O_2 can escape from the peroxisome and diffuse into the surrounding environment (Fransen et al., 2017, Lismont et al., 2015).

We showed that the expression of ROS scavenging enzyme the cytoplasmic *gst-4* is not upregulated in *isp-1;ctb-1* mutant animals and that the levels even went down upon *klf-1* depletion (Herholz et al., 2019). In *C. elegans*, transcriptional activation of *gst-4* is regulated by SKN-1-dependent pathways that are activated by stress (Detienne et al., 2016, Choe et al., 2009). The same group reported that *gst-4* can also be transcriptionally activated by EOR-1, a transcription factor of the epidermal growth factor (EGF) pathway (Detienne et al., 2016).

However, as already mentioned we could not detect any changes in overall $O2^-$ or H_2O_2 production rates after depletion of *acs-1*. Instead, these results suggest that not only increased mitochondrial ROS and changes in redox state, but also lipid peroxidation can trigger KLF-1 translocation to the nucleus

4.5 Outlook

To further understand the role of proteins specifically involved in peroxisomal fatty acid oxidation one should repeat experiments on *isp-1;ctb-1* mutant animals by downregulating genes involved in all four steps of peroxisomal FAO *acox-1*, *maoc-1*, *dhs-28,* and *daf-22*. There is evidence indicating that mammalian mitochondrial metabolism and ROS generation are a connecting factor in promoting adipocyte differentiation, thus directly influencing lipid metabolism. The dynamic of peroxisomal and mitochondrial networks can be followed using gut-specific reporter strains. It has been shown that mitochondrial mass and activity increases in the cell triggering the production of ROS through mitochondrial complex III, resulting in the induction of PPARγ transcriptional machinery which is necessary to initiate adipocyte differentiation (Tormos et al., 2011). Our preliminary data indicate that direct manipulation of ROS levels by the drugs paraquat or antimycin A affects lipid contents in worms. We also showed that depletion of the ROS scavenging enzyme, the cytoplasmic GST-4, leads to changes in lipid content in wild type worms. However, we still do not know to what extent these alterations and changes in lipid metabolism depend on KLF-1.

Although our initial analyses show that lipid uptake in *isp-1;ctb-1* mutant animals over time can reach wild type levels, we detected also delayed uptake, that could also influence lipid levels in mutant animals, as approximately 80% of fatty acids in worms originate from dietary fat. To further address if a decrease in fatty acid uptake might contribute to changes observed in *isp-1;ctb-1* mutant worms, depletion of *acs-3*, a long-chain acyl-CoA synthase, whose loss causes enhanced intestinal lipid uptake, *de novo* fat synthesis, and accumulation of enlarged, neutral lipid-rich intestinal depots would be of great significance for future experiments (Mullaney et al., 2010). Together with the effect on TAG and lipid droplets distribution and size, other critical experiments like measurement of mitochondrial respiration rate, and effect on the lifespan extension should be repeated, upon *acs-3* depletion.

Besides its known role in peroxisomal FAO, ACS-1 was proposed to have a role in the biosynthesis and activation of monomethyl branched-chain fatty acids (mmBCFAs) (Kniazeva et al., 2004). In *C. elegans,* mmBCFA are found in quite a lot of lipid species, including TAGs, PC, and PE, and have a critical role as structural components of sphingolipids (Watts and Ristow, 2017). The mmBCFAs are exclusively derived from

de novo synthesis because these fatty acids are not present in the *E. coli* diet and cannot be produced from modification of bacterial fatty acids in *C. elegans* (Watts and Ristow, 2017).

The increased lipid peroxidation could possibly lead to ferroptosis in mitochondrial *isp-1;ctb-1* mutant animals upon *acs-1* depletion. To test if the loss of peroxisomal function in mitochondrial mutants leads to massive lipid peroxidation resulting in ferroptosis, worms could be treated with (i) vitamin E; a lipophilic antioxidant; (ii) liproxstatin, a selective ferroptosis inhibitor; or (iii) salicylaldehyde isonicotinoyl hydrazone (SIH), lipophilic acyl hydrazine; all of which scavenge intracellular iron and mobilize it for extracellular clearance. In summary, our results display strong evidence that peroxisomes are important for the mitochondrial *isp-1;ctb-1* mutant animals for lipid metabolism and longevity assurance. Peroxisomal deficiency results in a decrease in lipid levels, respiration, shortened lifespan, and a massive increase in lipid peroxidation.

References

AARNIO, V., LEHTONEN, M., STORVIK, M., CALLAWAY, J. C., LAKSO, M. & WONG, G. 2011. Caenorhabditis Elegans Mutants Predict Regulation of Fatty Acids and Endocannabinoids by the CYP-35A Gene Family. *Front Pharmacol,* 2**,** 12.

ACKERMAN, D. & GEMS, D. 2012. The mystery of C. elegans aging: an emerging role for fat. Distant parallels between C. elegans aging and metabolic syndrome? *Bioessays,* 34**,** 466-71.

AGOSTINO, A., INVERNIZZI, F., TIVERON, C., FAGIOLARI, G., PRELLE, A., LAMANTEA, E., GIAVAZZI, A., BATTAGLIA, G., TATANGELO, L., TIRANTI, V. & ZEVIANI, M. 2003. Constitutive knockout of Surf1 is associated with high embryonic lethality, mitochondrial disease and cytochrome c oxidase deficiency in mice. *Human Molecular Genetics,* 12**,** 399-413.

ALTUN, Z. F. A. H., D.H. 2009. Introduction. In WormAtlas

AN, J. H. & BLACKWELL, T. K. 2003. SKN-1 links C. elegans mesendodermal specification to a conserved oxidative stress response. *Genes Dev,* 17**,** 1882-93.

ANTONENKOV, V. D., GRUNAU, S., OHLMEIER, S. & HILTUNEN, J. K. 2010. Peroxisomes are oxidative organelles. *Antioxid Redox Signal,* 13**,** 525-37.

APANASETS, O., GROU, C. P., VAN VELDHOVEN, P. P., BREES, C., WANG, B., NORDGREN, M., DODT, G., AZEVEDO, J. E. & FRANSEN, M. 2014. PEX5, the shuttling import receptor for peroxisomal matrix proteins, is a redox-sensitive protein. *Traffic,* 15**,** 94-103.

ARRESE, E. L. & SOULAGES, J. L. 2010. Insect fat body: energy, metabolism, and regulation. *Annu Rev Entomol,* 55**,** 207-25.

ASHRAFI, K. 2007. Obesity and the regulation of fat metabolism. *WormBook***,** 1-20.

AYALA, A., MUNOZ, M. F. & ARGUELLES, S. 2014. Lipid peroxidation: production, metabolism, and signaling mechanisms of malondialdehyde and 4-hydroxy-2-nonenal. *Oxid Med Cell Longev,* 2014**,** 360438.

BAARINE, M., ANDREOLETTI, P., ATHIAS, A., NURY, T., ZARROUK, A., RAGOT, K., VEJUX, A., RIEDINGER, J. M., KATTAN, Z., BESSEDE, G., TROMPIER, D., SAVARY, S., CHERKAOUI-MALKI, M. & LIZARD, G. 2012. Evidence of oxidative stress in very long chain fatty acid--treated oligodendrocytes and potentialization of ROS production using RNA interference-directed knockdown of ABCD1 and ACOX1 peroxisomal proteins. *Neuroscience,* 213**,** 1-18.

BACK, P., DE VOS, W. H., DEPUYDT, G. G., MATTHIJSSENS, F., VANFLETEREN, J. R. & BRAECKMAN, B. P. 2012. Exploring real-time in vivo redox biology of developing and aging Caenorhabditis elegans. *Free Radic Biol Med,* 52**,** 850-9.

BARBOSA, A. D., SAVAGE, D. B. & SINIOSSOGLOU, S. 2015. Lipid droplet-organelle interactions: emerging roles in lipid metabolism. *Curr Opin Cell Biol,* 35**,** 91-7.

BAUMGART, E., FAHIMI, H. D., STICH, A. & VOLKL, A. 1996. L-lactate dehydrogenase A4- and A3B isoforms are bona fide peroxisomal enzymes in rat liver. Evidence for involvement in intraperoxisomal NADH reoxidation. *J Biol Chem,* 271**,** 3846-55.

BAUMGART, E., VANHOREBEEK, I., GRABENBAUER, M., BORGERS, M., DECLERCQ, P. E., FAHIMI, H. D. & BAES, M. 2001. Mitochondrial alterations caused by defective peroxisomal biogenesis in a mouse model for Zellweger syndrome (PEX5 knockout mouse). *Am J Pathol,* 159**,** 1477-94.

BERDICHEVSKY, A., NEDELCU, S., BOULIAS, K., BISHOP, N. A., GUARENTE, L. & HORVITZ, H. R. 2010. 3-Ketoacyl thiolase delays aging of Caenorhabditis elegans and is required for lifespan extension mediated by sir-2.1. *Proc Natl Acad Sci U S A,* 107**,** 18927-32.

BERGER, J., DORNINGER, F., FORSS-PETTER, S. & KUNZE, M. 2016. Peroxisomes in brain development and function. *Biochim Biophys Acta,* 1863**,** 934-55.

BOVERIS, A., OSHINO, N. & CHANCE, B. 1972. The cellular production of hydrogen peroxide. *Biochem J,* 128**,** 617-30.

BRENNER, S. 1974. The genetics of Caenorhabditis elegans. *Genetics,* 77**,** 71-94.

BREY, C. W., NELDER, M. P., HAILEMARIAM, T., GAUGLER, R. & HASHMI, S. 2009. Kruppel-like family of transcription factors: an emerging new frontier in fat biology. *Int J Biol Sci,* 5**,** 622-36.

BROCK, T. J., BROWSE, J. & WATTS, J. L. 2006. Genetic regulation of unsaturated fatty acid composition in C. elegans. *PLoS Genet,* 2**,** e108.

BROWN, F. R., 3RD, MCADAMS, A. J., CUMMINS, J. W., KONKOL, R., SINGH, I., MOSER, A. B. & MOSER, H. W. 1982. Cerebro-hepato-renal (Zellweger) syndrome and neonatal adrenoleukodystrophy: similarities in phenotype and accumulation of very long chain fatty acids. *Johns Hopkins Med J,* 151**,** 344-51.

BUTLER, J. A., VENTURA, N., JOHNSON, T. E. & REA, S. L. 2010. Long-lived mitochondrial (Mit) mutants of Caenorhabditis elegans utilize a novel metabolism. *Faseb j,* 24**,** 4977-88.

CARRANO, A. C., DILLIN, A. & HUNTER, T. 2014. A Kruppel-like factor downstream of the E3 ligase WWP-1 mediates dietary-restriction-induced longevity in Caenorhabditis elegans. *Nat Commun,* 5**,** 3772.

CARUGNO, M., PESATORI, A. C., DIONI, L., HOXHA, M., BOLLATI, V., ALBETTI, B., BYUN, H.-M., BONZINI, M., FUSTINONI, S., COCCO, P., SATTA, G., ZUCCA, M., MERLO, D. F., CIPOLLA, M., BERTAZZI, P. A. & BACCARELLI, A. 2012. Increased mitochondrial DNA copy number in occupations associated with low-dose benzene exposure. *Environmental health perspectives,* 120**,** 210-215.

CATALA, A. & DIAZ, M. 2016. Editorial: Impact of Lipid Peroxidation on the Physiology and Pathophysiology of Cell Membranes. *Front Physiol,* 7**,** 423.

CHAN, D. C. 2006. Mitochondria: dynamic organelles in disease, aging, and development. *Cell,* 125**,** 1241-52.

CHANTREL-GROUSSARD, K., GEROMEL, V., PUCCIO, H., KOENIG, M., MUNNICH, A., ROTIG, A. & RUSTIN, P. 2001. Disabled early recruitment of antioxidant defenses in Friedreich's ataxia. *Hum Mol Genet,* 10**,** 2061-7.

CHOE, K. P., PRZYBYSZ, A. J. & STRANGE, K. 2009. The WD40 repeat protein WDR-23 functions with the CUL4/DDB1 ubiquitin ligase to regulate nuclear abundance and activity of SKN-1 in Caenorhabditis elegans. *Mol Cell Biol,* 29**,** 2704-15.

CIPOLLA, C. M. & LODHI, I. J. 2017. Peroxisomal Dysfunction in Age-Related Diseases. *Trends Endocrinol Metab,* 28**,** 297-308.

CONRAD, M., KAGAN, V. E., BAYIR, H., PAGNUSSAT, G. C., HEAD, B., TRABER, M. G. & STOCKWELL, B. R. 2018. Regulation of lipid peroxidation and ferroptosis in diverse species. *Genes Dev,* 32**,** 602-619.

COPELAND, J. M., CHO, J., LO, T., JR., HUR, J. H., BAHADORANI, S., ARABYAN, T., RABIE, J., SOH, J. & WALKER, D. W. 2009. Extension of Drosophila life span by RNAi of the mitochondrial respiratory chain. *Curr Biol,* 19**,** 1591-8.

CORSI AK, W. B., CHALFIE M.. 2005-2018. A Transparent window into biology: A primer on Caenorhabditis elegans.

CRISTINA, D., CARY, M., LUNCEFORD, A., CLARKE, C. & KENYON, C. 2009. A regulated response to impaired respiration slows behavioral rates and increases lifespan in Caenorhabditis elegans. *PLoS Genet,* 5**,** e1000450.

CULLINGFORD, T. E., BUTLER, M. J., MARSHALL, A. K., THAM EL, L., SUGDEN, P. H. & CLERK, A. 2008. Differential regulation of Kruppel-like factor family transcription factor expression in neonatal rat cardiac myocytes: effects of endothelin-1, oxidative stress and cytokines. *Biochim Biophys Acta,* 1783**,** 1229-36.

DANCY, B. M., SEDENSKY, M. M. & MORGAN, P. G. 2014. Effects of the mitochondrial respiratory chain on longevity in C. elegans. *Exp Gerontol,* 56**,** 245-55.

DANCY, B. M., SEDENSKY, M. M. & MORGAN, P. G. 2015. Mitochondrial bioenergetics and disease in Caenorhabditis elegans. *Front Biosci (Landmark Ed),* 20**,** 198-228.

DE DUVE, C. & BAUDHUIN, P. 1966. Peroxisomes (microbodies and related particles). *Physiol Rev,* 46**,** 323-57.

DEORI, N. M., KALE, A., MAURYA, P. K. & NAGOTU, S. 2018. Peroxisomes: role in cellular ageing and age related disorders. *Biogerontology,* 19**,** 303-324.

DETIENNE, G., VAN DE WALLE, P., DE HAES, W., SCHOOFS, L. & TEMMERMAN, L. 2016. SKN-1-independent transcriptional activation of glutathione S-transferase 4 (GST-4) by EGF signaling. *Worm,* 5**,** e1230585-e1230585.

DILLIN, A., HSU, A. L., ARANTES-OLIVEIRA, N., LEHRER-GRAIWER, J., HSIN, H., FRASER, A. G., KAMATH, R. S., AHRINGER, J. & KENYON, C. 2002. Rates of behavior and aging specified by mitochondrial function during development. *Science,* 298**,** 2398-401.

DODSON, M., CASTRO-PORTUGUEZ, R. & ZHANG, D. D. 2019. NRF2 plays a critical role in mitigating lipid peroxidation and ferroptosis. *Redox Biol,* 23**,** 101107.

DURIEUX, J., WOLFF, S. & DILLIN, A. 2011. The cell-non-autonomous nature of electron transport chain-mediated longevity. *Cell,* 144**,** 79-91.

ERKUT, C., GADE, V. R., LAXMAN, S. & KURZCHALIA, T. V. 2016. The glyoxylate shunt is essential for desiccation tolerance in C. elegans and budding yeast. *eLife,* 5**,** e13614.

FARESE, R. V., JR. & WALTHER, T. C. 2009. Lipid droplets finally get a little R-E-S-P-E-C-T. *Cell,* 139**,** 855-860.

FAUST, I. M., JOHNSON, P. R., STERN, J. S. & HIRSCH, J. 1978. Diet-induced adipocyte number increase in adult rats: a new model of obesity. *Am J Physiol,* 235**,** E279-86.

FENG, J., BUSSIERE, F. & HEKIMI, S. 2001. Mitochondrial electron transport is a key determinant of life span in Caenorhabditis elegans. *Dev Cell,* 1**,** 633-44.

FIRE, A., XU, S., MONTGOMERY, M. K., KOSTAS, S. A., DRIVER, S. E. & MELLO, C. C. 1998. Potent and specific genetic interference by double-stranded RNA in Caenorhabditis elegans. *Nature,* 391**,** 806-11.

FRANSEN, M., LISMONT, C. & WALTON, P. 2017. The Peroxisome-Mitochondria Connection: How and Why? *Int J Mol Sci,* 18.

FRANSEN, M., NORDGREN, M., WANG, B., APANASETS, O. & VAN VELDHOVEN, P. P. 2013. Aging, age-related diseases and peroxisomes. *Subcell Biochem,* 69**,** 45-65.

GAO, M., MONIAN, P., PAN, Q., ZHANG, W., XIANG, J. & JIANG, X. 2016. Ferroptosis is an autophagic cell death process. *Cell Res,* 26**,** 1021-32.

GAO, M., YI, J., ZHU, J., MINIKES, A. M., MONIAN, P., THOMPSON, C. B. & JIANG, X. 2019. Role of Mitochondria in Ferroptosis. *Molecular Cell,* 73**,** 354-363.e3.

GAO, Q. & GOODMAN, J. M. 2015. The lipid droplet-a well-connected organelle. *Front Cell Dev Biol,* 3**,** 49.

GASCHLER, M. M. & STOCKWELL, B. R. 2017. Lipid peroxidation in cell death. *Biochemical and biophysical research communications,* 482**,** 419-425.

GEBAUER, J., GENTSCH, C., MANSFELD, J., SCHMEISSER, K., WASCHINA, S., BRANDES, S., KLIMMASCH, L., ZAMBONI, N., ZARSE, K., SCHUSTER, S., RISTOW, M., SCHAUBLE, S. & KALETA, C. 2016. A Genome-Scale Database and Reconstruction of Caenorhabditis elegans Metabolism. *Cell Syst,* 2**,** 312-22.

HARTMAN, P. S., ISHII, N., KAYSER, E. B., MORGAN, P. G. & SEDENSKY, M. M. 2001. Mitochondrial mutations differentially affect aging, mutability and anesthetic sensitivity in Caenorhabditis elegans. *Mech Ageing Dev,* 122**,** 1187-201.

HASHMI, S., JI, Q., ZHANG, J., PARHAR, R. S., HUANG, C. H., BREY, C. & GAUGLER, R. 2008. A Kruppel-like factor in Caenorhabditis elegans with essential roles in fat regulation, cell death, and phagocytosis. *DNA Cell Biol,* 27**,** 545-51.

HASHMI, S., WANG, Y., PARHAR, R. S., COLLISON, K. S., CONCA, W., AL-MOHANNA, F. & GAUGLER, R. 2013. A C. elegans model to study human metabolic regulation. *Nutr Metab (Lond),* 10**,** 31.

HASHMI, S., WANG, Y., SUMAN, D. S., PARHAR, R. S., COLLISON, K., CONCA, W., AL-MOHANNA, F. & GAUGLER, R. 2015. Human cancer: is it linked to dysfunctional lipid metabolism? *Biochim Biophys Acta,* 1850**,** 352-64.

HASHMI, S., ZHANG, J., SIDDIQUI, S. S., PARHAR, R. S., BAKHEET, R. & AL-MOHANNA, F. 2011. Partner in fat metabolism: role of KLFs in fat burning and reproductive behavior. *3 Biotech,* 1**,** 59-72.

HAYASHI, G. & CORTOPASSI, G. 2015. Oxidative stress in inherited mitochondrial diseases. *Free radical biology & medicine,* 88**,** 10-17.

HERHOLZ, M., CEPEDA, E., BAUMANN, L., KUKAT, A., HERMELING, J., MACIEJ, S., SZCZEPANOWSKA, K., PAVLENKO, V., FROMMOLT, P. & TRIFUNOVIC, A. 2019. KLF-1 orchestrates a xenobiotic detoxification program essential for longevity of mitochondrial mutants. *Nat Commun,* 10**,** 3323.

HOLT, I. J., HARDING, A. E. & MORGAN-HUGHES, J. A. 1988. Deletions of muscle mitochondrial DNA in patients with mitochondrial myopathies. *Nature,* 331**,** 717-9.

HSIEH, P. N., ZHOU, G., YUAN, Y., ZHANG, R., PROSDOCIMO, D. A., SANGWUNG, P., BORTON, A. H., BORIUSHKIN, E., HAMIK, A., FUJIOKA, H., FEALY, C. E., KIRWAN, J. P., PETERS, M., LU, Y., LIAO, X., RAMÍREZ-BERGERON, D., FENG, Z. & JAIN, M. K. 2017. A conserved KLF-autophagy pathway modulates nematode lifespan and mammalian age-associated vascular dysfunction. *Nat Commun,* 8**,** 914.

HWANG, I., LEE, J., HUH, J. Y., PARK, J., LEE, H. B., HO, Y. S. & HA, H. 2012. Catalase deficiency accelerates diabetic renal injury through peroxisomal dysfunction. *Diabetes,* 61**,** 728-38.

IMANIKIA, S., HYLANDS, P. & STÜRZENBAUM, S. R. 2015. The double mutation of cytochrome P450's and fatty acid desaturases affect lipid regulation and longevity in C. elegans. *Biochemistry and biophysics reports,* 2**,** 172-178.

INGMAN, M., KAESSMANN, H., PÄÄBO, S. & GYLLENSTEN, U. 2000. Mitochondrial genome variation and the origin of modern humans. *Nature,* 408**,** 708-13.

ISHII, N., FUJII, M., HARTMAN, P. S., TSUDA, M., YASUDA, K., SENOO-MATSUDA, N., YANASE, S., AYUSAWA, D. & SUZUKI, K. 1998. A mutation in succinate dehydrogenase cytochrome b causes oxidative stress and ageing in nematodes. *Nature,* 394**,** 694-7.

ISHII, N., GOTO, S. & HARTMAN, P. S. 2002. Protein oxidation during aging of the nematode Caenorhabditis elegans. *Free Radic Biol Med,* 33**,** 1021-5.

IVASHCHENKO, O., VAN VELDHOVEN, P. P., BREES, C., HO, Y. S., TERLECKY, S. R. & FRANSEN, M. 2011. Intraperoxisomal redox balance in mammalian cells: oxidative stress and interorganellar cross-talk. *Mol Biol Cell,* 22**,** 1440-51.

KAGAN, V. E., MAO, G., QU, F., ANGELI, J. P., DOLL, S., CROIX, C. S., DAR, H. H., LIU, B., TYURIN, V. A., RITOV, V. B., KAPRALOV, A. A., AMOSCATO, A. A., JIANG, J., ANTHONYMUTHU, T., MOHAMMADYANI, D., YANG, Q., PRONETH, B., KLEIN-SEETHARAMAN, J., WATKINS, S., BAHAR, I., GREENBERGER, J., MALLAMPALLI, R. K., STOCKWELL, B. R., TYURINA, Y. Y., CONRAD, M. & BAYIR, H. 2017. Oxidized arachidonic and adrenic PEs navigate cells to ferroptosis. *Nat Chem Biol,* 13**,** 81-90.

KALETTA, T. & HENGARTNER, M. O. 2006. Finding function in novel targets: C. elegans as a model organism. *Nat Rev Drug Discov,* 5**,** 387-98.

KAMATH, R. S., FRASER, A. G., DONG, Y., POULIN, G., DURBIN, R., GOTTA, M., KANAPIN, A., LE BOT, N., MORENO, S., SOHRMANN, M., WELCHMAN, D. P., ZIPPERLEN, P. & AHRINGER, J. 2003. Systematic functional analysis of the Caenorhabditis elegans genome using RNAi. *Nature,* 421**,** 231-7.

KAYSER, E. B., MORGAN, P. G. & SEDENSKY, M. M. 1999. GAS-1: a mitochondrial protein controls sensitivity to volatile anesthetics in the nematode Caenorhabditis elegans. *Anesthesiology,* 90**,** 545-54.

KNIAZEVA, M., CRAWFORD, Q. T., SEIBER, M., WANG, C. Y. & HAN, M. 2004. Monomethyl branched-chain fatty acids play an essential role in Caenorhabditis elegans development. *PLoS Biol,* 2**,** E257.

KUMAR, V., BOUAMEUR, J. E., BAR, J., RICE, R. H., HORNIG-DO, H. T., ROOP, D. R., SCHWARZ, N., BRODESSER, S., THIERING, S., LEUBE, R. E., WIESNER,

R. J., VIJAYARAJ, P., BRAZEL, C. B., HELLER, S., BINDER, H., LOFFLER-WIRTH, H., SEIBEL, P. & MAGIN, T. M. 2015. A keratin scaffold regulates epidermal barrier formation, mitochondrial lipid composition, and activity. *J Cell Biol,* 211**,** 1057-75.

KWIECIEN, S., JASNOS, K., MAGIEROWSKI, M., SLIWOWSKI, Z., PAJDO, R., BRZOZOWSKI, B., MACH, T., WOJCIK, D. & BRZOZOWSKI, T. 2014. Lipid peroxidation, reactive oxygen species and antioxidative factors in the pathogenesis of gastric mucosal lesions and mechanism of protection against oxidative stress - induced gastric injury. *J Physiol Pharmacol,* 65**,** 613-22.

LAKOWSKI, B. & HEKIMI, S. 1998. The genetics of caloric restriction in Caenorhabditis elegans. *Proceedings of the National Academy of Sciences of the United States of America,* 95**,** 13091-13096.

LAMACCHIA, J. C., FRAZIER, H. N., 3RD & ROTH, M. B. 2015. Glycogen Fuels Survival During Hyposmotic-Anoxic Stress in Caenorhabditis elegans. *Genetics,* 201**,** 65-74.

LAPOINTE, J. & HEKIMI, S. 2008. Early mitochondrial dysfunction in long-lived Mclk1+/- mice. *J Biol Chem,* 283**,** 26217-27.

LEE, S. S., LEE, R. Y., FRASER, A. G., KAMATH, R. S., AHRINGER, J. & RUVKUN, G. 2003. A systematic RNAi screen identifies a critical role for mitochondria in C. elegans longevity. *Nat Genet,* 33**,** 40-8.

LEONARD, J. V. & SCHAPIRA, A. H. 2000. Mitochondrial respiratory chain disorders I: mitochondrial DNA defects. *Lancet,* 355**,** 299-304.

LETUNIC, I., YAMADA, T., KANEHISA, M. & BORK, P. 2008. iPath: interactive exploration of biochemical pathways and networks. *Trends Biochem Sci,* 33**,** 101-3.

LI, J., CAO, F., YIN, H. L., HUANG, Z. J., LIN, Z. T., MAO, N., SUN, B. & WANG, G. 2020. Ferroptosis: past, present and future. *Cell Death Dis,* 11**,** 88.

LING, J., BREY, C., SCHILLING, M., LATEEF, F., LOPEZ-DEE, Z. P., FERNANDES, K., THIRUCHELVAM, K., WANG, Y., CHANDEL, K., RAU, K., PARHAR, R., AL-MOHANNA, F., GAUGLER, R. & HASHMI, S. 2017. Defective lipid metabolism associated with mutation in klf-2 and klf-3: important roles of essential dietary salts in fat storage. *Nutr Metab (Lond),* 14**,** 22.

LISMONT, C., NORDGREN, M., VAN VELDHOVEN, P. P. & FRANSEN, M. 2015. Redox interplay between mitochondria and peroxisomes. *Front Cell Dev Biol,* 3**,** 35.

LODHI, I. J. & SEMENKOVICH, C. F. 2014. Peroxisomes: a nexus for lipid metabolism and cellular signaling. *Cell Metab,* 19**,** 380-92.

MA, C., HAGSTROM, D., POLLEY, S. G. & SUBRAMANI, S. 2013. Redox-regulated cargo binding and release by the peroxisomal targeting signal receptor, Pex5. *J Biol Chem,* 288**,** 27220-31.

MACELUCH, J. A. & NIEDZIELA, M. 2006. The clinical diagnosis and molecular genetics of kearns-sayre syndrome: a complex mitochondrial encephalomyopathy. *Pediatr Endocrinol Rev,* 4**,** 117-37.

MAK, H. Y. 2012. Lipid droplets as fat storage organelles in Caenorhabditis elegans: Thematic Review Series: Lipid Droplet Synthesis and Metabolism: from Yeast to Man. *J Lipid Res,* 53**,** 28-33.

MCBRIDE, H. M., NEUSPIEL, M. & WASIAK, S. 2006. Mitochondria: more than just a powerhouse. *Curr Biol,* 16**,** R551-60.

MCCONNELL, B. B. & YANG, V. W. 2010. Mammalian Kruppel-like factors in health and diseases. *Physiol Rev,* 90**,** 1337-81.

MULLANEY, B. C., BLIND, R. D., LEMIEUX, G. A., PEREZ, C. L., ELLE, I. C., FAERGEMAN, N. J., VAN GILST, M. R., INGRAHAM, H. A. & ASHRAFI, K. 2010. Regulation of C. elegans fat uptake and storage by acyl-CoA synthase-3 is dependent on NR5A family nuclear hormone receptor nhr-25. *Cell Metab,* 12**,** 398-410.

NARAYAN, V., LY, T., POURKARIMI, E., MURILLO, A. B., GARTNER, A., LAMOND, A. I. & KENYON, C. 2016. Deep Proteome Analysis Identifies Age-Related Processes in C. elegans. *Cell Systems,* 3**,** 144-159.

NUNNARI, J. & SUOMALAINEN, A. 2012. Mitochondria: in sickness and in health. *Cell,* 148**,** 1145-59.

OLZMANN, J. A. & CARVALHO, P. 2019. Dynamics and functions of lipid droplets. *Nat Rev Mol Cell Biol,* 20**,** 137-155.

PALGUNOW, D., KLAPPER, M. & DORING, F. 2012. Dietary restriction during development enlarges intestinal and hypodermal lipid droplets in Caenorhabditis elegans. *PLoS One,* 7**,** e46198.

PALIKARAS, K., LIONAKI, E. & TAVERNARAKIS, N. 2015. Coordination of mitophagy and mitochondrial biogenesis during ageing in C. elegans. *Nature,* 521**,** 525-8.

PALMEIRA, C. M., TEODORO, J. S., AMORIM, J. A., STEEGBORN, C., SINCLAIR, D. A. & ROLO, A. P. 2019. Mitohormesis and metabolic health: The interplay between ROS, cAMP and sirtuins. *Free Radical Biology and Medicine,* 141**,** 483-491.

PASCUAL-AHUIR, A., MANZANARES-ESTREDER, S. & PROFT, M. 2017. Pro- and Antioxidant Functions of the Peroxisome-Mitochondria Connection and Its Impact on Aging and Disease. *Oxid Med Cell Longev,* 2017**,** 9860841.

PEREZ, M. A., MAGTANONG, L., DIXON, S. J. & WATTS, J. L. 2019. Dietary Induction and Modulation of Ferroptosis in Caenorhabditis elegans. 772079.

POIRIER, Y., ANTONENKOV, V. D., GLUMOFF, T. & HILTUNEN, J. K. 2006. Peroxisomal beta-oxidation--a metabolic pathway with multiple functions. *Biochim Biophys Acta,* 1763**,** 1413-26.

PORTER, N. A. 1986. Mechanisms for the autoxidation of polyunsaturated lipids. *Accounts of Chemical Research,* 19**,** 262-268.

RASHID, T., NEMAZANYY, I., PAOLINI, C., TATSUTA, T., CRESPIN, P., DE VILLENEUVE, D., BRODESSER, S., BENIT, P., RUSTIN, P., BARAIBAR, M. A., AGBULUT, O., OLIVIER, A., PROTASI, F., LANGER, T., CHRAST, R., DE LONLAY, P., DE FOUCAULD, H., BLAAUW, B. & PENDE, M. 2019. Lipin1 deficiency causes sarcoplasmic reticulum stress and chaperone-responsive myopathy. *Embo j,* 38.

REISER, G., SCHONFELD, P. & KAHLERT, S. 2006. Mechanism of toxicity of the branched-chain fatty acid phytanic acid, a marker of Refsum disease, in astrocytes involves mitochondrial impairment. *Int J Dev Neurosci,* 24**,** 113-22.

RIDDICK, D. S., DING, X., WOLF, C. R., PORTER, T. D., PANDEY, A. V., ZHANG, Q.-Y., GU, J., FINN, R. D., RONSEAUX, S., MCLAUGHLIN, L. A., HENDERSON, C. J., ZOU, L. & FLÜCK, C. E. 2013. NADPH-cytochrome P450 oxidoreductase: roles in physiology, pharmacology, and toxicology. *Drug metabolism and disposition: the biological fate of chemicals,* 41**,** 12-23.

RIDDLE, B. T., MEYER BJ, ET AL. 1997. *C. elegans II*.

RISTOW, M. & ZARSE, K. 2010. How increased oxidative stress promotes longevity and metabolic health: The concept of mitochondrial hormesis (mitohormesis). *Experimental Gerontology,* 45**,** 410-418.

RODEHEFFER, M. S., BIRSOY, K. & FRIEDMAN, J. M. 2008. Identification of white adipocyte progenitor cells in vivo. *Cell,* 135**,** 240-9.

SCHAAR, C. E., DUES, D. J., SPIELBAUER, K. K., MACHIELA, E., COOPER, J. F., SENCHUK, M., HEKIMI, S. & VAN RAAMSDONK, J. M. 2015. Mitochondrial and cytoplasmic ROS have opposing effects on lifespan. *PLoS genetics,* 11**,** e1004972-e1004972.

SCHONFELD, P., SCHLUTER, T., FISCHER, K. D. & REISER, G. 2011. Non-esterified polyunsaturated fatty acids distinctly modulate the mitochondrial and cellular ROS production in normoxia and hypoxia. *J Neurochem,* 118**,** 69-78.

SCHRADER, M. & FAHIMI, H. D. 2006. Peroxisomes and oxidative stress. *Biochim Biophys Acta,* 1763**,** 1755-66.

SEBASTIÁN, D., GUITART, M., GARCÍA-MARTÍNEZ, C., MAUVEZIN, C., ORELLANA-GAVALDÀ, J. M., SERRA, D., GÓMEZ-FOIX, A. M., HEGARDT, F. G. & ASINS, G. 2009. Novel role of FATP1 in mitochondrial fatty acid oxidation in skeletal muscle cells. *Journal of lipid research,* 50**,** 1789-1799.

SHERRATT, H. S. 1991. Mitochondria: structure and function. *Rev Neurol (Paris),* 147**,** 417-30.

SRINIVASAN, S. 2015. Regulation of body fat in Caenorhabditis elegans. *Annu Rev Physiol,* 77**,** 161-78.

SU, L. J., ZHANG, J. H., GOMEZ, H., MURUGAN, R., HONG, X., XU, D., JIANG, F. & PENG, Z. Y. 2019. Reactive Oxygen Species-Induced Lipid Peroxidation in Apoptosis, Autophagy, and Ferroptosis. *Oxid Med Cell Longev,* 2019**,** 5080843.

SUOMALAINEN, A. & BATTERSBY, B. J. 2018. Mitochondrial diseases: the contribution of organelle stress responses to pathology. *Nat Rev Mol Cell Biol,* 19**,** 77-92.

SUTHAMMARAK, W., MORGAN, P. G. & SEDENSKY, M. M. 2010. Mutations in mitochondrial complex III uniquely affect complex I in Caenorhabditis elegans. *J Biol Chem,* 285**,** 40724-31.

THIERINGER, H., MOELLERS, B., DODT, G., KUNAU, W. H. & DRISCOLL, M. 2003. Modeling human peroxisome biogenesis disorders in the nematode Caenorhabditis elegans. *J Cell Sci,* 116**,** 1797-804.

TOWLE, H. C., KAYTOR, E. N. & SHIH, H. M. 1997. Regulation of the expression of lipogenic enzyme genes by carbohydrate. *Annu Rev Nutr,* 17**,** 405-33.

TOZZI, G., NUCCETELLI, M., LO BELLO, M., BERNARDINI, S., BELLINCAMPI, L., BALLERINI, S., GAETA, L. M., CASALI, C., PASTORE, A., FEDERICI, G., BERTINI, E. & PIEMONTE, F. 2002. Antioxidant enzymes in blood of patients with Friedreich's ataxia. *Arch Dis Child,* 86**,** 376-9.

TRALAU, T. & LUCH, A. 2013. The evolution of our understanding of endo-xenobiotic crosstalk and cytochrome P450 regulation and the therapeutic implications. *Expert Opin Drug Metab Toxicol,* 9**,** 1541-54.

TROJANOWSKI, N. F., RAIZEN, D. M. & FANG-YEN, C. 2016. Pharyngeal pumping in Caenorhabditis elegans depends on tonic and phasic signaling from the nervous system. *Sci Rep,* 6**,** 22940.

TUPPEN, H. A. L., BLAKELY, E. L., TURNBULL, D. M. & TAYLOR, R. W. 2010. Mitochondrial DNA mutations and human disease. *Biochimica et Biophysica Acta (BBA) - Bioenergetics,* 1797**,** 113-128.

VAN VELDHOVEN, P. P. & BAES, M. 2013. Peroxisome deficient invertebrate and vertebrate animal models. *Front Physiol,* 4**,** 335.

VENTURA, N. & REA, S. L. 2007. Caenorhabditis elegans mitochondrial mutants as an investigative tool to study human neurodegenerative diseases associated with mitochondrial dysfunction. *Biotechnol J,* 2**,** 584-95.

VENTURA, N., REA, S. L. & TESTI, R. 2006. Long-lived C. elegans mitochondrial mutants as a model for human mitochondrial-associated diseases. *Exp Gerontol,* 41**,** 974-91.

VIOLANTE, S., IJLST, L., VAN LENTHE, H., DE ALMEIDA, I. T., WANDERS, R. J. & VENTURA, F. V. 2010. Carnitine palmitoyltransferase 2: New insights on the substrate specificity and implications for acylcarnitine profiling. *Biochim Biophys Acta,* 1802**,** 728-32.

VISCOMI, C. & ZEVIANI, M. 2020. Strategies for fighting mitochondrial diseases. *J Intern Med*.

VRABLIK, T. L., PETYUK, V. A., LARSON, E. M., SMITH, R. D. & WATTS, J. L. 2015. Lipidomic and proteomic analysis of Caenorhabditis elegans lipid droplets and identification of ACS-4 as a lipid droplet-associated protein. *Biochim Biophys Acta,* 1851**,** 1337-45.

WALLACE, D. C. 2005. A mitochondrial paradigm of metabolic and degenerative diseases, aging, and cancer: a dawn for evolutionary medicine. *Annu Rev Genet,* 39**,** 359-407.

WALLACE, D. C., SINGH, G., LOTT, M. T., HODGE, J. A., SCHURR, T. G., LEZZA, A. M., ELSAS, L. J., 2ND & NIKOSKELAINEN, E. K. 1988. Mitochondrial DNA mutation associated with Leber's hereditary optic neuropathy. *Science,* 242**,** 1427-30.

WALLIS, J. G., WATTS, J. L. & BROWSE, J. 2002. Polyunsaturated fatty acid synthesis: what will they think of next? *Trends Biochem Sci,* 27**,** 467.

WALTHER, T. C., CHUNG, J. & FARESE, R. V., JR. 2017. Lipid Droplet Biogenesis. *Annu Rev Cell Dev Biol,* 33**,** 491-510.

WANDERS, R. J. 2004. Peroxisomes, lipid metabolism, and peroxisomal disorders. *Mol Genet Metab,* 83**,** 16-27.

WANDERS, R. J., FERDINANDUSSE, S., BRITES, P. & KEMP, S. 2010. Peroxisomes, lipid metabolism and lipotoxicity. *Biochim Biophys Acta,* 1801**,** 272-80.

WANDERS, R. J., WATERHAM, H. R. & FERDINANDUSSE, S. 2015. Metabolic Interplay between Peroxisomes and Other Subcellular Organelles Including Mitochondria and the Endoplasmic Reticulum. *Front Cell Dev Biol,* 3**,** 83.

WANG, R., KNIAZEVA, M. & HAN, M. 2013. Peroxisome protein transportation affects metabolism of branched-chain fatty acids that critically impact growth and development of C. elegans. *PLoS One,* 8**,** e76270.

WANG, X., LUO, F. & ZHAO, H. 2014. Paraquat-induced reactive oxygen species inhibit neutrophil apoptosis via a p38 MAPK/NF-κB-IL-6/TNF-α positive-feedback circuit. *PloS one,* 9**,** e93837-e93837.

WATKINS, P. A. & ELLIS, J. M. 2012. Peroxisomal acyl-CoA synthetases. *Biochim Biophys Acta,* 1822**,** 1411-20.

WATTS, J. L. 2009. Fat synthesis and adiposity regulation in Caenorhabditis elegans. *Trends Endocrinol Metab,* 20**,** 58-65.

WATTS, J. L. 2016. Using Caenorhabditis elegans to Uncover Conserved Functions of Omega-3 and Omega-6 Fatty Acids. *J Clin Med,* 5.

WATTS, J. L. & BROWSE, J. 2002. Genetic dissection of polyunsaturated fatty acid synthesis in Caenorhabditis elegans. *Proceedings of the National Academy of Sciences of the United States of America,* 99**,** 5854-5859.

WATTS, J. L. & RISTOW, M. 2017. Lipid and Carbohydrate Metabolism in Caenorhabditis elegans. *Genetics,* 207**,** 413-446.

WEEKS, J. C., ROBERTS, W. M., LEASURE, C., SUZUKI, B. M., ROBINSON, K. J., CURREY, H., WANGCHUK, P., EICHENBERGER, R. M., SAXTON, A. D., BIRD, T. D., KRAEMER, B. C., LOUKAS, A., HAWDON, J. M., CAFFREY, C. R. & LIACHKO, N. F. 2018. Sertraline, Paroxetine, and Chlorpromazine Are Rapidly Acting Anthelmintic Drugs Capable of Clinical Repurposing. *Scientific reports,* 8**,** 975-975.

WEIR, H. J., YAO, P., HUYNH, F. K., ESCOUBAS, C. C., GONCALVES, R. L., BURKEWITZ, K., LABOY, R., HIRSCHEY, M. D. & MAIR, W. B. 2017. Dietary Restriction and AMPK Increase Lifespan via Mitochondrial Network and Peroxisome Remodeling. *Cell Metab,* 26**,** 884-896.e5.

WEISS, S. B., KENNEDY, E. P. & KIYASU, J. Y. 1960. The enzymatic synthesis of triglycerides. *J Biol Chem,* 235**,** 40-4.

WELTE, M. A. 2015. Expanding roles for lipid droplets. *Curr Biol,* 25**,** R470-81.

WICKS, S. E., VANDANMAGSAR, B., HAYNIE, K. R., FULLER, S. E., WARFEL, J. D., STEPHENS, J. M., WANG, M., HAN, X., ZHANG, J., NOLAND, R. C. & MYNATT, R. L. 2015. Impaired mitochondrial fat oxidation induces adaptive remodeling of muscle metabolism. *Proc Natl Acad Sci U S A,* 112**,** E3300-9.

WITKOWSKI, A., THWEATT, J. & SMITH, S. 2011. Mammalian ACSF3 protein is a malonyl-CoA synthetase that supplies the chain extender units for mitochondrial fatty acid synthesis. *J Biol Chem,* 286**,** 33729-36.

WOOD, W. B. 1988. Determination of pattern and fate in early embryos of Caenorhabditis elegans. *Dev Biol (N Y 1985),* 5**,** 57-78.

WU, Z. & WANG, S. 2013. Role of kruppel-like transcription factors in adipogenesis. *Dev Biol,* 373**,** 235-43.

YANASE, S., YASUDA, K. & ISHII, N. 2002. Adaptive responses to oxidative damage in three mutants of Caenorhabditis elegans (age-1, mev-1 and daf-16) that affect life span. *Mech Ageing Dev,* 123**,** 1579-87.

YANG, W. & HEKIMI, S. 2010. A mitochondrial superoxide signal triggers increased longevity in Caenorhabditis elegans. *PLoS Biol,* 8**,** e1000556.

YANG, W. S., KIM, K. J., GASCHLER, M. M., PATEL, M., SHCHEPINOV, M. S. & STOCKWELL, B. R. 2016. Peroxidation of polyunsaturated fatty acids by lipoxygenases drives ferroptosis. *Proc Natl Acad Sci U S A,* 113**,** E4966-75.

YANG, W. S. & STOCKWELL, B. R. 2016. Ferroptosis: Death by Lipid Peroxidation. *Trends Cell Biol,* 26**,** 165-176.

YILMAZ, L. S. & WALHOUT, A. J. 2016. A Caenorhabditis elegans Genome-Scale Metabolic Network Model. *Cell Syst,* 2**,** 297-311.

YLIKALLIO, E. & SUOMALAINEN, A. 2012. Mechanisms of mitochondrial diseases. *Ann Med,* 44**,** 41-59.

YOKOTA, S., TOGO, S. H., MAEBUCHI, M., BUN-YA, M., HARAGUCHI, C. M. & KAMIRYO, T. 2002. Peroxisomes of the nematode Caenorhabditis elegans: distribution and morphological characteristics. *Histochem Cell Biol,* 118**,** 329-36.

YU, J. & LI, P. 2017. The size matters: regulation of lipid storage by lipid droplet dynamics. *Sci China Life Sci,* 60**,** 46-56.

ZHANG, J., BAKHEET, R., PARHAR, R. S., HUANG, C. H., HUSSAIN, M. M., PAN, X., SIDDIQUI, S. S. & HASHMI, S. 2011. Regulation of fat storage and reproduction by Kruppel-like transcription factor KLF3 and fat-associated genes in Caenorhabditis elegans. *J Mol Biol,* 411**,** 537-53.

ZHANG, J., HASHMI, S., CHEEMA, F., AL-NASSER, N., BAKHEET, R., PARHAR, R. S., AL-MOHANNA, F., GAUGLER, R., HUSSAIN, M. M. & HASHMI, S. 2013. Regulation of lipoprotein assembly, secretion and fatty acid beta-oxidation by Kruppel-like transcription factor, klf-3. *J Mol Biol,* 425**,** 2641-55.

ZHANG, W., SHIELDS, J. M., SOGAWA, K., FUJII-KURIYAMA, Y. & YANG, V. W. 1998. The gut-enriched Kruppel-like factor suppresses the activity of the CYP1A1 promoter in an Sp1-dependent fashion. *J Biol Chem,* 273**,** 17917-25.

Acknowledgments

First I would like to thank Sandra (Prof. Dr. Aleksandra Trifunovic), because without you the last four years would not have been possible. Thank you for your support and incredible patience and letting me be part of your research group.

Next, I would like to thank the mito-RTG manager Dr. Katerina Vlantis.
You always had an open ear for me no matter what or when. You always encouraged and built me up. You were one of the most important mental supports for me during my PhD.

Dr. Marija Herholz, the goddess of *C. elegans*, without you this work would not have been possible as well. I thank you so much for your immense energy, your help, and your patience. For guiding me and accompanying me throughout my PhD.

Linda Baumann, thank you for your technical assistance especially during the first and last year of my PhD journey. Thanks for your helping hands, support, and your time which you spend for me during all the experiments last months. Special thanks for keeping my Fortuna Düsseldorf cup alive!

Dr. Alexandra Kukat, thanks a lot for our funny lunch breaks and delicious shared salads.

Thanks to Matthijs (Johannes) Hermeling, my first and best coffee buddy ever. I am glad to have a colleague in the lab like you who was uncomplicated, always helpful and friendly. I will never forget that Wednesday means “It’s almost weekend!”

Grüß Gott, Frau Hien Ho! Thank you so much for seeing me as an “easy target” for socializing and for going with me to Austria. By the way, you still owe me a second visit for eating nougat parfait together. I am thankful for always cuddling me, and making me happy, being there in case of need. Also, for funny German lessons, where you got to know that “LACHS ist ein besonders fröhlicher Fisch”, for singing and for becoming a friend. Remember “Under the sea, under the sea darlin' it's better down where it's wetter”.

Milica Popovic, you were the last one who joined the lab one a half year ago, but it seems you were there from the beginning. Thank you so much for letting me get to know you, and together with the others you made the last year of my doctoral thesis so much happier and more bearable. Thank you for being there in case of need, for the best pancakes I ever ate and for becoming a friend.

Anastasia Rumyantseva thank you for your help and support and to reveal all the “secrets” during daily lab routine.

„Der Cottbuser Postkutscher putzt den Cottbuser Postkutschkasten“ thanks to Gregor Fink.

Thank you to all other present and former members of the Trifunovic lab for help and expertise and a great time: Harshita Kaul, Katharina Senft, Dr. Sophie Kaspar, Dr. Eduard Hofsetz, Dr. Marijana Aradjanski and Dr. Karolina Szczepanowska.

Ein sehr großer Dank geht an Mama und Papa. Ich habe euch sehr lieb!

Ich danke allen Freunden, die abseits vom Labor für einen enormen Ausgleich in den letzten vier Jahren gesorgt haben. @ Anne wir sind langsam „zu alt für so einen Sch…!“

Der größte Dank geht an Alex! Danke für deine Geduld und die Liebe, die du mir jeden Tag schenkst.

Erklärung

Ich versichere, dass ich die von mir vorgelegte Dissertation selbständig angefertigt, die benutzten Quellen und Hilfsmittel vollständig angegeben und die Stellen der Arbeit einschließlich Tabellen, Karten und Abbildungen -, die anderen Werken im Wortlaut oder dem Sinn nach entnommen sind, in jedem Einzelfall als Entlehnung kenntlich gemacht habe; dass diese Dissertation noch keiner anderen Fakultät oder Universität zur Prüfung vorgelegen hat; dass sie abgesehen von unten angegebenen Teilpublikationen noch nicht veröffentlicht worden ist sowie, dass ich eine solche Veröffentlichung vor Abschluss des Promotionsverfahrens nicht vornehmen werde.

Die Bestimmungen der Promotionsordnung sind mir bekannt. Die von mir vorgelegte Dissertation ist von Prof. Dr. Aleksandra Trifunovic betreut worden.

Köln, 27. April 2020

_____

(Sarah Maciej)